# CARBON FORMATION FROM ACETYLENE IN THE SHOCK TUBE

Eugene N. Bennett

Library
U. S. Naval Postgraduate School
Monterey, California

ACE - ACETYLENE
CAR - CARBON
SHR - SHOCK TUBE

8854

BARRETT

1951

[illegible]
B37p

Letter on cover:

. [illegible]
[illegible]

Eugene H. Barrett

# CARBON FORMATION FROM ACETYLENE IN THE SHOCK TUBE

Thesis by

Eugene N. Bennett

Major, U. S. Marine Corps

In Partial Fulfillment of the Requirements

For the Degree of

Aeronautical Engineer

California Institute of Technology

Pasadena, California

1956

Thesis
B372

## ACKNOWLEDGMENTS

The author is indebted to Dr. S. S. Penner for suggesting the studies on carbon formation and for his continued interest and advice during the progress of the work. He is grateful to Messrs. D. Weber, W. Hooker and, particularly, to F. Harshbarger for his assistance with the experimental studies. He also wishes to acknowledge helpful suggestions from Professor L. Lees and Mr. T. Harshbarger concerning some of the computations.

Support for the experimental and theoretical studies, through the U. S. Navy (Office of Naval Research) under Contract Nonr-220(03), NR 015 401, and the U. S. Air Force under Contract AF 18(603)-2, is gratefully acknowledged.

23924

ABSTRACT

The use of the shock tube for the study of carbon formation from acetylene has been considered theoretically and studied experimentally.

In the calculations, the state of the gas is determined behind incident and reflected shocks for a wide range of shock strengths and for various excitation models of the internal degrees of freedom. A simple mechanism has been assumed for the thermal decomposition, namely, the formation of solid carbon and hydrogen. Estimates are presented for the minimum times spent by the gas in a uniform state at the elevated temperatures behind reflected shocks.

The shock strengths required to initiate decomposition of acetylene at various pressures have been investigated experimentally. Temperature estimates and shock velocity measurements suggest that the effective specific heat ratio approaches the equilibrium value. Spectroscopic studies have been carried out to determine the light emitted in a narrow wave length region during chemical decomposition behind reflected shocks. The results show that the intensity distribution follows the black-body emission law. Therefore, a two-color method may be used in future studies for determining the temperature as a function of time behind carbon-forming shocks.

TABLE OF CONTENTS

PAGE

Acknowledgements

Abstract

Table of Contents

List of Figures

Symbols

I. INTRODUCTION 1

II. CALCULATION OF VARIOUS LIMITING TEMPERATURES BEHIND INCIDENT AND REFLECTED SHOCKS, PRIOR TO CHEMICAL REACTION 3

A. Equilibrium Calculations For the Ideal One-Dimensional Shock Tube 3

B. Non-Equilibrium Calculations 10

1. Excitation of Translational Degrees of Freedom 11

2. Excitation of Translational and Rotational Degrees of Freedom 11

III. ESTIMATES FOR THE TEMPERATURE RISE ASSOCIATED WITH THE DECOMPOSITION OF ACETYLENE 13

A. Temperature Rise Assuming Thermal Equilibrium After Decomposition 13

B. Temperature Rise Assuming Non-Equilibrium Partition of Energy 17

IV. CALCULATION OF THE MINIMUM TIME AT PEAK TEMPERATURE BEHIND A REFLECTED SHOCK WAVE 20

A. Calculation of Minimum Time at $T_5$ 21

B. Time at Which the First Reflected Rarefaction Wave Intersects the Contact Surface 22

PAGE

C. Interaction Between the Reflected Shock Wave and the Contact Surface 23

V. APPARATUS AND EXPERIMENTAL PROCEDURE 26

A. The Shock Tube 26

B. Auxiliary Apparatus 26

C. Instrumentation and Experimental Procedures 27

1. Incident Shock Velocity Measurements 27

2. Detection of Carbon Formation 28

3. Spectral Survey of Light Emitted During Chemical Reaction 28

VI. EXPERIMENTAL INVESTIGATIONS 30

A. Determination of the Minimum Pressure Ratio Required for Carbon Formation 30

B. Studies of the Light Emitted Behind a Reflected Shock Passing Through Acetylene 33

VII. CONCLUSIONS AND RECOMMENDATIONS 37

References 39

Appendix 40

Figures 42

## LIST OF FIGURES


| FIGURE | | PAGE |
|---|---|---|
| 1 | Ideal flow model in the uniform shock tube. | 42 |
| 2 | Incident shock Mach number vs. log $p_4/p_1$ for acetylene; $\gamma$ = equilibrium value. | 43 |
| 3 | Temperature ratios $T_2/T_1$ and $T_5/T_1$ vs. log $p_4/p_1$ for acetylene; $\gamma$ = equilibrium value. | 44 |
| 4 | Pressure ratios $p_2/p_1$ and $p_5/p_1$ vs. log $p_4/p_1$ for acetylene; $\gamma$ = equilibrium value. | 45 |
| 5 | Incident and reflected shock velocities vs. log $p_4/p_1$ for acetylene; $\gamma$ = equilibrium value. | 46 |
| 6 | Incident shock Mach number vs. log $p_4/p_1$ for a mixture of 95 °/o argon and 5 °/o acetylene; $\gamma$ = equilibrium value. | 47 |
| 7 | Temperature ratios $T_2/T_1$ and $T_5/T_1$ vs. log $p_4/p_1$ for a mixture of 95 °/o argon and 5 °/o acetylene; $\gamma$ = equilibrium value; $\rho_2 a_2/\rho_3 a_3 = 1$ at log $p_4/p_1 = 1.973$. | 48 |
| 8 | Pressure ratios $p_2/p_1$ and $p_5/p_1$ vs. log $p_4/p_1$ for a mixture of 95 °/o argon and 5 °/o acetylene; $\gamma$ = equilibrium value. | 49 |
| 9 | Incident and reflected shock velocities vs. log $p_4/p_1$ for a mixture of 95 °/o argon and 5 °/o acetylene; $\gamma$ = equilibrium value. | 50 |
| 10 | Incident shock Mach number vs. log $p_4/p_1$ for acetylene; $\gamma = 7/5$. | 51 |
| 11 | Temperature ratios $T_2/T_1$ and $T_5/T_1$ vs. log $p_4/p_1$ for acetylene; $\gamma = 7/5$. | 52 |
| 12 | Pressure ratios $p_2/p_1$ and $p_5/p_1$ vs. log $p_4/p_1$ for acetylene; $\gamma = 7/5$. | 53 |

| FIGURE | | PAGE |
|---|---|---|
| 13 | Incident and reflected shock velocities vs. $\log p_4/p_1$ for acetylene; $\gamma = 7/5$. | 54 |
| 14 | Incident shock Mach number vs. $\log p_4/p_1$ for acetylene; $\gamma = 5/3$. | 55 |
| 15 | Temperature ratios $T_2/T_1$ and $T_5/T_1$ vs. $\log p_4/p_1$ for acetylene; $\gamma = 5/3$. | 56 |
| 16 | Pressure ratios $p_2/p_1$ and $p_5/p_1$ vs. $\log p_4/p_1$ for acetylene; $\gamma = 5/3$. | 57 |
| 17 | Incident and reflected shock velocities vs. $\log p_4/p_1$ for acetylene; $\gamma = 5/3$. | 58 |
| 18 | Incident shock Mach number vs. $\log p_4/p_1$ for a mixture of 95 $^{o}$/o argon and 5 $^{o}$/o acetylene; $\gamma = 5/3$. | 59 |
| 19 | Temperature ratios $T_2/T_1$ and $T_5/T_1$ vs. $\log p_4/p_1$ for a mixture of 95 $^{o}$/o argon and 5 $^{o}$/o acetylene; $\gamma = 5/3$; $\rho_2 a_2/\rho_3 a_3 = 1$ at $\log p_4/p_1 > 3.5$. | 60 |
| 20 | Pressure ratios $p_2/p_1$ and $p_5/p_1$ vs. $\log p_4/p_1$ for a mixture of 95 $^{o}$/o argon and 5 $^{o}$/o acetylene; $\gamma = 5/3$. | 61 |
| 21 | Incident and reflected shock velocities vs. $\log p_4/p_1$ for a mixture of 95 $^{o}$/o argon and 5 $^{o}$/o acetylene; $\gamma = 5/3$. | 62 |
| 22 | Molar heat release ($Q$) vs. temperature for the decomposition of acetylene to solid carbon and hydrogen; $\gamma$ = equilibrium value. | 63 |
| 23 | Temperature ratios $T_2'/T_1$ and $T_5'/T_1$ vs. $\log p_4/p_1$ for acetylene; constant-pressure reaction; $\gamma$ = equilibrium value. | 64 |

| FIGURE | | PAGE |
|---|---|---|
| 24 | Temperature ratios $T_2'/T_1$ and $T_5'/T_1$ vs. $\log p_4/p_1$ for acetylene; constant-volume reaction; $\gamma$ = equilibrium value. | 65 |
| 25 | Temperature ratio $T_2'/T_1$ and $T_5'/T_1$ vs. $\log p_4/p_1$ for a mixture of 95 °/o argon and 5 °/o acetylene; constant-pressure reaction; $\gamma$ = equilibrium value. | 66 |
| 26 | Temperature ratio $T_2'/T_1$ and $T_5'/T_1$ vs. $\log p_4/p_1$ for a mixture of 95 °/o argon and 5 °/o acetylene; constant-volume reaction; $\gamma$ = equilibrium value. | 67 |
| 27 | Molar heat release (Q) vs. temperature for the decomposition of acetylene to solid carbon and hydrogen; $\gamma$ = 7/5 or 5/3 for $C_2H_2$ and $H_2$. | 68 |
| 28 | Temperature ratios $T_2'/T_1$ and $T_5'/T_1$ vs. $\log p_4/p_1$ for acetylene; constant-pressure reaction; $\gamma$ = 5/3. | 69 |
| 28a | Temperature ratios $T_2'/T_1$ and $T_5'/T_1$ vs. $\log p_4/p_1$ for acetylene; constant-volume reaction; $\gamma$ = 7/5. | 70 |
| 29 | Temperature ratio $T_2'/T_1$ and $T_5'/T_1$ vs. $\log p_4/p_1$ for acetylene; constant-volume reaction; $\gamma$ = 5/3. | 71 |
| 30 | Temperature ratios $T_2'/T_1$ and $T_5'/T_1$ vs. $\log p_4/p_1$ for acetylene; constant-pressure reaction; $\gamma$ = 7/5. | 72 |
| 31 | Temperature ratios $T_2'/T_1$ and $T_5'/T_1$ vs. $\log p_4/p_1$ for a mixture of 95 °/o argon and 5 °/o acetylene; constant-pressure reaction; $\gamma$ = 5/3. | 73 |

| FIGURE | | PAGE |
|---|---|---|
| 32 | Temperature ratios $T_2'/T_1$ and $T_5'/T_1$ vs. $\log p_4/p_1$ for a mixture of 95 °/o argon and 5 °/o acetylene; constant-volume reaction; $\gamma = 5/3$. | 74 |
| 33 | The x-t diagram, showing coordinates defined in Section IV. | 75 |
| 34 | Minimum time ( $\tau$ ) at $T_5$ vs. $\log p_4/p_1$ for acetylene. | 76 |
| 35 | Minimum time ($\tau$) at $T_5$ vs. $\log p_4/p_1$ for a mixture of 95 °/o argon and 5 °/o acetylene. | 77 |
| 36 | The time $(t_r - t_c)$ vs. $\log p_4/p_1$ for acetylene. | 78 |
| 37 | The time $(t_r - t_c)$ vs. $\log p_4/p_1$ for a mixture of 95 °/o argon and 5 °/o acetylene. | 79 |
| 38 | Two x - t diagrams, showing wave reflection resulting from the interaction between the reflected shock and the contact surface. | 80 |
| 39 | Schematic diagram of the shock tube and gas supply manifold. | 81 |
| 40 | Minimum pressure ratio ($p_4/p_1$) vs. initial pressure ($p_1$) required for carbon formation. | 82 |
| 41 | Minimum temperatures and pressures required for carbon formation behind reflected shocks in acetylene mixtures, assuming various excitation models of the internal degrees of freedom. | 83 |
| 42 | Log $p_5$ vs. $1/T_5$ (data from figure 41). | 84 |
| 43 | Emitted spectral intensity distribution measured behind carbon-forming shocks in acetylene. | 85 |

## SYMBOLS

| | |
|---|---|
| $a$ | local speed of sound |
| $c_1$ | first radiation constant |
| $c_2$ | second radiation constant |
| $C_p$ | molar heat capacity at constant pressure |
| $C_v$ | molar heat capacity at constant volume |
| $E$ | molar internal energy |
| $E'$ | effective activation energy |
| $H$ | molar enthalpy |
| $h$ | specific enthalpy |
| $\Delta H_f^\circ$ | standard molar heat of formation |
| $I_\lambda$ | radiation intensity at the wave length $\lambda$ |
| $M$ | Mach number |
| $p$ | pressure |
| $Q$ | molar heat release during chemical reaction |
| $R$ | universal gas constant |
| $R_g$ | specific gas constant |
| $S_\lambda$ | spectrometer spectral response |
| $T$ | absolute temperature |
| $t$ | time |
| $u$ | gas velocity |
| $U_s$ | incident shock velocity |
| $U_{sr}$ | reflected shock velocity |
| $v$ | gas velocity relative to a shock front |
| $v_{2r}$ | gas velocity relative to the reflected shock in the region between the incident shock and the contact surface |
| $\gamma$ | specific heat ratio |
| $\lambda$ | wave length of light |

$\rho$ density

$\tau$ minimum time spent by the gas at the elevated temperature behind a reflected shock wave

Subscripts

$( )_1$ initial conditions of low-pressure gas

$( )_2$ flow properties between the incident shock and the contact surface

$( )_3$ flow properties behind the contact surface

$( )_4$ initial conditions of the high-pressure gas

$( )_5$ flow properties behind the reflected shock

# I. INTRODUCTION

The pyrolysis of acetylene to form carbon and hydrogen and/or other hydrocarbons is of considerable basic interest in studies on aerothermochemistry. The detailed mechanism of pyrolysis is as yet understood incompletely.

The problem of carbon formation from hydrocarbons is also of practical importance in a variety of propulsion applications. A recent paper by C. Foure[1] is concerned with carbon formation in flame tubes and around injector orifices of turbo-jet engines. One of the theories of carbon formation from hydrocarbons, advanced particularly by G. Porter,[2] involves the assumption that carbon formation is preceded by the production of acetylene as an intermediate step, viz., "The thermal decomposition of hydrocarbons results in dehydrogenation and cracking to smaller molecules and the last stable hydrocarbon to be observed before carbon formation is acetylene".

Slow pyrolysis (i.e., heating of acetylene with maintenance of chemical equilibrium) to decomposition temperatures often involves heterogenous processes and usually leads to a variety of polymerization reactions at lower temperatures. The shock tube provides a unique tool for preparing acetylene, under uniform conditions, at elevated temperatures where the decomposition and/or polymerization rates may be studied conveniently.

The theoretical and experimental work reported in this thesis are parts of a more extensive kinetic study of carbon formation from acetylene. The subjects which will be considered in this study are the following: (1) the probable state of acetylene behind incident and reflected shocks; (2) the conditions of temperature and pressure

necessary to initiate the decomposition of acetylene with the formation of solid carbon; (3) the presentation of a new optical method for determining the temperature behind a shock wave in acetylene as a function of time; (4) the use of the experimental results to obtain preliminary data concerning the rate of formation of carbon from acetylene at elevated temperatures.

In Section II a theoretical calculation is described for the change of state in acetylene and in acetylene-argon mixtures produced by incident and reflected shock waves. The calculations are made for the uniform shock tube. Models considered for the studies are: (a) thermally equilibrated acetylene; (b) various states of the acetylene in which non-equilibrium conditions prevail and either the translational degrees of freedom or both the translational and rotational degrees of freedom are fully excited.

Section III is restricted to a discussion of thermal effects, based upon a simple mechanism for the decomposition of acetylene to solid carbon and hydrogen. Upper and lower limits for the final temperatures are computed for incident and reflected shocks. In Section IV, criteria are established for the minimum time at peak temperature behind reflected shocks; these criteria have been obtained for a particular shock-tube geometry. A brief discussion of the apparatus and experimental procedures is given in Section V. The results of the experimental investigations of (a) conditions required for carbon formation and (b) of light emission studies and temperature estimates are contained in Section VI. Finally, in Section VII, the experimental results are used to draw some preliminary conclusions regarding the mechanism of carbon formation.

## II. CALCULATION OF VARIOUS LIMITING TEMPERATURES BEHIND INCIDENT AND REFLECTED SHOCKS, PRIOR TO CHEMICAL REACTION

For the interpretation of experiments on carbon formation from acetylene in shock tubes, the state of the acetylene behind the shock must be known. Three limiting cases may be considered, namely, (a) the case in which complete thermal equilibrium is reached, (b) the case in which only the translational degrees of freedom are excited, and (c) the case in which both translational and rotational degrees of freedom are excited. In general, we expect to obtain in cases (a) and (b) estimates for the lower and upper limits of temperature, respectively, for the acetylene behind the shock and prior to chemical decomposition.

### A. Equilibrium Calculations For The Ideal One-Dimensional Shock Tube

The values of enthalpies are needed for the calculation of temperatures. Enthalpy data may be found in the literature[3, 4] for a large number of gases. In the present treatment the temperatures will be calculated for the short period of quasi-steady flow behind the shock wave, before the arrival of the rarefaction wave. The assumptions in these calculations are the following:

(1) There are no chemical reactions or phase changes, i.e., the change of state produced by the shock wave occurs in a time short compared with the time required for chemical reactions. The gas is assumed to be in thermal equilibrium before chemical reactions occur. Thus it is assumed that internal relaxation times are short compared with times necessary for chemical reactions.

(2) The compression by the shock wave is assumed to be adiabatic.

(3) Frictional effects are neglected.

(4) The ideal gas law is obeyed.

The temperature rise behind the incident shock may be calculated from the conservation equations if the initial state of the gas and the incident shock velocity are known. The quantities to be considered are the following:

$\rho$ = density ($g/cm^3$),

$p$ = pressure ($dynes/cm^2$),

$T$ = absolute temperature ($^oK$),

$h$ = specific enthalpy (ergs/g),

$R_g$ = specific gas constant ($ergs/g\text{-}^oK$),

$u$ = gas velocity in fixed coordinates (cm/sec),

$U_s$ = incident shock velocity (cm/sec),

$U_{sr}$ = reflected shock velocity (cm/sec),

$v$ = gas velocity relative to the shock front (cm/sec)

$= u - U_s$ or $u - U_{sr}$.

Subscripts refer to conditions in the regions shown in the one-dimensional shock tube and $x$ vs. $t$ (i.e., distance along the shock tube vs. time) diagram given in figure 1.

The initial values and boundary conditions are as follows:

Region 1: Initially occupied by low-pressure gas; all state quantities are known; $u_1 = 0$, $v_1 = -U_s < 0$.

Region 2: The gas behind the incident shock; $u_2 = -(v_1 - v_2) > 0$.

Region 3: Expanded high-pressure gas; $u_3 = u_2$ , $p_3 = p_2$ .

Region 4: Initially filled with high-pressure gas; all state quantities are known; $u_4 = 0$ .

Region 5: Low-pressure gas behind the reflected shock; $v_5 = -U_{sr} > 0$ , $v_{2r} = u_2 - U_{sr}$ . Here $v_5$ and $v_{2r}$ are the gas velocities relative to the reflected shock wave.

Consider a coordinate system fixed in the moving incident shock front. The continuity equation for steady, one-dimensional, flow is then

$$\rho_1 v_1 = \rho_2 v_2 . \tag{1}$$

The momentum equation for steady, inviscid, flow becomes

$$p_1 + \rho_1 v_1^2 = p_2 + \rho_2 v_2^2 . \tag{2}$$

The condition for conservation of energy for inviscid, adiabatic, flow may be written in the form

$$h_1 + \frac{v_1^2}{2} = h_2 + \frac{v_2^2}{2} . \tag{3}$$

The equation of state for ideal gases is

$$p = \rho R_g T . \tag{4}$$

Using equation 4 to eliminate $p$ from equation 2, we obtain

$$\rho_1 (R_g T_1 + v_1^2) = \rho_2 (R_g T_2 + v_2^2) . \tag{5}$$

Equation 1 is now used to eliminate $\rho$ from equation 5 with the result

$$\frac{R_g T_1 + v_1^2}{v_1} = \frac{R_g T_2 + v_2^2}{v_2} . \tag{6}$$

Equation 3 may be solved for $v_2$ , viz.,

$$v_2 = -\sqrt{v_1^2 - 2(h_1 - h_2)} \quad . \tag{7}$$

Here we choose the negative sign since $v_1$ and $v_2$ must have the same signs, as is apparent from equation 6. By substituting equation 7 into equation 6 and solving for the temperature ratio across the shock front, we obtain

$$\frac{T_2}{T_1} = -\sqrt{v_1^2 + 2(h_1 - h_2)}\left(\frac{1}{v_1} + \frac{v_1}{R_g T_1}\right) - \frac{v_1^2 + 2(h_1 - h_2)}{R_g T_1}$$

$$= v_2\left[\frac{1}{v_1} + \frac{v_1 - v_2}{R_g T_1}\right] > 0 \, . \tag{8}$$

Equation 8 may be solved for $v_1$, this being the negative of the propagation velocity of the shock wave into the undisturbed gas. The result is (see the Appendix for details)

$$U_s = -v_1 = \sqrt{\frac{-b + \sqrt{b^2 - 4ac}}{2a}} \, , \tag{9}$$

where $a = 2\left[(h_2 - h_1) - R_g(T_2 - T_1)\right]$, $b = 4R_g(h_2 - h_1)(T_2 - T_1) - R_g^2(T_2^2 - T_1^2) - 4(h_2 - h_1)^2$, and $c = -2R_g^2 T_1^2 (h_2 - h_1)$.

It is a simple matter to compute $U_s = -v_1$ from equation 9 for various values of $T_1$ and $T_2$ by using the tabulated data of $h_1$ and $h_2$.

For conditions behind the reflected shock, it is convenient to use the conservation equations and the equation of state for a coordinate system fixed in the reflected shock front. The resulting equations are similar to those given above in equations 1 to 8. It is necessary only to replace $v_1$ by $v_{2r}$, subscript 1 by subscript 2, and subscript 2

by subscript 5. In terms of $v_{2r}$, the solution of the relevant equations is [compare equation 8 and note $v_5 > 0$ whereas $v_2 < 0$]

$$\frac{T_5}{T_2} = v_5\left[\frac{1}{v_{2r}} + \frac{v_{2r} - v_5}{R_g T_2}\right] > 0. \tag{10}$$

It is clear from previous statements of the conditions in region 5 that

$$v_{2r} = u_2 - U_{sr} = v_5 - (v_1 - v_2). \tag{11}$$

An equation analogous to equation 7 is readily obtained for $v_5$, viz.,

$$v_5 = \sqrt{v_{2r}^2 + 2(h_2 - h_5)}. \tag{12}$$

Simultaneous solution of equations 11 and 12 yields the result

$$v_{2r} = -\left[\frac{(h_5 - h_2)}{(v_1 - v_2)} + \frac{(v_1 - v_2)}{2}\right]. \tag{13}$$

Combining equations 11 and 13 leads to

$$v_5 = -\frac{(h_5 - h_2)}{(v_1 - v_2)} + \frac{(v_1 - v_2)}{2}. \tag{14}$$

Substituting equations 13 and 14 into equation 10 and solving for $T_5$ yields the relation

$$T_5 = \left[(h_5 - h_2) - \frac{(v_1 - v_2)^2}{2}\right]\left[\frac{T_2}{(h_5 - h_2) + \frac{(v_1 - v_2)^2}{2}} + \frac{1}{R_g}\right]. \tag{15}$$

This expression, with $T_5$ and $h_5$ unknown, can be solved for $T_5$ by iteration using data from the literature[3, 4] after obtaining $v_2$ from equation 6.

The pressure ratio across the incident shock is readily obtained

from equations 1 and 4. It is found to be

$$\frac{p_2}{p_1} = \frac{v_1}{v_2} \frac{T_2}{T_1} \tag{16}$$

provided $R_g$ is constant, i.e, provided the molecular weight of the gas is unchanged, as has been assumed to be the case in the present calculations. A similar expression is obtained for the pressure ratio across the reflected shock, viz.,

$$\frac{p_5}{p_1} = \frac{p_5}{p_2} \frac{p_2}{p_1} = \left(\frac{v_5}{v_{2R}} \frac{T_5}{T_2}\right)\left(\frac{v_1}{v_2} \frac{T_2}{T_1}\right) = \left(\frac{v_5}{v_{2R}}\right)\left(\frac{v_1}{v_2} \frac{T_5}{T_1}\right).$$

Using equations 13 and 14 it is now apparent that

$$\frac{p_5}{p_1} = \frac{(h_5 - h_2) + \frac{(v_1 - v_2)^2}{2}}{(h_5 - h_2) - \frac{(v_1 - v_2)^2}{2}} \frac{v_1}{v_2} \frac{T_5}{T_1}. \tag{17}$$

Assuming the incident shock velocity has been calculated for various states of the gas behind the incident shock, it now remains to find the initial pressure ratios, $p_4/p_1$, which will produce these states. The high-pressure gas chosen in our experiments was an inert gas and hence has a constant specific heat ratio. Then the Riemann condition (Cf. references 5 or 6) for unsteady isentropic expansion of the high-pressure gas is

$$u_3 + \frac{2}{\gamma - 1} a_3 = \text{constant} = \frac{2}{\gamma - 1} a_4, \tag{18}$$

where $a$ is the local velocity of sound. The pressures in the isentropic expansion are related to the local sound velocity by

$$\frac{p_4}{p_3} = \left(\frac{a_4}{a_3}\right)^{\frac{2\gamma}{\gamma - 1}}. \tag{19}$$

By solving equation 18 for $a_4/a_3$ in terms of $u_3$ and $a_4$ and substituting the result into equation 19 we obtain

$$\frac{p_4}{p_3} = \left(1 - \frac{\gamma-1}{2}\,\frac{u_3}{a_4}\right)^{\frac{-2\gamma}{\gamma-1}} . \tag{20}$$

Using the boundary conditions $p_3 = p_2$ and $u_3 = u_2$ , and multiplying both sides of equation 20 by $p_3/p_1$ , yields the desired relation for the initial pressure ratio

$$\frac{p_4}{p_1} = \frac{p_2}{p_1}\left(1 - \frac{\gamma-1}{2}\,\frac{u_2}{a_4}\right)^{\frac{-2\gamma}{\gamma-1}} . \tag{21}$$

Computations were made for shocks passing either through pure acetylene or through a mixture containing 95 °/o argon and 5 °/o acetylene by volume, at an initial temperature of 298.16°K. The high-pressure gas was assumed to be helium and was also taken to be at an initial temperature of 298.16°K. The computations for pure acetylene were carried out as follows:

(1) $T_2$ was raised in 100°K increments from 400°K to 1500°K. Values of molar enthalpy from the literature[4] for $T_1$ and each chosen value of $T_2$ were converted to specific enthalpies, $h_1$ and $h_2$. The incident shock velocity, $U_s$ , and also $v_1$ were then computed from equation 9.

(2) With $v_1$ known, $v_2$ was computed from equation 6.

(3) Equation 15 was solved by trial and error to obtain $T_5$ and $h_5$ for each assumed value of $T_2$ .

(4) Equation 13 was then used to calculate $v_{2r}$ .

(5) The reflected shock velocity, $U_{sr} = -v_5$ , was obtained

from equation 14.

(6) Pressure ratios $p_2/p_1$ and $p_5/p_1$ were obtained from equations 16 and 17, respectively.

(7) The speed of sound, $a_4$, was computed for helium at 298.16°K from the relation $a_4 = \sqrt{\gamma_4 R_g T_4}$, where $\gamma_4 = 5/3$.

(8) With $u_2 = -(v_1 - v_2)$, $p_4/p_1$ was calculated from equation 21.

The computation for the mixture of 95 °/o argon and 5 °/o acetylene was done in the same manner. It was necessary only to modify the specific ideal gas constant and construct an enthalpy - temperature table for the mixture from data given in the literature.[4] The results of computations for both pure acetylene and the acetylene-argon mixture are presented graphically in figures 2 to 9.

## B. Non-Equilibrium Calculations

The assumptions 2 to 4 made in the equilibrium calculations are again made. However, the chemical reactions are now taken to occur before thermal equilibrium is attained. Thus it is assumed that internal relaxation times are long compared with the chemical reaction times, an assumption which implies that the heat capacities and the specific heat ratios are independent of temperature.

The assumption that the heat capacities are constant greatly simplifies the problem of calculating changes of flow properties across shock waves. In fact, the need for tabulated data of enthalpy is eliminated, and algebraic solutions, which do not require an iteration procedure, are obtained. For steady one-dimensional flow, the develop-

ment of relations across shock waves from the conservation laws and equation of state, equations 1 to 4, is well known (Cf. references 5, 6, 7, or 8) and the results are referred to as the normal or plane shock relations.

Tables of these relations for various specific heat ratios have been prepared by J. Lukasiewicz[5] for both the incident shock and the shock reflected from a rigid wall. In these tables, the independent variable may be considered to be the pressure ratio across the shock, $p_2/p_1$ .

1. Excitation of Translational Degrees of Freedom

Non-equilibrium calculations with translational excitation only yield possible upper limits for the temperature and pressure before chemical reaction begins. In this case, an ideal gas exhibits a molar heat capacity at constant pressure of $5/2\ R$ , and a molar heat capacity at constant volume of $3/2\ R$. Thus the specific heat ratio, $\gamma$ , is 5/3.

From Lukasiewicz[5] values of $T_2/T_1$ , $v_1/a_1$, $(v_1-v_2)/a$ , $p_5/p_2$, $T_5/T_2$ , and $|U_{s_R}/U_s|$ are obtained for various values of $p_2/p_1$. For pure acetylene and the mixture of 95 °/o argon and 5 °/o acetylene, $a_1$ may be calculated from the relation $a_1 = \sqrt{\gamma_1 R_g T_1}$ with $\gamma_1 = 5/3$ . The flow and state properties are then related to the initial pressure ratio, $p_4/p_1$ , by equation 21.

2. Excitation of Translational and Rotational Degrees of Freedom

The molar heat capacities at constant pressure and constant volume are $7/2\ R$ and $5/2\ R$ , respectively, for acetylene with only

the translational and rotational degrees of freedom fully excited, since acetylene is a linear molecular with two degrees of rotational freedom. The specific heat ratio $\gamma$ , becomes 7/5 in this case. Values of $T_2/T_1$ , $v_1/a_1$ , $(v_1-v_2)/a_1$, $p_5/p_2$ , $T_5/T_2$ , and $|U_{sr}/U_s|$ are obtained for various values of $p_2/p_1$ from Lukasiewicz.[5] For pure acetylene, $a_1$ is calculated as in paragraph 1, using $\gamma_1 = 7/5$ . Equation 21 may now be used to relate the state and flow properties to the initial pressure ratio, $p_4/p_1$.

For the mixture containing 95 °/o argon we neglect the influence of the acetylene and use always $\gamma_1 = 5/3$ since the specific heat ratio for monatomic gases is constant at the temperatures considered here. With this approximation, results of the calculations for a mixture containing 95 °/o argon and 5 °/o acetylene are therefore the same as those given for pure acetylene with only translational excitation.

Results of the non-equilibrium calculations are presented graphically in figures 10 to 21.

## III. ESTIMATES FOR THE TEMPERATURE RISE ASSOCIATED WITH THE DECOMPOSITION OF ACETYLENE

One possible mechanism for the decomposition of acetylene is represented by the equation

$$C_2H_2(g) \longrightarrow 2C(s) + H_2(g). \tag{22}$$

For the sake of simplicity we shall ignore the possible formation of hydrocarbons and base our analysis on the assumed decomposition mechanism described by equation 22. The heat released by this reaction equals the heat of formation of acetylene from the elements. The standard heat of formation, $\Delta H_f^\circ$, (i.e., the heat of formation at 298.16°K and zero pressure) is well known. For ideal gases $\Delta H_f^\circ$ is, of course, independent of the pressure. We use the value [see references 3 and 4], $\Delta H_f^\circ = 54.194$ Kcal/mol. Thus the reaction represented by equation 22 is highly exothermic under standard conditions and also behind relatively weak shocks of the type considered here.

The molar heat release, $Q$, for the reaction described by equation 22 can be obtained at any temperature from the relation

$$Q = 2\int_{298.16}^{T} C_p[C(s)]\,dT + \int_{298.16}^{T} C_p[H_2(g)]\,dT - \Delta H_f^\circ[C_2H_2(g)] - \int_{298.16}^{T} C_p[C_2H_2(g)]\,dT. \tag{23}$$

### A. Temperature Rise Assuming Thermal Equilibrium After Decomposition

For equilibrium calculations, the heat capacities are, in general, functions of the temperature. The heat capacity integrals of equation 23

can be replaced by molar enthalpy differences and determined from tabulated data.[3, 4] Thus equation 23 becomes

$$Q_T = 2\left(H_T - H_{298.16}\right)_{C(s)} + \left(H_T - H_{298.16}\right)_{H_2(g)} - \Delta H_f^\circ \left[C_2H_2(g)\right] - \left(H_T - H_{298.16}\right)_{C_2H_2(g)}. \quad (24)$$

Equation 24 applies both at constant pressure and at constant volume since there is no change in the number of moles of gas for the reaction given by equation 22. The equilibrium heat release calculated from equation 24 as a function of temperature is shown in figure 22.

In order to evaluate the effect of heat release on the temperature behind the shock, two simplifying assumptions are made:

(1) The heat release occurs adiabatically at the local temperature behind the shock, for each assumed model of excitation, following passage of the shock.

(2) The reaction goes to completion according to equation 22.

To obtain the final temperature behind the incident and reflected shocks, $T_2'$ and $T_5'$, respectively, at constant pressure, the heat release calculated from equation 24 is equated to the enthalpy rise of the products of reaction. Thus

$$Q_{T_2} = 2\left(H_{T_2'} - H_{T_2}\right)_{C(s)} + \left(H_{T_2'} - H_{T_2}\right)_{H_2(g)} \quad (25)$$

and

$$Q_{T_5} = 2\left(H_{T_5'} - H_{T_5}\right)_{C(s)} + \left(H_{T_5'} - H_{T_5}\right)_{H_2(g)}. \quad (26)$$

Since the heats of reaction and molar enthalpies are known, interpolation in the enthalpy tables of carbon and hydrogen for values of $H_{T_5'}\left[C(s)\right]$ or $H_{T_2'}\left[C(s)\right]$ and $H_{T_5'}\left[H_2(g)\right]$ or $H_{T_2'}\left[H_2(g)\right]$, which

satisfy equations 25 or 26, will yield the final temperatures, $T_2'$ and $T_5'$ . The results of these calculations for $T_2'/T_1$ and $T_5'/T_1$ are shown in figure 23 as functions of the initial pressure ratio, $p_4/p_1$ .

In order to obtain the final temperature, assuming a constant-volume process for the chemical decomposition leading to carbon formation, the heat release calculated from equation 24 is equated to the internal energy rise of the products. The internal energy for hydrogen may be obtained by subtracting $RT$ from the molar enthalpy. The difference between molar enthalpy and internal energy for solid carbon is small and may be neglected. The equations for the determination of $T_2'$ and $T_5'$ in the case of constant volume decomposition are

$$Q_{T_2} = 2\left(H_{T_2'} - H_{T_2}\right)_{C(s)} + \left(E_{T_2'} - E_{T_2}\right)_{H_2(g)} , \qquad (27)$$

and

$$Q_{T_5} = 2\left(H_{T_5'} - H_{T_5}\right)_{C(s)} + \left(E_{T_5'} - E_{T_5}\right)_{H_2(g)} . \qquad (28)$$

Results obtained by using equations 24, 27, and 28 for the determination of $T_2'/T_1$ and $T_5'/T_1$ are presented in figure 24.

For a mixture containing 95 °/o argon and 5 °/o acetylene, the decomposition reaction may be written as

$$0.05\,C_2H_2(g) + 0.95\,A(g) \longrightarrow 0.1\,C(s) + 0.05\,H_2(g) + 0.95\,A(g) . \qquad (29)$$

It is clear that the heat release per mole of mixture is 5 °/o of that given by equation 24. The enthalpy and internal energy changes for argon can be written as $(5/2)RT$ and $(3/2)RT$ , respectively, since

the heat capacities at constant pressure and volume are constant in the temperature range which is of interest in the present calculations. Equating the heat release to the enthalpy rise for the products of the reaction we obtain

$$Q_{T_2} = 0.1(H_{T_2'} - H_{T_2})_{C(s)} + 0.05(H_{T_2'} - H_{T_2})_{H_2(g)} + 5/2\, R(T_2' - T_2) \qquad (30)$$

and

$$Q_{T_5} = 0.1(H_{T_5'} - H_{T_5})_{C(s)} + 0.05(H_{T_5'} - H_{T_5})_{H_2(g)} + 5/2\, R(T_5' - T_5) \qquad (31)$$

Proper use in equations 30 and 31 of the enthalpy tables for carbon and hydrogen yields the final temperatures, $T_2'$ and $T_5'$, at constant pressure. Similarly, at constant volume, the equations become

$$Q_{T_2} = 0.1(H_{T_2'} - H_{T_2})_{C(s)} + 0.05(E_{T_2'} - E_{T_2})_{H_2(g)} + 3/2\, R(T_2' - T_2) \qquad (32)$$

and

$$Q_{T_5} = 0.1(H_{T_5'} - H_{T_5})_{C(s)} + 0.05(E_{T_5'} - E_{T_5})_{H_2(g)} + 3/2\, R(T_5' - T_5) \qquad (33)$$

Values of $T_2'$ and $T_5'$ have been obtained for various initial pressure ratios, $p_4/p_1$, and are shown in figures 25 and 26. It is evident that the effect of adding a large amount of inert diluent, such as argon, is to decrease the ultimate temperature rise produced by the chemical reaction.

B. Temperature Rise Assuming Non-Equilibrium Partition of Energy

The molar heat release from chemical reaction is easily calculated for non-equilibrium partition of energy. If only translational excitation occurs, the molar heat capacities for the gases are constant, viz., $C_p = 5/2\,R$ and $C_v = 3/2\,R$. For translational and rotational excitation, the heat capacities are $C_p = 7/2\,R$ and $C_v = 5/2\,R$. With these postulates, the heat capacity integrals for hydrogen and acetylene in equation 23 cancel. The assumption of non-equilibrium conditions for excitation of internal degrees of freedom of the gases does not affect the enthalpy of solid carbon. Replacing the molar heat capacity integrals in equation 23 for carbon by molar enthalpy differences, we obtain the non-equilibrium heat release equation

$$Q_T = 2(H_T - H_{298.16})_{C(s)} - \Delta H_f^\circ\,[C_2H_2(g)]. \qquad (34)$$

The heat release as a function of temperature, calculated from equation 34, is shown in figure 27.

With the assumption of constant heat capacity for gaseous components, the final temperatures behind the incident and reflected shocks are easily calculated. Molar enthalpy tables are needed only for solid carbon.

For shocks in pure acetylene, with the products of reaction having only the translational degrees of freedom excited, we proceed as follows. For constant-pressure processes, $C_p = 5/2\,R$. Equating the heat release from equation 34 to the enthalpy rise of the products we obtain

$$Q_{T_2} = 2(H_{T_2'} - H_{T_2})_{C(s)} + 5/2\,R(T_2' - T_2), \qquad (35)$$

and

$$Q_{T_5} = 2(H_{T_5'} - H_{T_5})_{C(s)} + 5/2\, R(T_5' - T_5). \tag{36}$$

For a constant-volume process, $C_v = 3/2\, R$ ,

$$Q_{T_2} = 2(H_{T_2'} - H_{T_2})_{C(s)} + 3/2\, R(T_2' - T_2), \tag{37}$$

and

$$Q_{T_5} = 2(H_{T_5'} - H_{T_5})_{C(s)} + 3/2\, R(T_5' - T_5). \tag{38}$$

Next consider shocks in pure acetylene, with the products of reaction fully excited in the translational and rotational degrees of freedom. For a constant-pressure process, $C_p = (7/2)R$ . Then

$$Q_{T_2} = 2(H_{T_2'} - H_{T_2})_{C(s)} + 7/2\, R(T_2' - T_2), \tag{39}$$

and

$$Q_{T_5} = 2(H_{T_5'} - H_{T_5})_{C(s)} + 7/2\, R(T_5' - T_5). \tag{40}$$

For a constant volume process, $C_v = 5/2R$. The resulting relations are identical with equations 35 and 36.

For a mixture of 5°/o acetylene and 95°/o argon the heat release is 5°/o of that given by equation 34. For a constant-pressure process, $C_p = 5/2\, R$ if the products have only the translational degrees of freedom excited. Equating the heat release to the enthalpy change of the products, we obtain

$$Q_{T_2} = 0.1(H_{T_2'} - H_{T_2})_{C(s)} + 5/2\, R(T_2' - T), \tag{41}$$

and

$$Q_{T_5} = 0.1(H_{T_5'} - H_{T_5})_{C(4)} + 5/2\, R(T_5' - T_5). \quad (42)$$

For a constant-volume process, $C_v = 3/2\ R$ if only the translational degrees of freedom are excited. Hence

$$Q_{T_2} = 0.1(H_{T_2'} - H_{T_2})_{C(4)} + 3/2\, R(T_2' - T_2), \quad (43)$$

and

$$Q_{T_5} = 0.1(H_{T_5'} - H_{T_5})_{C(4)} + 3/2\, R(T_5' - T_5). \quad (44)$$

The case in which the translational and rotational degrees of freedom are excited for a mixture containing 95% argon leads to essentially the same results as those which have been given in equations 41 to 44 since the specific heat of monatomic argon remains unchanged.

The results of calculations of $T_2'/T_1$ and $T_5'/T_1$, using equations 34 to 44, are presented graphically in figures 28 to 32 for various initial pressure ratios.

## IV. CALCULATION OF THE MINIMUM TIME AT PEAK TEMPERATURE BEHIND A REFLECTED SHOCK WAVE

It is important to obtain an estimate for the lower limit of the time spent at the maximum temperature by the gas behind a reflected shock wave. If the geometry of the shock tube is fixed, two processes may produce a change of the temperature behind the reflected shock, namely, (1) arrival of the rarefaction wave reflected from the end of the high-pressure section of the shock tube, or (2) reflected waves associated with the interaction between the reflected shock wave and the contact surface.

The arrival of the reflected rarefaction wave can be controlled by varying the length of the high-pressure section of the shock tube, as will be described below in greater detail. The nature of the waves produced by interaction between the reflected shock wave and the contact surface depends on the initial pressure ratio, the model of excitation for the internal degrees of freedom assumed, the gas under consideration and the shock-tube geometry. However, a lower limit for the time, $\tau$, during which the gas is at the uniform maximum temperature behind the reflected shock is obtained very simply by estimating the time interval between passage of the reflected shock at the observation station and interception of the reflected shock by the contact surface. *

---

* Neglecting the influence of the reflected rarefaction wave from the high-pressure section of the shock tube, it is obvious that no wave motion can affect the temperature behind the reflected shock at the observation station in the time $\tau$, provided, of course, that the tube geometry has been chosen in such a way as to place the observation station behind the reflected shock relative to the point of intersection of the shock and the contact surface.

## A. Calculation of Minimum Time at $T_5$

In order to compute the minimum time, $\tau$ , at temperature $T_5$ we define the following quantities which are shown also in figure 33:

$X_e$ = distance from the diaphragm to the end of the shock tube (meters).

$X_o$ = distance from the diaphragm to the position where observations are made (meters).

$X_c$ = distance from diaphragm to the position of interaction between the reflected shock wave and the contact surface (meters).

$t_o$ = time before the reflected shock wave passes the observation station (sec), measured from the time at which the diaphragm is ruptured.

$t_c$ = time before the reflected shock wave intersects the contact surface (sec), measured from the time at which the diaphragm is ruptured.

$t_r$ = time before the first reflected rarefaction wave would intercept the contact surface in an infinite shock tube (sec), measured from the time at which the diaphragm is ruptured.

The velocities of the incident shock, $U_s$ , of the reflected shock $U_{sr}$, and of the contact surface $u_2$ , have been calculated in Section II. It is convenient to take these velocities as positive in relating the times and distances defined above. It is clear that

$$t_c = \frac{X_c}{u_2} = \frac{X_e}{U_s} + \frac{X_e - X_c}{U_{sr}} . \qquad (45)$$

From equation 45 it is apparent that $X_c$ and $X_e$ are related through the expression

$$X_c = X_e \frac{U_s + U_{sr}}{u_2 + U_{sr}} \frac{u_2}{U_s} , \tag{46}$$

and

$$t_c = \frac{X_e}{U_s} \frac{U_s + U_{sr}}{u_2 + U_{sr}} . \tag{47}$$

The time at which the reflected shock wave passes the observation station is given by

$$t_o = \frac{X_e - X_o}{U_{sr}} + \frac{X_e}{U_s} . \tag{48}$$

From equations 47 and 48 the minimum time $\tau$ at peak temperature is seen to be

$$\tau = t_c - t_o = \frac{X_e}{U_s} \left[ \frac{U_s - u_2}{u_2 - U_{sr}} \right] - \frac{X_e - X_o}{U_{sr}} . \tag{49}$$

The minimum times, $\tau$, at the temperature $T_5$ computed from equation 49, for the various assumed models of internal excitation in pure acetylene, are shown in figure 34; the corresponding results are given in figure 35 for the mixture containing 5°/o acetylene and 95°/o argon. All calculations refer to a shock tube with $X_e$ = 2.323 meters and $X_o$ = 2.287 meters.

## B. Time at Which the First Reflected Rarefaction Wave Intersects the Contact Surface

The minimum time computed from equation 49 is significant only if the time $t_r$ required before the first reflected rarefaction wave intersects the contact surface is longer than $t_c$. The time $t_r$ can

be expressed analytically as a function of the design variables by using ideal shock tube theory. The result has been given, for example, by R. K. Lobb[9] and is, in our notation,

$$t_r = \frac{2 X_l}{a_4} \frac{p_4/p_1}{p_2/p_1} \frac{\gamma_4+1}{4\gamma_4} \qquad (50)$$

Here $X_l$ is the length of the high-pressure section of the shock and the other symbols have their usual meaning. Values of $t_r - t_c$ for $X_l = 0.914$ meters have been calculated by using equations 47 and 50 for various gas mixture and excitation models. The results are shown in figures 36 and 37. Experiments of other investigators show that the theoretical values of $\tau$ and $t_r - t_c$ may be reduced by a factor of one-half for very strong shocks in real shock tubes.

## C. Interaction Between the Reflected Shock Wave and the Contact Surface

In order to prove that the temperature $T_5$ behind the reflected shock is the maximum temperature to which the gas is subjected before chemical reactions begin, it is necessary to examine the nature of the interaction between the reflected shock wave and the contact surface. If the acoustic impedance $\rho a$ in region 3 is less than that in region 2, then the reflected shock wave will be refracted at the contact surface and will be accelerated upon passing from region 2 to region 3. The condition $\rho_3 a_3 < \rho_2 a_2$ is satisfied at low initial pressure ratios $p_4/p_1$ (see figure 38). The boundary conditions that the pressures and velocities must be the same on both sides of the contact surface are satisfied only if an expansion wave is reflected from the contact surface into region 5 when the reflected shock wave passes the contact surface. This reflected rarefaction wave lowers the temperature at the observation station, $X_o$.

some time later than $t_c$ and, therefore, does not invalidate equation 49 for estimates of lower time limits at peak temperature. When the acoustic impedances in regions 2 and 3 are equal, the reflected shock passes the contact surface unchanged and no reflection of any kind occurs at the contact surface (see figure 33). At sufficiently high initial pressure ratios, $p_4/p_1$, the acoustic impedance in region 3 ($\rho_3 a_3$) exceeds that in region 2 ($\rho_2 a_2$); in this case, the reflected shock is decelerated upon passing the contact surface and a shock is reflected back into region 5, which can raise the temperature above $T_5$. This state of affairs is shown schematically in figure 38.

Thus $T_5$, as calculated in Section II, is the actual maximum temperature behind the reflected shock before chemical reaction occurs only if

$$\frac{\rho_2 a_2}{\rho_3 a_3} \geq 1 . \tag{51}$$

In terms of the quantities calculated previously, equation 51 can be expressed as

$$\frac{\rho_2 a_2}{\rho_3 a_3} = \left(1 - \frac{\gamma_4 - 1}{2} \frac{u_2}{a_4}\right) \sqrt{\frac{\gamma_2 W_2 T_4}{\gamma_4 W_4 T_2}} \geq 1 . \tag{52}$$

where $W_2$ and $W_4$ represent the molecular weights of the gases concerned. The critical values for $p_4/p_1$ at which the right-hand side of equation 52 equals unity are indicated in figures 3, 7, 11, 15, and 19. It should perhaps be emphasized that the temperature rise in region 5, after any of the interactions involving the contact surface, can be estimated satisfactorily only by detailed numerical calculations if

$\rho_2 a_2 < \rho_3 a_3$. For values of the ratio $\rho_2 a_2 / \rho_3 a_3$ only slightly less than unity, the shock reflected from the contact surface will be so weak that it may be neglected.

In the strict sense, the generalized impedance ratio, $\frac{\rho_2 a_2 \sqrt{1 + \frac{1}{2}\left(\frac{p_5}{p_2} - 1\right)\left(1 + \frac{1}{\gamma_2}\right)}}{\rho_3 a_3 \sqrt{1 + \frac{1}{2}\left(\frac{p_5}{p_2} - 1\right)\left(1 + \frac{1}{\gamma_3}\right)}}$, should be introduced into equation 51. This ratio will equal unity for slightly higher initial pressure ratios than those obtained by use of equation 52. For the relatively weak shocks considered here, equation 52 is sufficiently accurate for estimating the initial pressure ratio below which the calculated values of $T_5$ can be considered valid.

# V. APPARATUS AND EXPERIMENTAL PROCEDURE

## A. The Shock Tube

The shock tube is constructed of flanged sections of three inch diameter cold-rolled steel pipe. Since the flanged sections are made of different lengths, a variety of shock tube geometries can be obtained. The sections are bolted together, using neoprene O-rings to provide the necessary seals. A carbon steel structure, thirty-two inches high, twenty-four inches wide, and bolted to the laboratory floor, serves as a rigid support for the shock tube.

The high-pressure sections have a wall thickness of 1/4 inch and were hydraulically tested to a pressure of 2000 psi. A screw-plunger (for breaking the stressed diaphram separating the high- and low-pressure sections) is incorporated in the high-pressure section (see figure 39). The high-pressure section rests on rollers so that the tube may be easily separated for changing diaphragms or cleaning.

The low-pressure sections have a wall thickness of 1/8 inch. Observations are made through three pairs of one inch diameter circular openings in the tube walls. Glass or lucite windows are held in these openings by threaded plugs and are sealed with O-rings. The end of the low-pressure section is closed with a threaded plug. Shock-tube dimensions and locations of the observation stations are shown in figure 39.

## B. Auxiliary Apparatus

The gas supply for the shock tube is controlled by a six-valve manifold shown schematically in figure 39. Helium was used as driver

gas in the high-pressure section; commercial acetylene or a mixture of 5 °/o acetylene and 95 °/o argon served as driven gas in the low-pressure section of the shock tube.

A Kinney high-capacity vacuum pump, capable of reducing the pressure to less than 0.01 mm of mercury (absolute), was used to evacuate both high- and low-pressure sections of the shock tube before admitting the gases. The pressure in the high-pressure section was measured with a calibrated Bourdon gage. The absolute pressure of the low-pressure gas was measured with a mercury manometer.

High- and low-pressure sections of the shock tube were separated by one or more thicknesses of 0.003 or 0.005 inch copper sheet, depending upon the shock strengths and pressure ratios across the diaphragm.

## C. Instrumentation and Experimental Procedures

### 1. Incident Shock Velocity Measurements

Pressure-sensing devices were used to determine the incident shock velocity. The apparatus consists of a metal holder containing a barium titanate crystal. The pressure pick-ups are mounted in place of a window at each of the observing stations nearest the diaphragm. The pressure change resulting from passage of the incident shock causes a one to two volt electrical pulse from the crystals. The shock velocity is determined by measuring the time interval between the two pulses with a Berkeley Universal Electronic Counter and Timer, Model 5510. The rise time of the pulses leads to an uncertainty in the shock velocity of $\pm$ 2 °/o. These pulses may be used to trigger other electronic equipment when convenient. An oscilloscope and the Berkeley counter were satisfactorily triggered without the use of pulse amplifiers.

2. Detection of Carbon Formation

A simple optical method, utilizing light absorption by solid particles, was devised for the detection of carbon formation. The light from a rheostat-controlled six-volt lamp was allowed to pass through the shock-tube observation station near the end of the tube. The intensity of the transmitted light was measured with a 931-A photomultiplier tube. Carbon formation reduces the amount of transmitted light, and thus changes the voltage output of the phototube. This output was observed with a Tektronix oscilloscope type 535, operated with single sweep control and triggered through the output of the second pressure pick-up used for velocity measurements. Results were recorded by use of a Polaroid oscilloscope camera. Intense light emission, associated with chemical reaction after passage of the shock, precludes the use of this method for measuring the rate of carbon formation.

3. Spectral Survey of Light Emitted During Chemical Reaction

In order to study the emission of light during chemical reactions, a spectrometer was placed at the observation window nearest to the end of the shock tube. The opposite window was masked to prevent transmitted light from reaching the spectrograph.

A Jarrel - Ash Spectrometer, Model 8200, was used for spectroscopic studies. This instrument consists of a JACO - Ebert Scanning Monochromator, with a suitable photomultiplier detector behind the exit slit. A Leeds and Northrup Recorder and stabilized high-voltage power supply for the phototube complete the instrument. The monochromator is designed for operation in the visible and ultraviolet

ranges of the spectrum. A 52 x 52 mm grating ruled to 1200 lines per mm gives a dispersion of 16 Å/mm in the first order at the exit slit. The scanning range is 2000 to 8000 Å in the first order with resolution better than 0.2 Å.

The three-inch shock tube was not constructed in time to obtain spectrometric data. For this reason, preliminary measurements were made with the spectrometer mounted near a one-inch diameter shock tube. These preliminary experiments clearly established that the intense emitted radiation from carbon-forming acetylene was grey and, therefore, could be used for making measurements of the effective temperatures as a function of time. More refined experiments, using the three-inch shock tube, are being conducted by F. Harshbarger.

A 2.0 ft. long high-pressure section, and a 6.5 ft. long low-pressure section, were used in the one-inch diameter shock tube. The low-pressure section had appended to it an end consisting of a four inch lucite section and a metal plate to close the tube. Measurements with the monochromator were made at a position 1/4 inch from the end of the tube using a 40 micron entrance slit and a 25 micron exit slit. The output of the 1P21 photo tube multiplier was observed and photographed by use of the Tektronix oscilloscope. The oscilloscope was triggered through the incident shock after it passed a barium titanate pressure pick-up located twenty-six inches from the end of the shock tube.

# VI. EXPERIMENTAL INVESTIGATIONS

## A. Determination of the Minimum Pressure Ratio Required for Carbon Formation

The minimum pressure ratio $p_4/p_1$ required for carbon formation as a function of the downstream pressure, $p_1$, was determined by use of the method described in Section V, paragraph C-2. The phototube output in light transmission experiments decreased approximately 10 volts as the light source was switched from "on" to "off". The threshold value for carbon formation, which was detected by wiping the end-plug of the shock tube carefully with white tissue, decreased the phototube output approximately two volts. The phototube output was greatly reduced, however, by obtaining carbon formation at initial pressure ratios only slightly above the threshold value.

For acetylene, measurements were made at initial pressures ($p_1$) of 10, 50, and 150 mm of mercury; for the mixture of 95 °/o argon and 5 °/o acetylene, initial pressures ($p_1$) of 50, 100, and 150 mm of mercury were used. The results of these experiments are shown in figure 40. The oscilloscope recordings of these measurements revealed two interesting results: (1) The onset of carbon formation occurs at an initial pressure ratio which is defined within narrow limits; the density of the carbon deposits changes from "very light" to "very heavy" with a small increase in initial pressure ratio (of the order of 2 °/o to 5 °/o). (2) The formation of detectable amounts of carbon from pure acetylene is invariably accompanied by intense light emission in the visible region of the spectrum; the light output increases in intensity and duration

with increased carbon formation. No particular significance can be attached to light emission from the argon-acetylene mixture since argon is excited and emits light at temperatures corresponding to shock strengths below those used in experiments on carbon formation.

From the experimental data for $p_4/p_1$ and $p_1$ at the threshold of carbon formation, the minimum temperatures, $T_5$, and pressures, $p_5$, required for carbon formation were estimated. The computations were made for the various models of excitation of the internal degrees of freedom considered in Section II. The results are shown in figure 41. The length of the times available at $T_5$ and $p_5$ for carbon formation were taken from figures 34 to 37, and are also indicated in figure 41.

Shock velocity measurements for carbon-forming experiments were normally 2 to 10 $^{o}/_{o}$ below the theoretical values calculated for thermal equilibrium, (see figure 5). Comparison of temperature measurements (see figure 43) with temperatures calculated from various excitation models, suggest that the effective specific heat ratio approaches the equilibrium value for exothermic reaction. Therefore, the actual conditions for carbon formation probably approach those shown in figure 41 assuming equilibrium excitation of the internal degrees of freedom. The temperatures and pressures required to initiate decomposition of acetylene in times less than two milliseconds are much greater than those reported for explosive decomposition in slow pyrolysis.[13]

A rough kinetic interpretation of the experimental data presented in figure 41 can be made in the following manner. The rate of change of carbon concentration with time can be written from the law of mass

action[11] in the Arrhenius form as

$$\frac{d[C(s)]}{dt} = B \exp\left[-E'/RT_5\right](p_5)^n, \tag{53}$$

where $n$ is a small number, $E'$ is the effective molar activation energy, $B$ equals the frequency factor (independent of temperature), and $R$ is the molar gas constant. The thermal decomposition of many hydrocarbons obeys first-order kinetics;[12] therefore, a choice of $n$ near unity appears to be reasonable.

We now assume that at the conditions for minimum detectable carbon formation, the rates of formation of carbon are roughly similar since the times at $T_5$ and minimum detectable amounts of carbon are roughly the same. Therefore,

$$\frac{d[C(s)]}{dt} \approx \frac{\Delta C(s)}{\Delta t(\text{at } T_5)} = \text{constant for all values of } p_5 \text{ and}$$

$T_5$ determined experimentally. Hence it follows from equation 53 that $\ln B - E'/RT_5 + n \ln p_5 = \text{constant}$ or

$$E' = \frac{2.303nR\, d \log_{10} p_5}{d(1/T_5)}. \tag{54}$$

Since the activation energy is independent of temperature and pressure, a plot of $\log_{10} p_5$ versus $1/T_5$ should be linear with a slope equal to $E'/2.303nR$. Using the values of $p_5$ and $T_5$ calculated from the experimental data, such a plot was made and is given in figure 42. Reference to figure 42 shows that the interpretation suggested by equation 54 is useful only for the data obtained with a mixture of 95 °/o

argon and 5 °/o acetylene. The assumption that $\Delta C(s)/\Delta t$ is constant for all $T_5$ and $p_5$ does not hold when the initial concentration of acetylene becomes large because the times at peak temperature are variable (see the data for $\tau$ given in figure 41).

The value obtained for the effective activation energy, corresponding to carbon formation in the argon-acetylene mixture, is about $54n$ Kcal/mol, assuming that the equilibrium value of $\gamma$ applies. For pure acetylene, the effective activation energy is not defined by our crude experiments.

B. Studies of the Light Emitted Behind a Reflected Shock Passing Through Acetylene

A spectral survey of the light emission behind reflected shocks in acetylene has been made by using the procedures described in Section V, Paragraph C-3. It seemed possible that intense radiation would occur at wave lengths corresponding to the $C_2$ and $CH$ emission bands commonly observed in hydrocarbon flames. However, the observed radiation at the time of maximum light output actually appeared to be grey (or black).

The light intensity was measured as a function of time in 100 Å intervals for the spectral range between 3500 and 7000 Å. The initial pressure ratio was 465, and the acetylene pressure, $p_1$, was 24 mm of mercury for each of the measurements. For all wave lengths, the light intensity reached a relative maximum value in 350 to 400 microseconds after the beginning of emission.

To show that the emitted radiation follows the black- (or grey-)

body distribution law, we consider Planck's equation for the spectral distribution of thermal radiation, viz.,

$$I_\lambda = \frac{c_1}{\lambda^5} \frac{1}{e^{c_2/\lambda T} - 1} S_\lambda . \qquad (55)$$

In equation 55, $I_\lambda$ is the measured intensity at the wave length $\lambda$, $c_1$, and $c_2$ are universal constants, $T$ is again the absolute temperature, and $S_\lambda$ is the spectral response of the spectrograph-phototube combination. $S_\lambda$ is independent of the temperature and may be assumed to be characteristic of the instrument as long as the spectrograph entrance slit is maintained at a fixed value.

In order to determine $S_\lambda$ for the system, the temperature of a standard tungsten light source was measured with a Leeds and Northrup optical pyrometer. This light source was then placed in the lucite section of the shock tube. The intensity of this source was measured with the spectrometer over the range of wave lengths from 3500 $\mathring{A}$ to 7000 $\mathring{A}$. To obtain the spectral response, the measured intensities at each wave length were divided by the maximum observed intensity.

The peak intensities (which occurred 350 to 400 microseconds after the beginning of emitted radiation) measured behind the reflected shock in acetylene were corrected for the spectral response of the system by using the calibration curve and equation 55. The resulting values of the emitted spectral intensity are shown in figure 43 as a function of wave length. The Planck spectral distribution curves for various temperatures, normalized to an absolute value of 0.02 at 4000 $\mathring{A}$, are also indicated in figure 43. Reference to figure 43 shows

that the wave length dependence of the emitted light, at the time of maximum intensity, follows roughly the black-body distribution curve for thermal radiation at a temperature of 2000°K. The scatter of the experimental points is considerable and may be attributed to the difficulty in reproducing shock velocities exactly. Although the initial pressure ratio is carefully duplicated for each measurement, a 10 °/o scatter in shock velocity can generally be expected as a result of non-uniform diaphragm rupture.

The fact that the radiant energy emitted from decomposing acetylene in the shock tube follows the black-body distribution law may be used to advantage for temperature measurements based on a two-color technique. An experimental program, using two narrow-pass light filters and photoelectric receivers in order to obtain simultaneous intensity measurements at two different wave lengths, is currently being pursued by F. Harshbarger. It is possible that the addition of small amounts of acetylene to air may allow temperature-time measurements also in gas-dynamic studies using the shock tube. Measurements of this sort would constitute a valuable addition to available techniques for studying these problems.

In principle, it should be possible to compute the temperature as a function of time from the available light intensity vs. time data at fixed wave lengths. The same method of interpretation used for temperature determination for the time when the emitted intensity was a maximum should apply at other times. We have obtained a temperature estimate of about 2200°K at a time 100 $\mu$ sec. after the beginning of emission, compared with about 2000°K (see figure 43) for times between 350 and

400 $\mu$ sec. after emission. However, the experimental scatter was large and, therefore, the absolute significance of this last result is doubtful. The preceding temperature estimates are somewhat lower than the values which are predicted on the basis of equilibrium excitation followed by complete decomposition of acetylene to solid carbon and hydrogen.

Light intensity vs. time experiments are now being conducted in the three-inch shock tube. It appears likely that some kinetic information will be obtained from the time delay preceding the emission of radiation.

## VII. CONCLUSIONS AND RECOMMENDATIONS

The theoretical and experimental studies on carbon formation behind reflected shocks in acetylene, which are described in the preceding sections, constitute little more than a beginning to an investigation of the mechanism of carbon formation at elevated temperatures and pressures. The principal conclusions, which we are justified in drawing, are the following:

(1) The effective value of the specific heat ratio $\gamma$, for the incident shock probably is close to the equilibrium value. Since relaxation times decrease with temperature, it therefore appears likely also that the effective $\gamma$ for the reflected shock, prior to chemical decomposition, is close to the equilibrium value.

(2) Threshold experiments on carbon formation, in the times available for a fixed shock-tube geometry, show that the rate of carbon formation is well defined by the design pressure ratio $p_4/p_1$ and by $p_1$; these, in turn determine the values of $T_5$ and $p_5$ reproducibly. Estimates for $T_5$ and $p_5$ at the threshold of carbon formation may possibly be used to obtain crude indications for the activation energy involved in carbon formation.

(3) The relative intensity for the spectral distribution of the radiation emitted behind the reflected shock in carbon-forming experiments follows the black- (or grey-) body distribution curve for the wave length region between 3500 and 7000 $\mathring{A}$ at times 100 and 350 to 400 $\mu$ sec. after the beginning of light emission. Since the intense CH and $C_2$ emission bands occur in this spectral range, but were not

distinguishable from the continuous background radiation, it appears likely that in carbon-forming shocks the emitted relative radiant energy really follows, over all wave length regions, the black-body distribution curve some time after chemical decomposition occurs. Therefore, a simple two-color technique can be used to obtain the temperature as a function of time behind carbon-forming shocks. This last conclusion may well prove to be of importance also for gas-dynamic studies in which it may be advantageous to add a small amount of acetylene in order to obtain conditions suitable for optical observations of the temperature as a function of time.

Future studies on the mechanism of carbon formation at elevated temperatures and pressures may profitably start from the preliminary studies described in this thesis.

## REFERENCES


1. Foure, C., "Formation et Depot de Carbone Dans Les Foyers de Turbo-Machines D'Aviation", Combustion Researches and Reviews, AGARDograph No. 9, Butterworths Scientific Publications, London (1955), pp. 125-139.

2. Porter, G., "The Mechanism of Carbon Formation", ibid, pp. 108-123.

3. National Bureau of Standards, Tables of Selected Values of Chemical Thermodynamic Properties, (1949), Series III, Vol. II.

4. Rossini, F. D., et al., Selected Values of Physical and Thermodynamic Properties of Hydrocarbons and Related Compounds, American Petroleum Institute Research Project 44, Carnegie Press, Pittsburgh (1953).

5. Lucasiewicz, J., "Shock Tube Theory and Applications", NAEC Report 15, Ottawa (1952), pp. 8-69.

6. Courant, R., and Friedrichs, K. O., Supersonic Flow and Shock Waves, Interscience Publishers, Inc., New York (1948), pp. 107-191.

7. Liepmann, H. W., and Puckett, A. E., Aerodynamics of a Compressible Fluid, John Wiley and Sons, New York (1947), pp. 38-45.

8. Bonney, A. E., Engineering Supersonic Aerodynamics, Mc Graw Hill Book Co., New York (1950), pp. 50-60.

9. Lobb, R. K., "On the Length of a Shock Tube", UTIA Report No. 4, Toronto (1950), p. 6.

10. Copenhaver, J. W., and Bigelow, M. H., Acetylene and Carbon Monoxide Chemistry, Reinhold Publishing Corporation, New York (1949), pp. 310-326.

11. Penner, S. S., Introduction to the Study of Chemical Reactions in Flow Systems, AGARDograph No. 7, Butterworths Scientific Publications, London (1955), pp. 3-6.

12. Hinshelwood, C. N., et. al., Proceedings of the Royal Society of London, A203, (1950), pp. 486-501; A214, (1952), pp. 20-35.

## APPENDIX

### Solution of Equation 8 for the Incident Shock Velocity

Equation 8 can be rewritten as

$$= \sqrt{v_1^2 + 2(h_1 - h_2)} \left( \frac{1}{v_1} + \frac{v_1}{R_g T_1} \right) = \frac{T_2}{T_1} + \frac{v_1^2 + 2(h_1 - h_2)}{R_g T_1} \quad . \quad (A-1)$$

Combining fraction on the right-hand side of equation A-1 and squaring both sides we obtain

$$1 + \frac{2 v_1^2}{R_g T_1} + \frac{v_1^4}{(R_g T_1)^2} + \frac{2(h_1 - h_2)}{v_1^2} + \frac{4(h_1 - h_2)}{R_g T_1} + \frac{2 v_1^2 (h_1 - h_2)}{R_g T_1^2} =$$

$$\frac{(R_g T_2)^2 + 2 v_1^2 R_g T_2 + 4 R_g T_2 (h_1 - h_2) + v_1^4 + 4 v_1^2 (h_1 - h_2) + 4(h_1 - h_2)^2}{(R_g T_1)^2} . \quad (A-2)$$

It is clear that the terms in $v_1^4$ cancel; the terms involving $v_1^2 (h_1 - h_2)$ may be combined. It is then easily shown, after multiplication by $v_1^2 (R_g T_1)^2$, that

$$v_1^2 (R_g T_1)^2 + 2 v_1^4 R_g T_1 + 2 (R_g T_1)^2 (h_1 - h_2) + 4 v_1^2 (h_1 - h_2) =$$

$$v_1^2 (R_g T_2)^2 + 2 v_1^4 R_g T_2 + 4 v_1^2 R_g T_2 (h_1 - h_2) + 2 v_1^4 (h_1 - h_2) + 4 v_1^2 (h_1 - h_2),$$

or

$$v_1^4 \left[ 2 R_g T_1 - 2 R_g T_2 - 2(h_1 - h_2) \right] + v_1^2 \left[ (R_g T_1)^2 + 4 R_g T_1 (h_1 - h_2) \right. \quad (A-3)$$

$$\left. - (R_g T_2)^2 - 4 R_g T_2 (h_1 - h_2) - 4 (h_1 - h_2)^2 \right] + 2 (R_g T_1)^2 (h_1 - h_2) = 0.$$

Simplification of the coefficients of various powers of $v_1$ in equation A-3, as well as rearrangement of temperature and enthalpy differences so that these differences will all be positive (i.e.,

$T_2 > T_1$, $h_2 > h_1$ for compression by shocks), leads to

$$a v_1^4 + b v_1^2 + c = 0$$

where

$$\left.\begin{aligned} a &= 2\left[(h_2 - h_1) - R_g(T_2 - T_1)\right], \quad b = 4R_g(h_2 - h_1)(T_2 - T_1) \\ &- R_g^2(T_2^2 - T_1^2) - 4(h_2 - h_1)^2, \text{ and } c = -2R_g^2 T_1^2 (h_2 - h_1). \end{aligned}\right\} \quad (A-4)$$

Equation A-4 may now be solved for $v_1^2$ with the result

$$v_1^2 = \frac{-b \pm \sqrt{b^2 - 4ac}}{2a}. \quad (A-5)$$

It is obvious that $a$ is positive and that $b$ and $c$ are negative. Thus, for real values of $v_1$, the positive sign must be taken with the radical in equation A-5.

Since $v_1$ is negative in the chosen coordinate system, equation 7 is obtained directly from equation A-5, viz.,

$$U_\infty = -v_1 = \sqrt{\frac{b + \sqrt{b^2 - 4ac}}{2a}}.$$

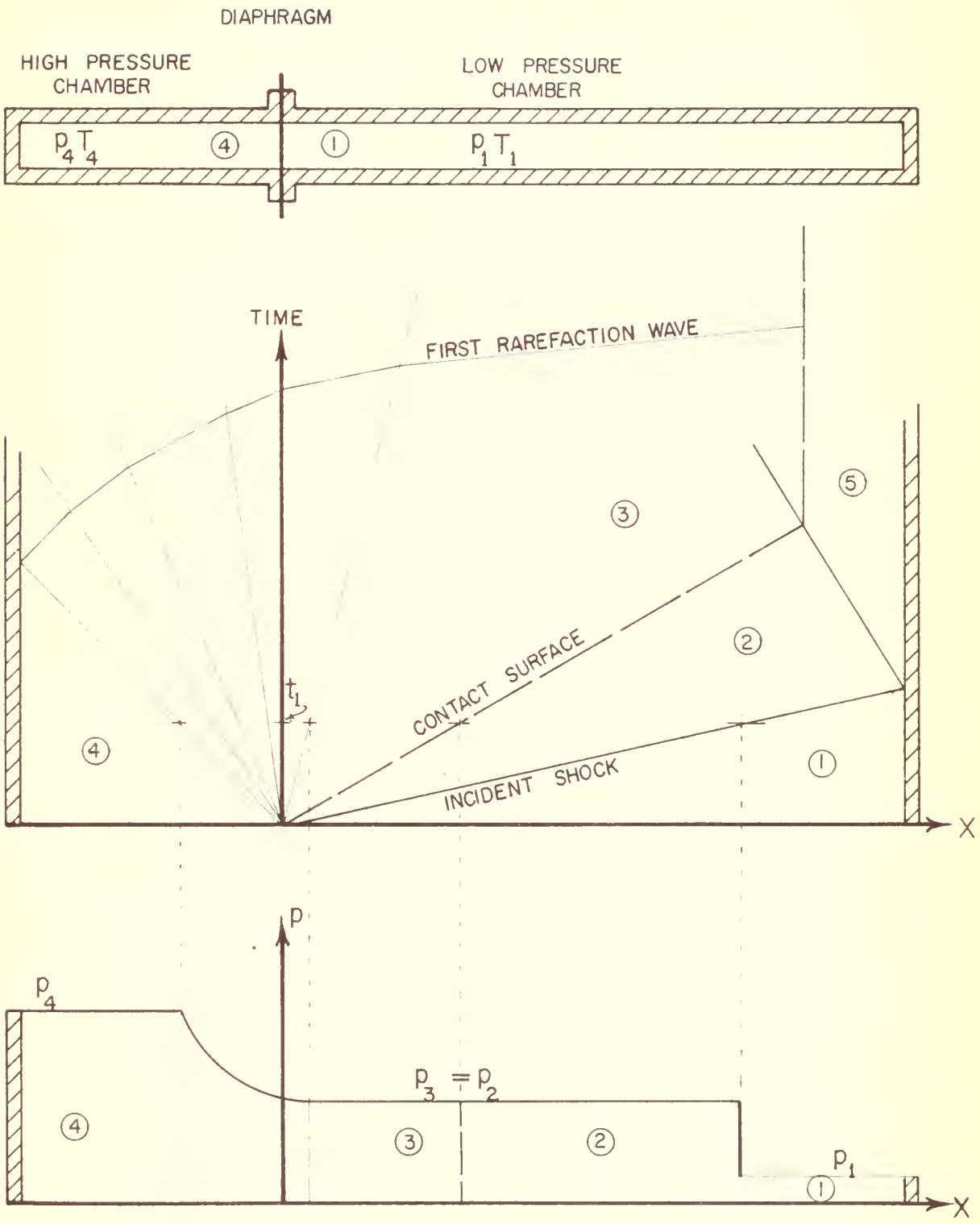


Fig. 1. Ideal flow model in the uniform shock tube.

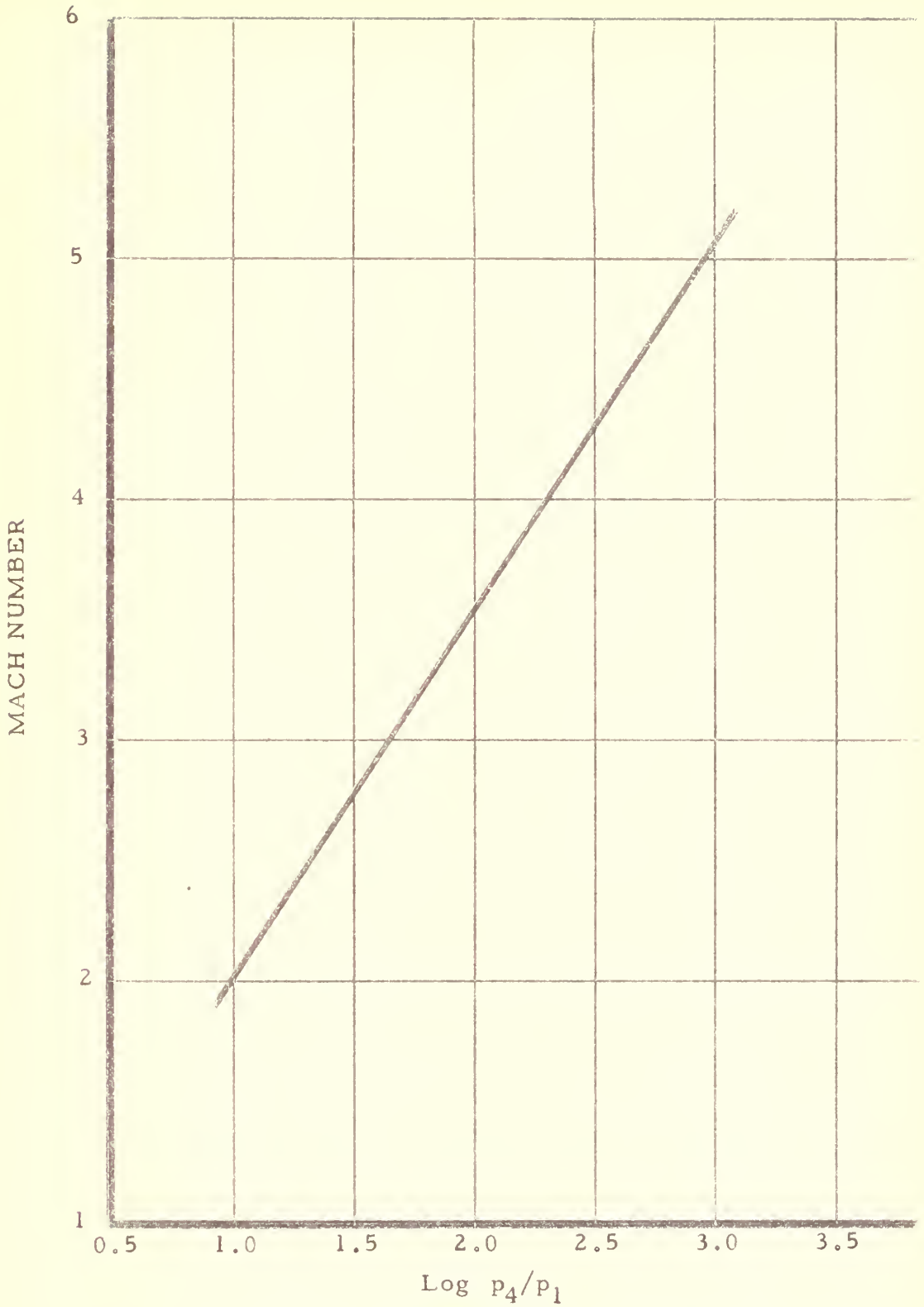


Fig. 2. Incident shock Mach number vs. log $p_4/p_1$ for acetylene; $\gamma$ = equilibrium value.

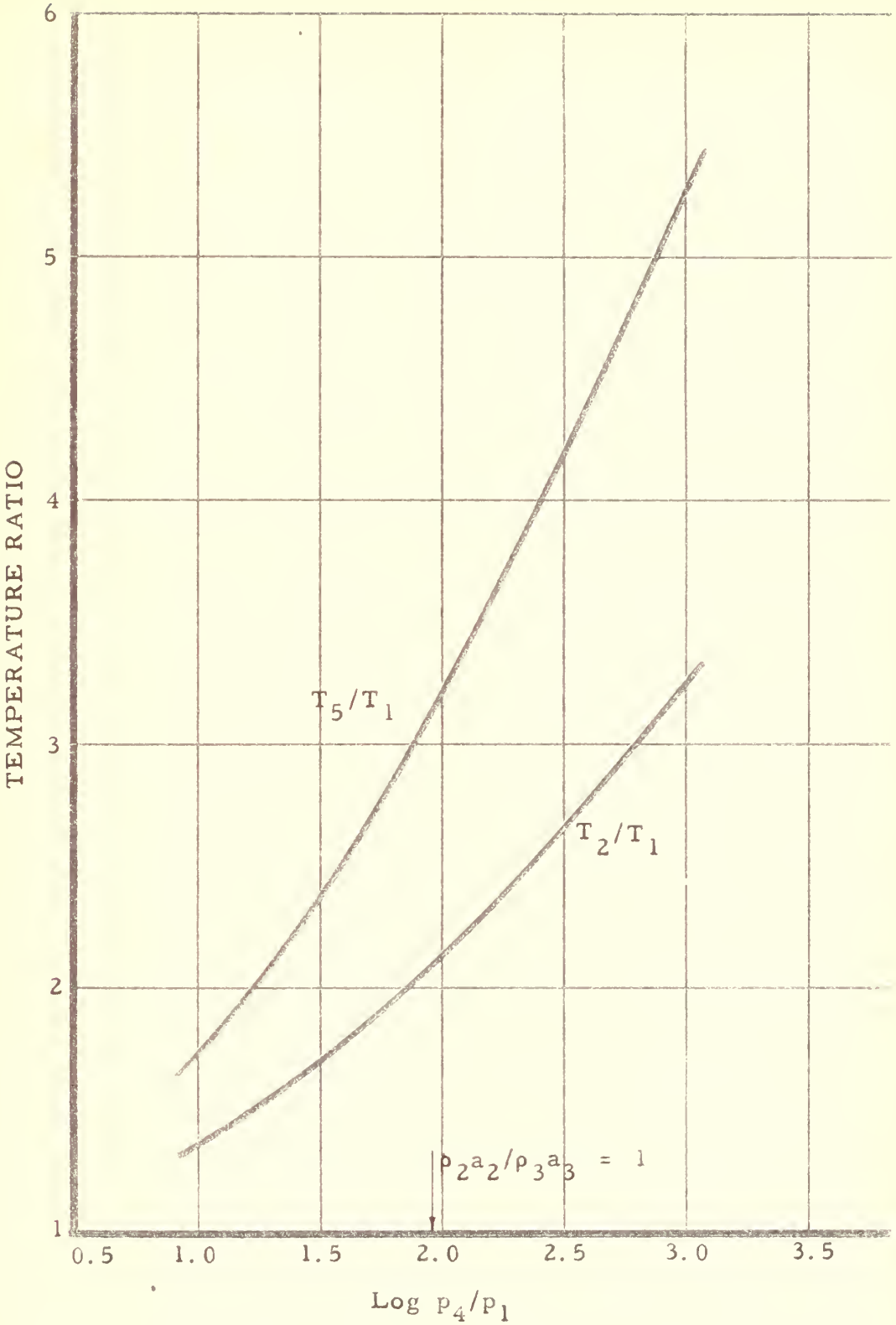


Fig. 3. Temperature ratios $T_2/T_1$ and $T_5/T_1$ vs. log $p_4/p_1$ for acetylene; $\gamma$ = equilibrium value.

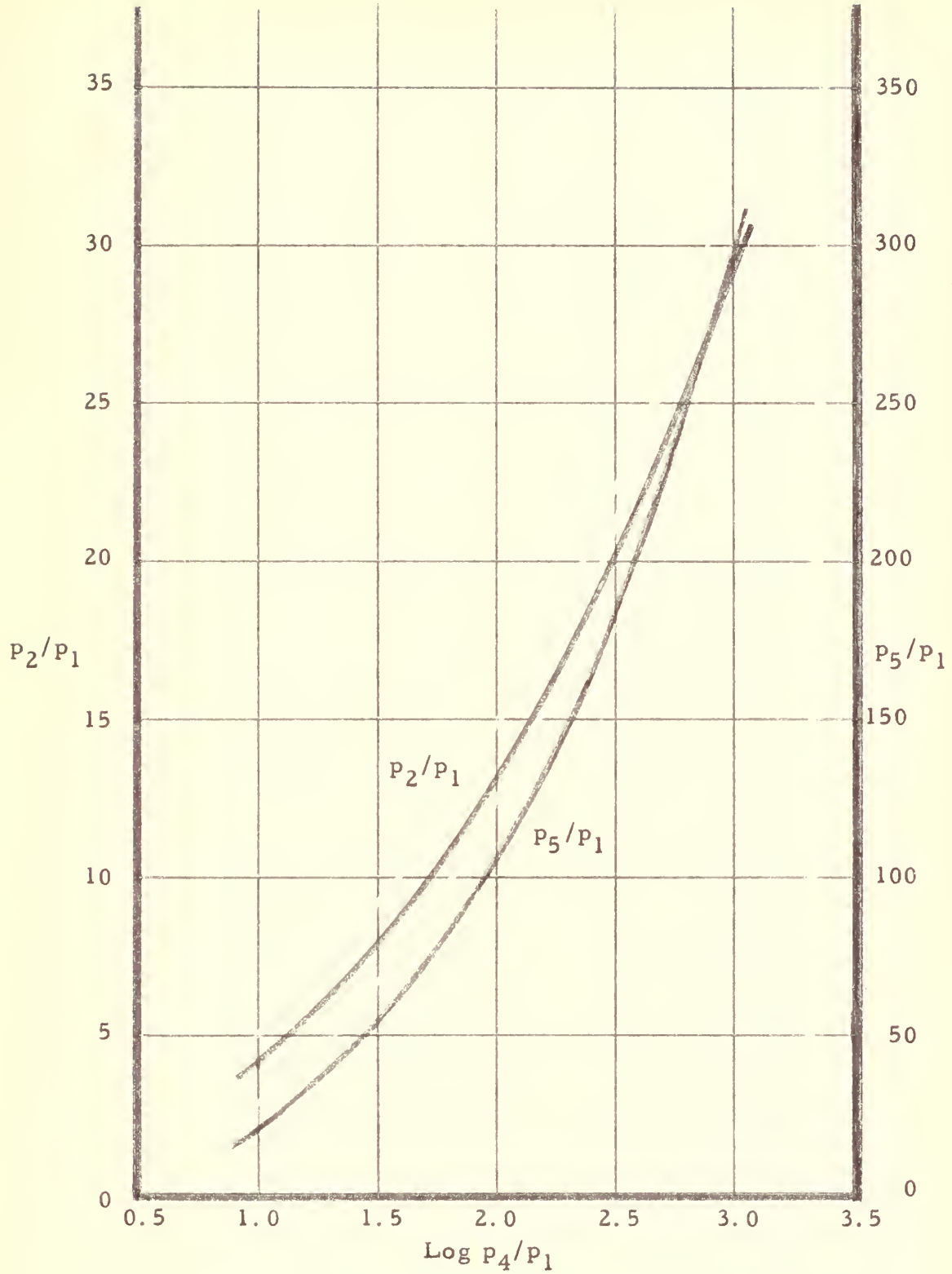


Fig. 4. Pressure ratios $p_2/p_1$ and $p_5/p_1$ vs. log $p_4/p_1$ for acetylene; $\gamma$ = equilibrium value.

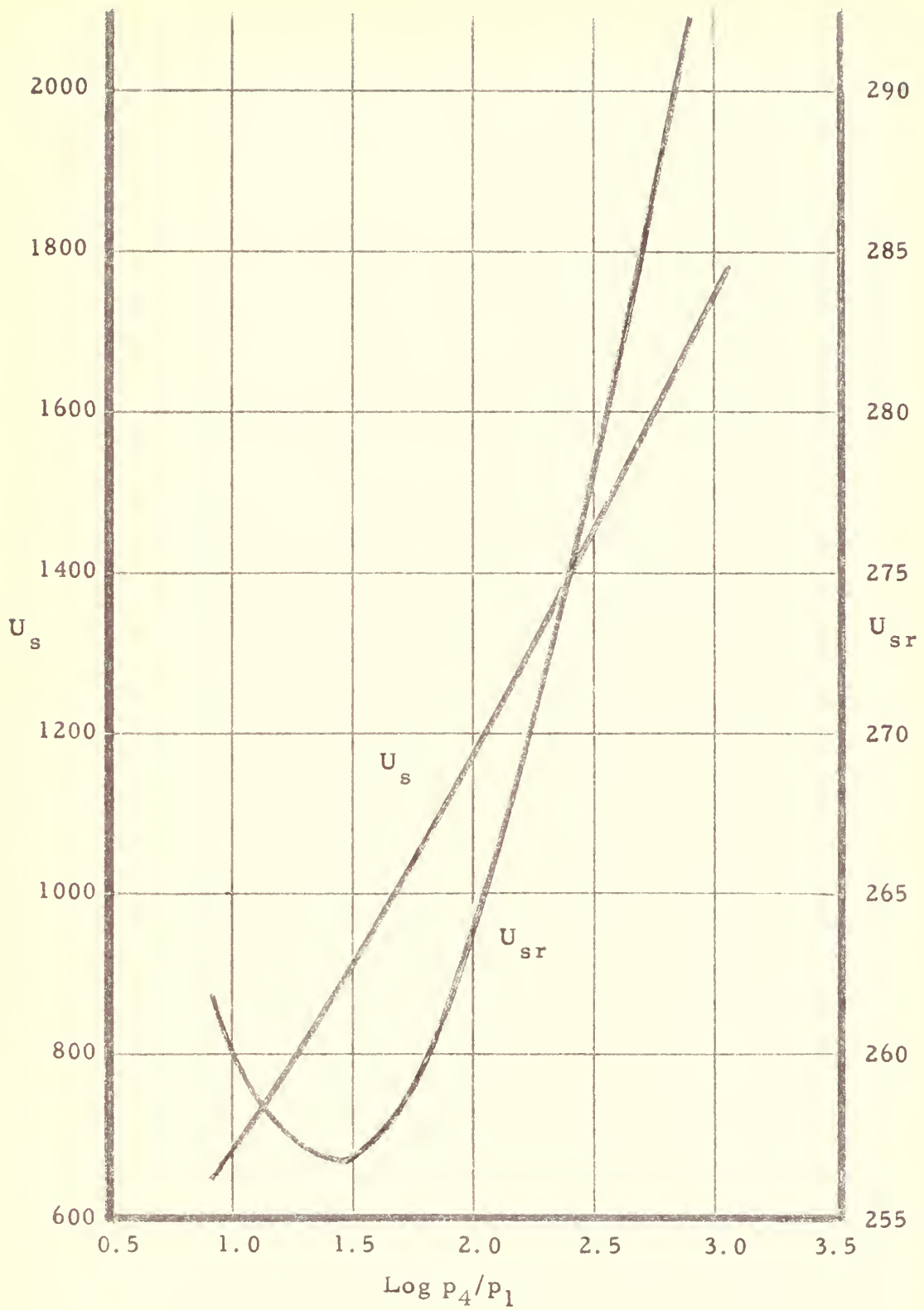


Fig. 5. Incident and reflected shock velocities vs. log $p_4/p_1$ for acetylene; $\gamma$ = equilibrium value.

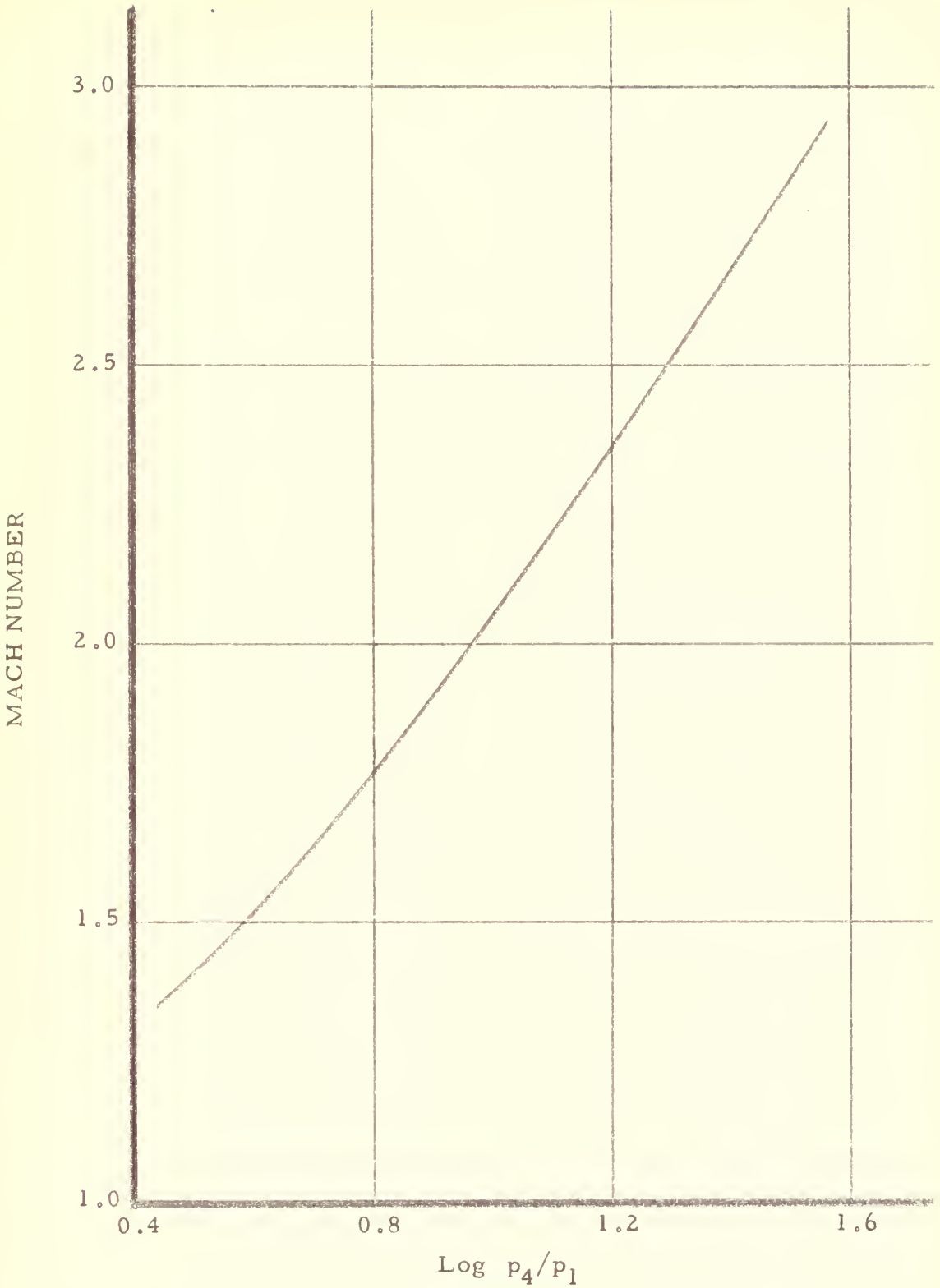


Fig. 6. Incident shock Mach number vs. log $p_4/p_1$ for a mixture of 95 °/o argon and 5 °/o acetylene; $\gamma$ = equilibrium value.

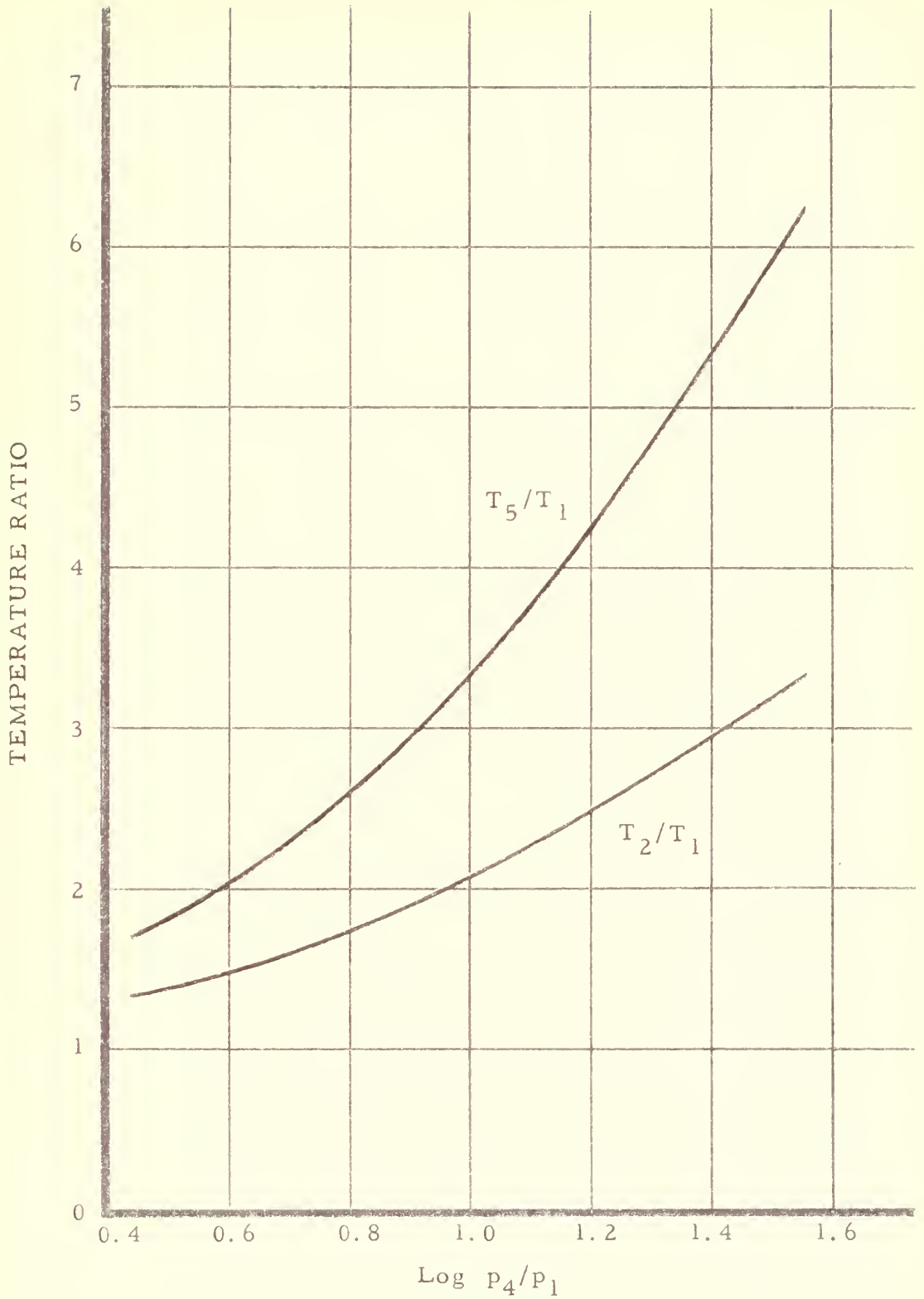


Fig. 7. Temperature ratios $T_2/T_1$ and $T_5/T_1$ vs. log $p_4/p_1$ for a mixture of 95 °/o argon and 5 °/o acetylene; $\gamma$ = equilibrium value; $\rho_2 a_2/\rho_3 a_3 = 1$ at log $p_4/p_1 = 1.973$.

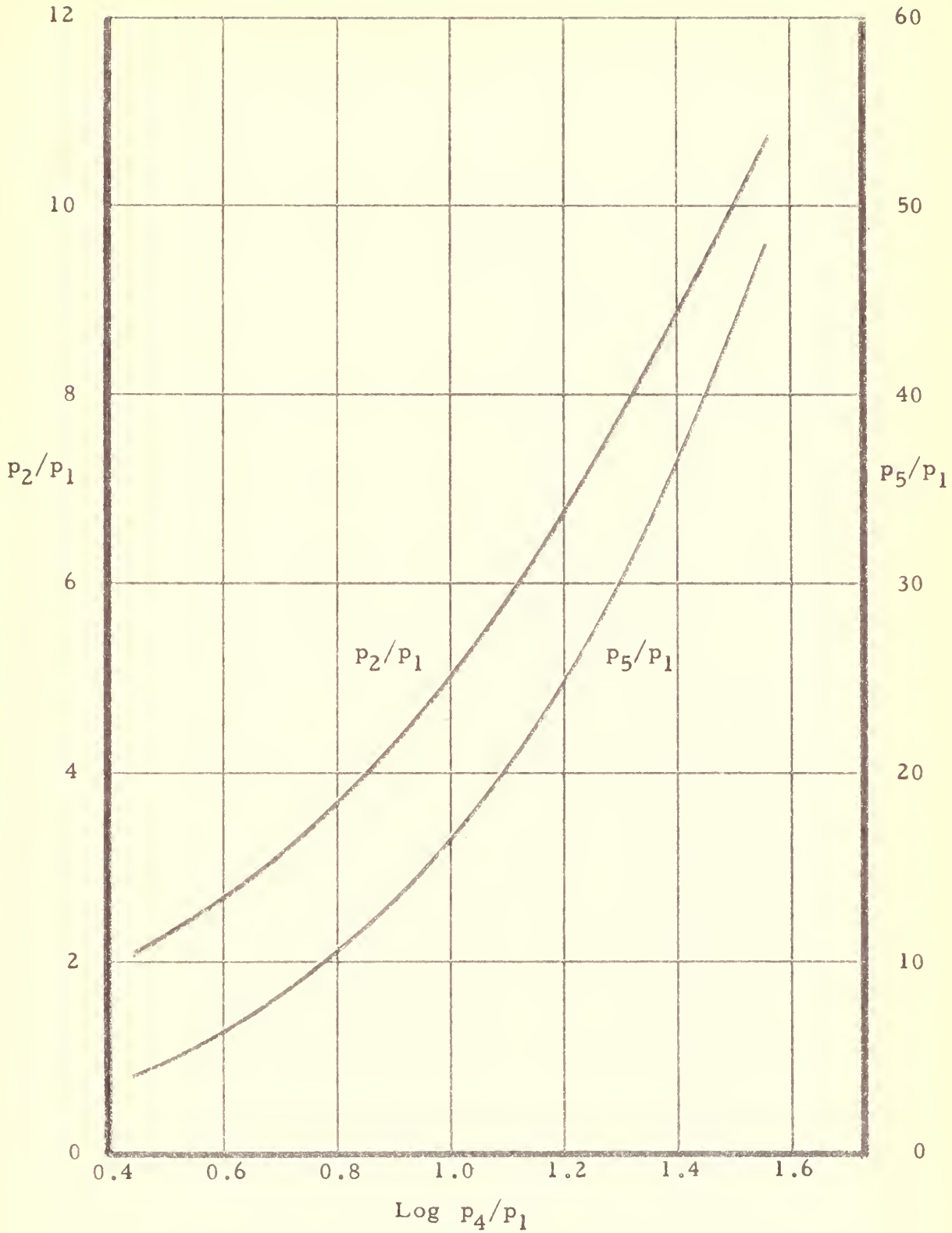


Fig. 8. Pressure ratios $p_2/p_1$ and $p_5/p_1$ vs. log $p_4/p_1$ for a mixture of 95 %/o argon and 5 %/o acetyene; $\gamma$ = equilibrium value.

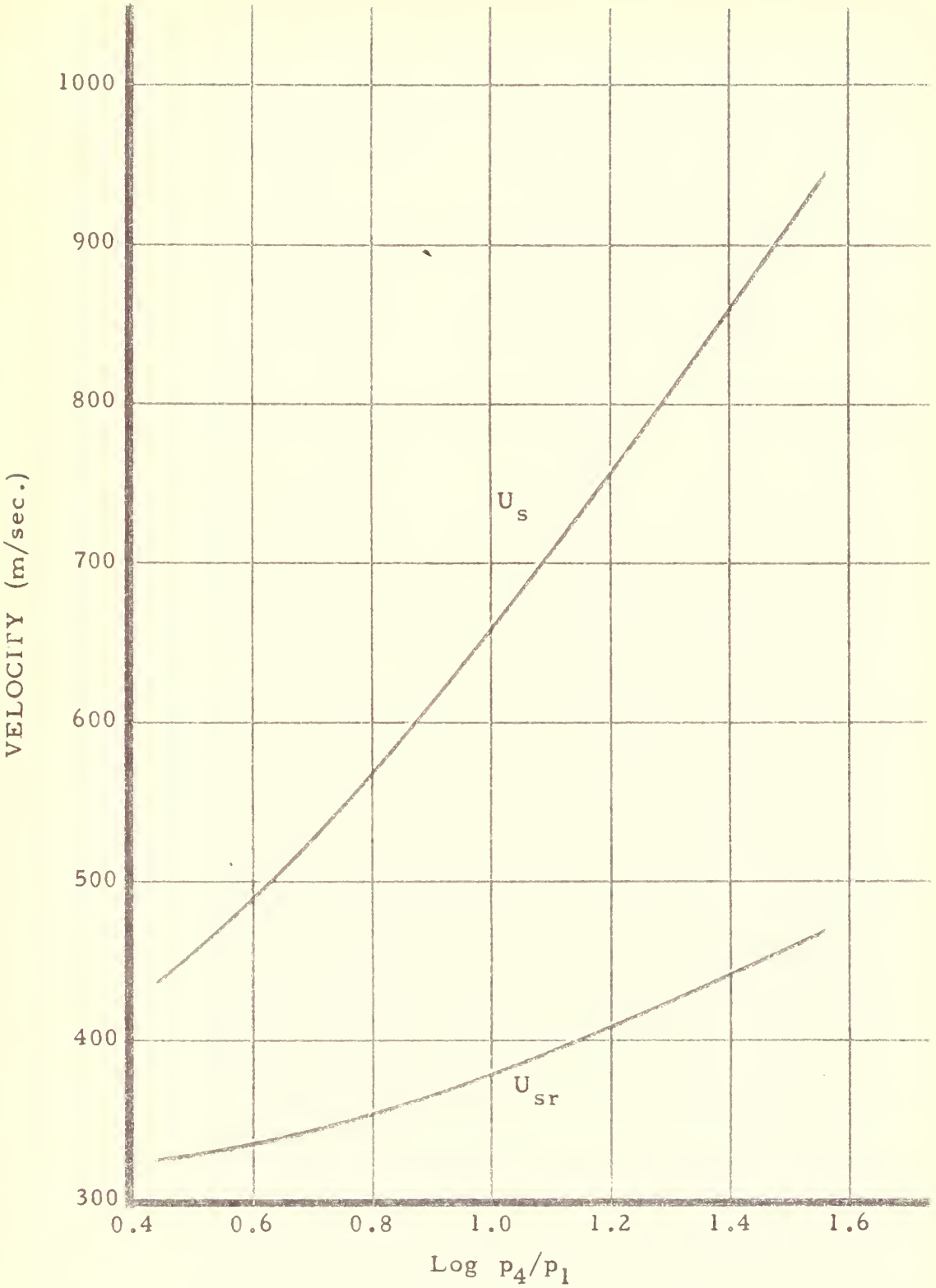


Fig. 9. Incident and reflected shock velocities vs. log $p_4/p_1$ for a mixture of 95 °/o argon and 5 °/o acetylene; $\gamma$ = equilibrium value.

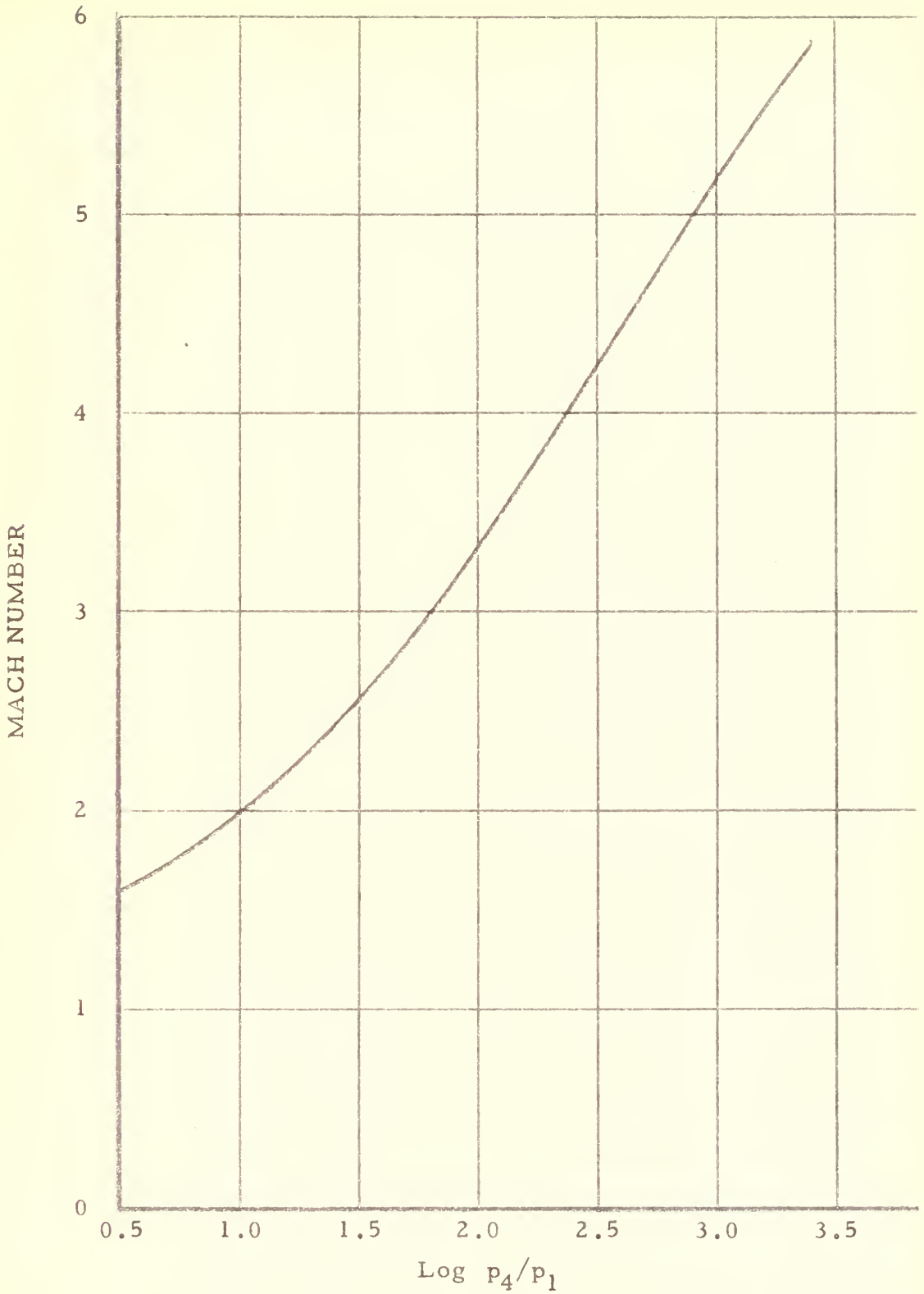


Fig. 10. Incident shock Mach number vs. log $p_4/p_1$ for acetylene; $\gamma = 7/5$.

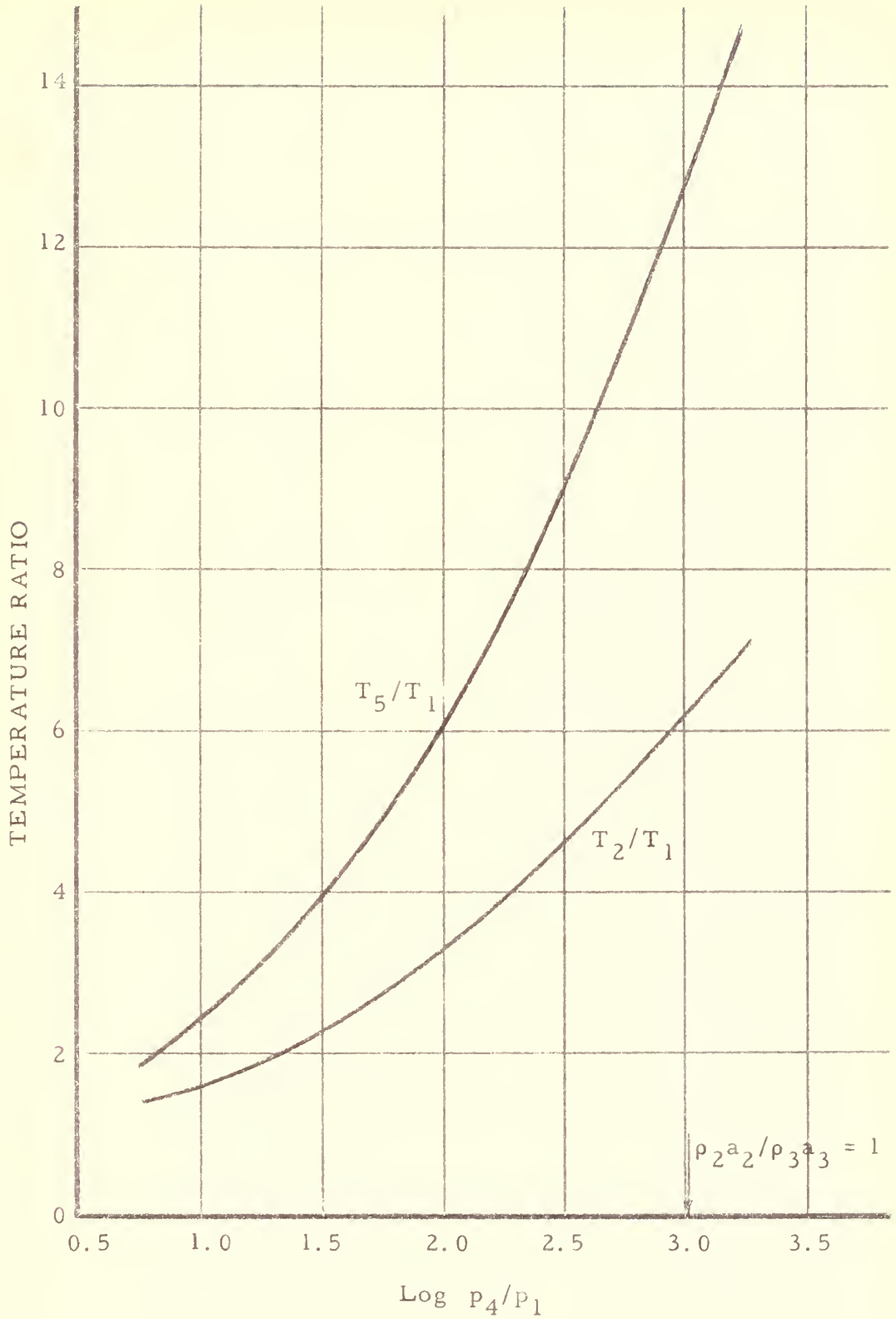


Fig. 11. Temperature ratios $T_2/T_1$ and $T_5/T_1$ vs. log $p_4/p_1$ for acetylene; $\gamma = 7/5$.

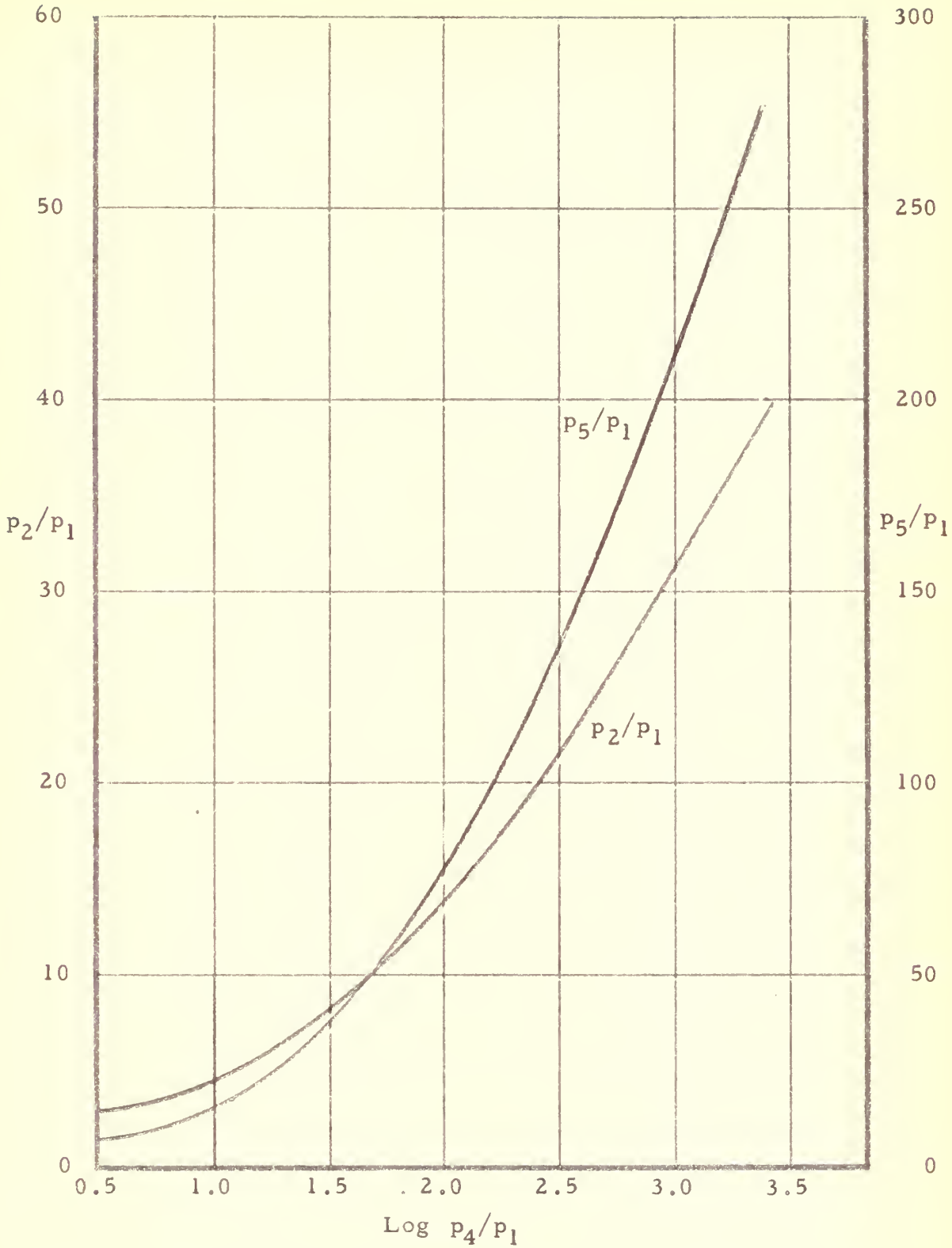


Fig. 12. Pressure ratios $p_2/p_1$ and $p_5/p_1$ vs. log $p_4/p_1$ for acetylene; $\gamma = 7/5$.

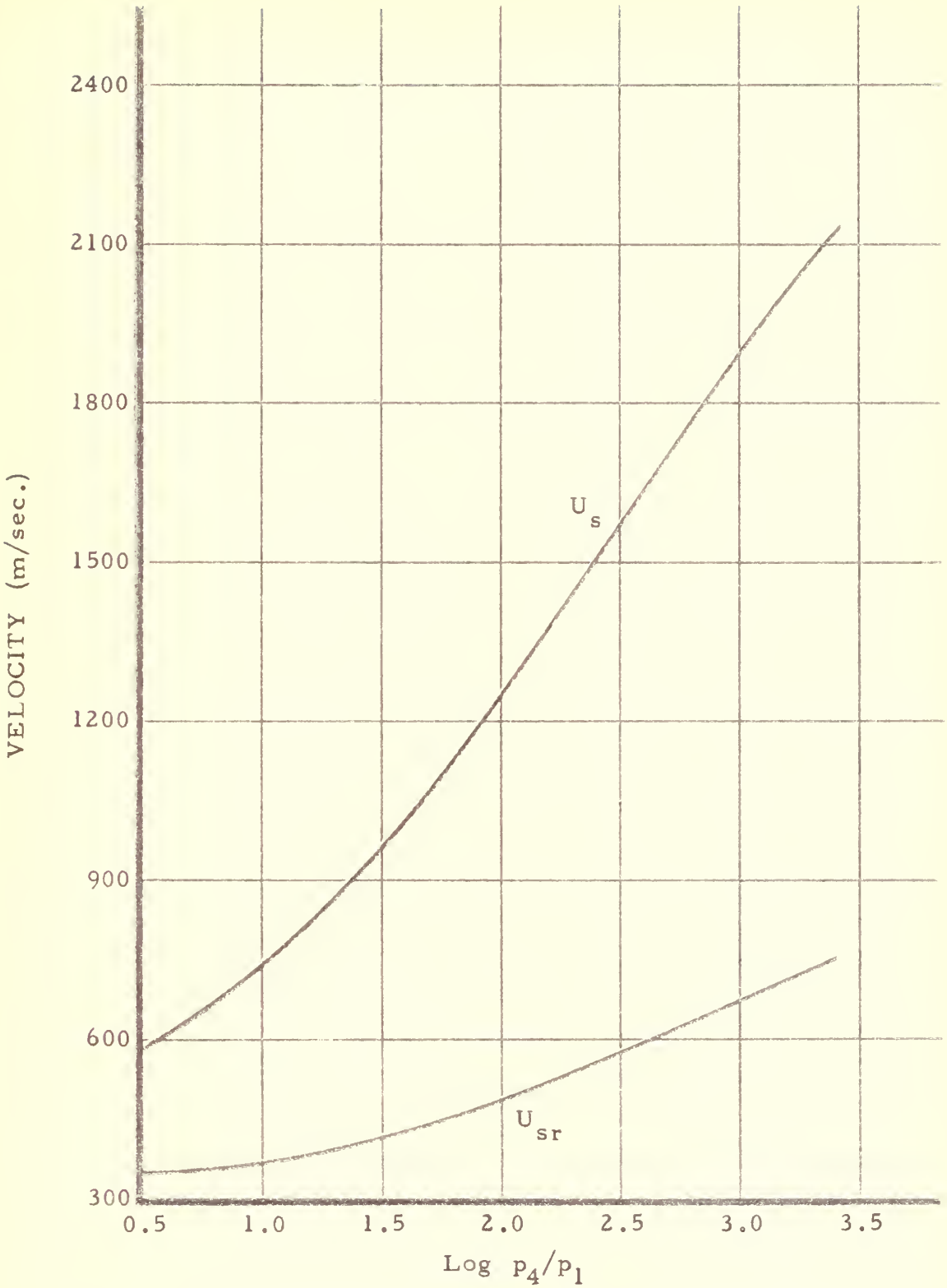


Fig. 13. Incident and reflected shock velocities vs. log $p_4/p_1$ for acetylene; $\gamma = 7/5$.

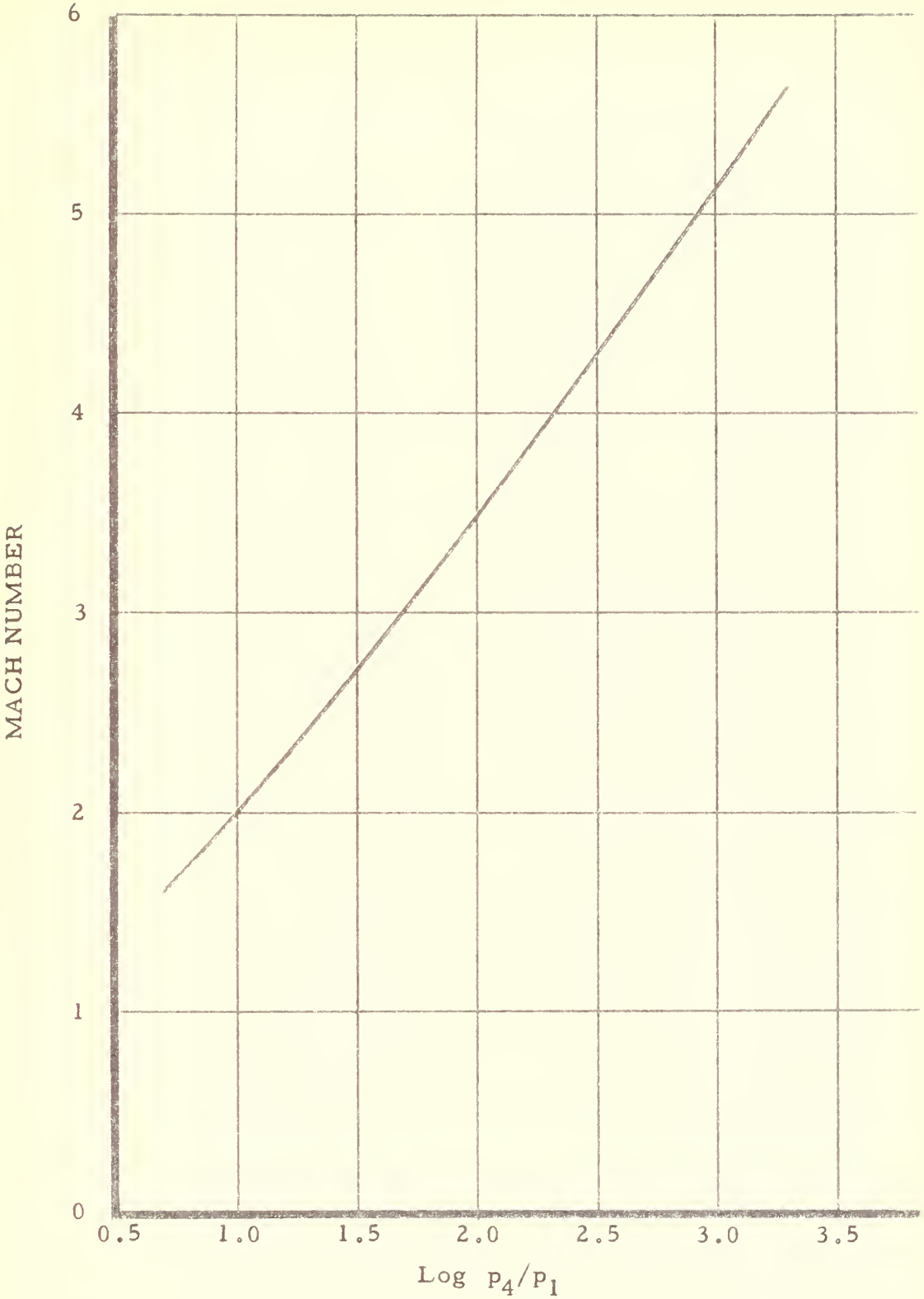


Fig. 14. Incident shock Mach number vs. log $p_4/p_1$ for acetylene; $\gamma = 5/3$.

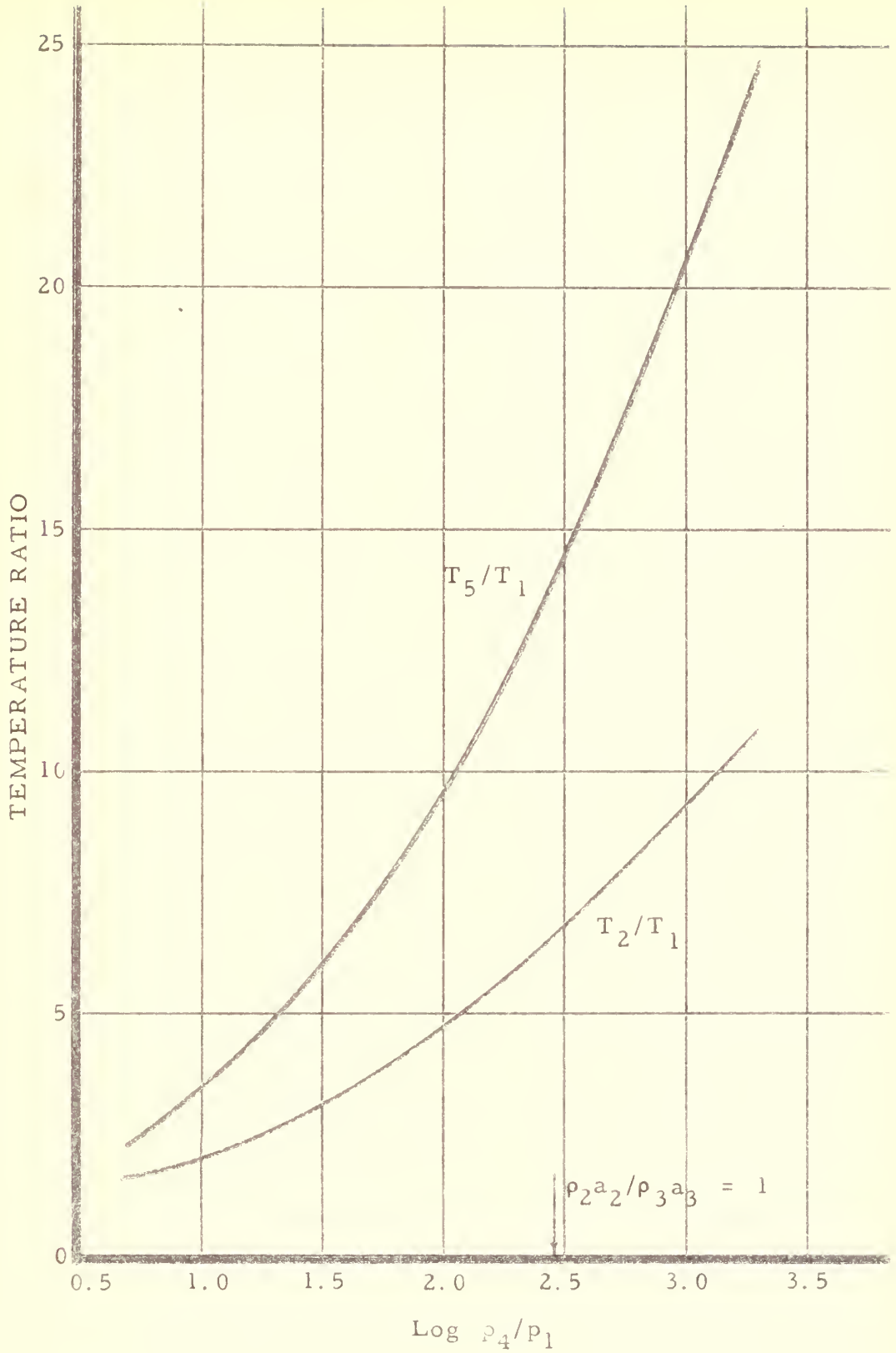


Fig. 15. Temperature ratios $T_2/T_1$ and $T_5/T_1$ vs. log $p_4/p_1$ for acetylene; $\gamma = 5/3$.

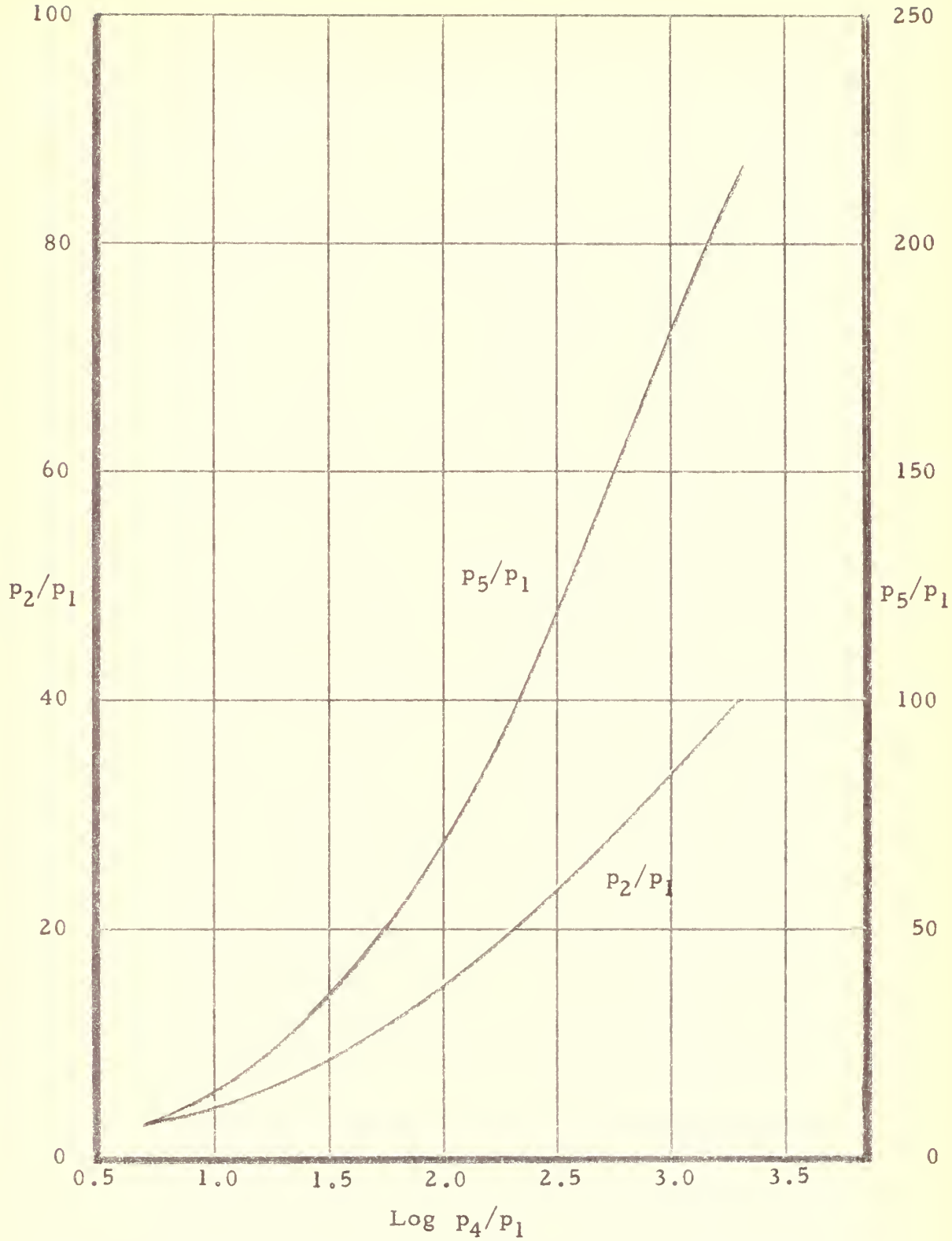


Fig. 16. Pressure ratios $p_2/p_1$ and $p_5/p_1$ vs. log $p_4/p_1$ for acetylene; $\gamma = 5/3$.

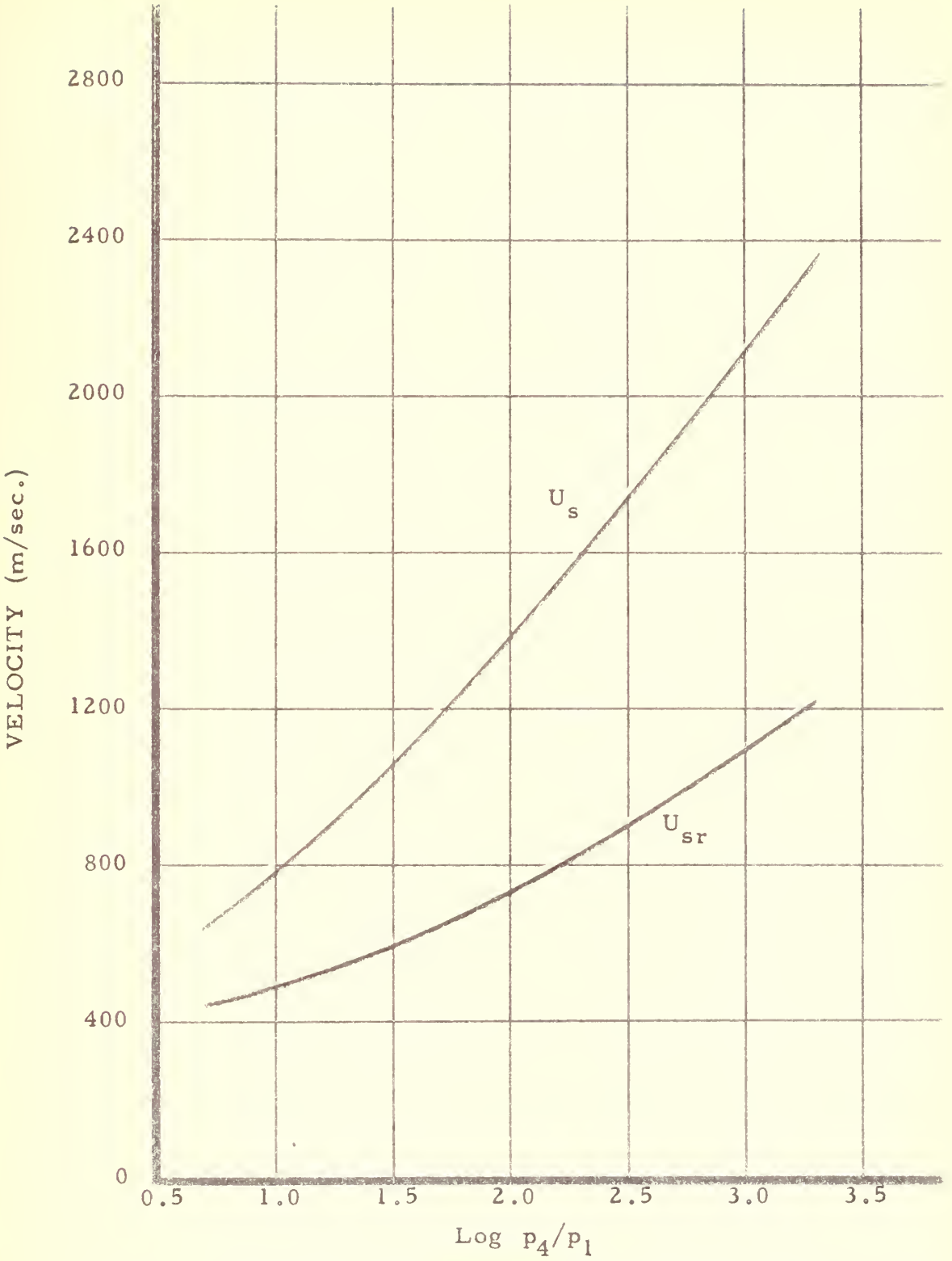


Fig. 17. Incident and reflected shock velocities vs. log $p_4/p_1$ for acetylene; $\gamma = 5/3$.

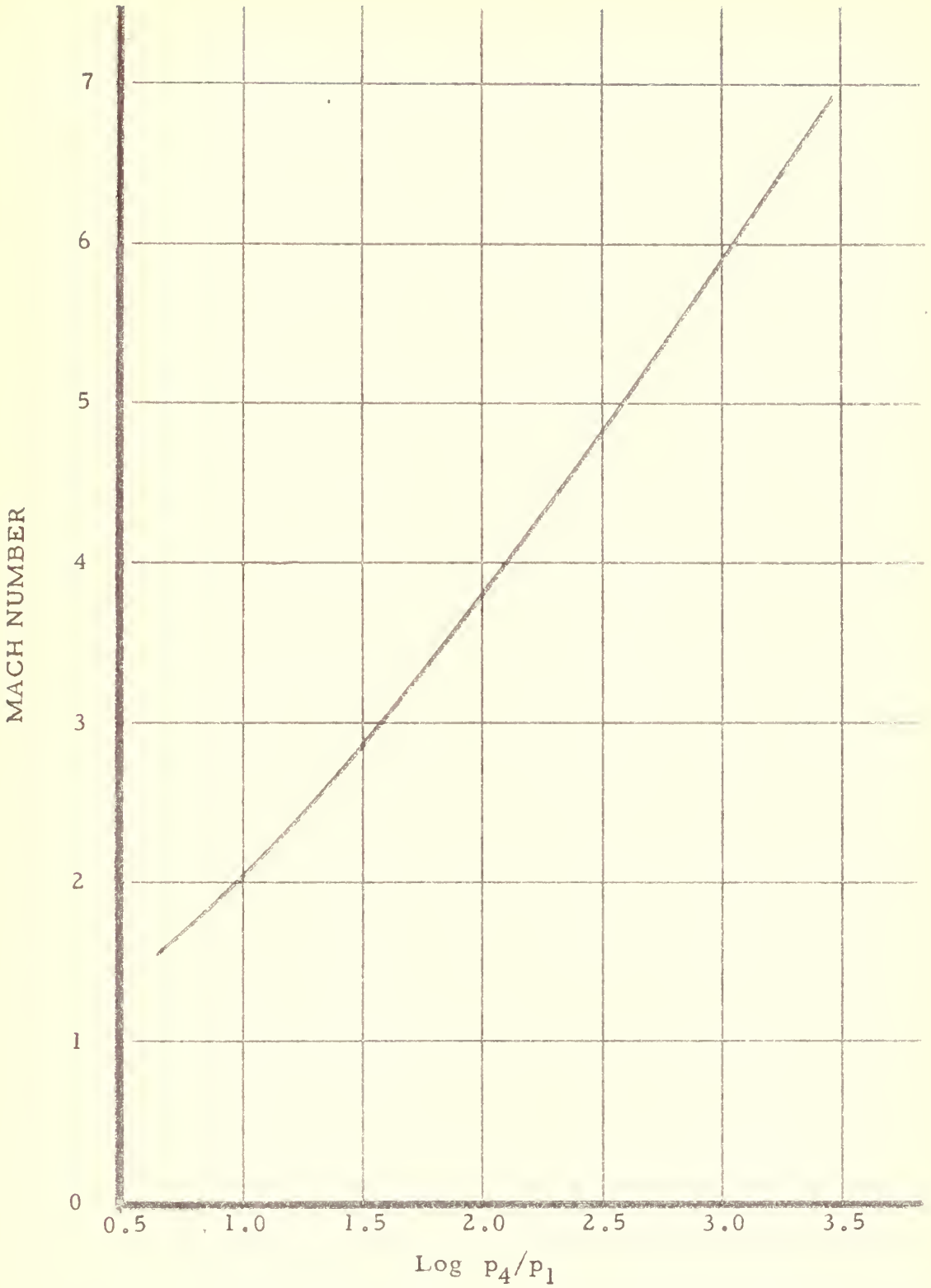


Fig. 18. Incident shock Mach number vs. log $p_4/p_1$ for a mixture of 95 °/o argon and 5 °/o acetylene; $\gamma = 5/3$.

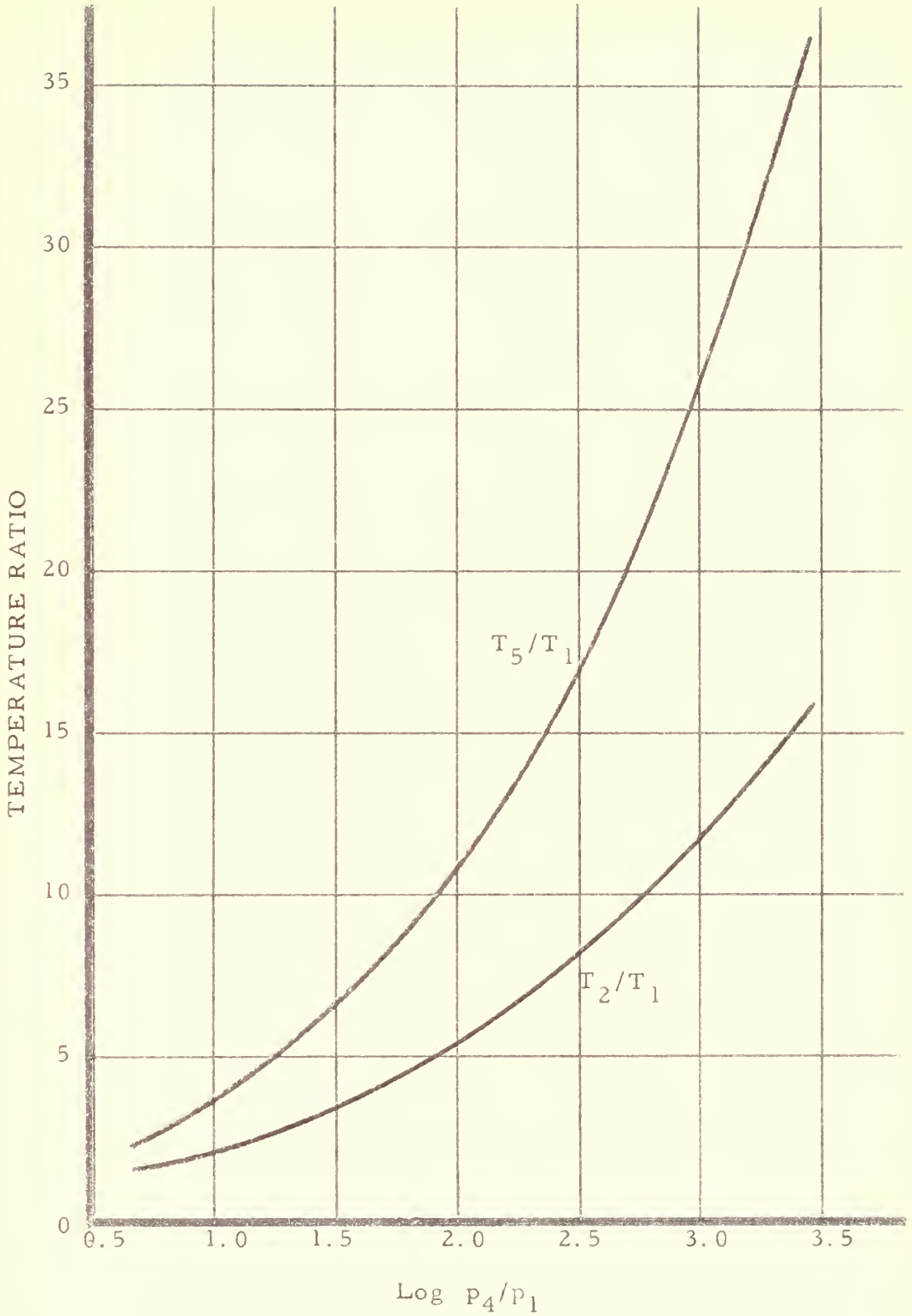


Fig. 19. Temperature ratios $T_2/T_1$ and $T_5/T_1$ vs. log $p_4/p_1$ for a mixture of 95 °/o argon and 5 °/o acetylene; $\gamma = 5/3$; $\rho_2 a_2/\rho_3 a_3 = 1$ at log $p_4/p_1 > 3.5$ .

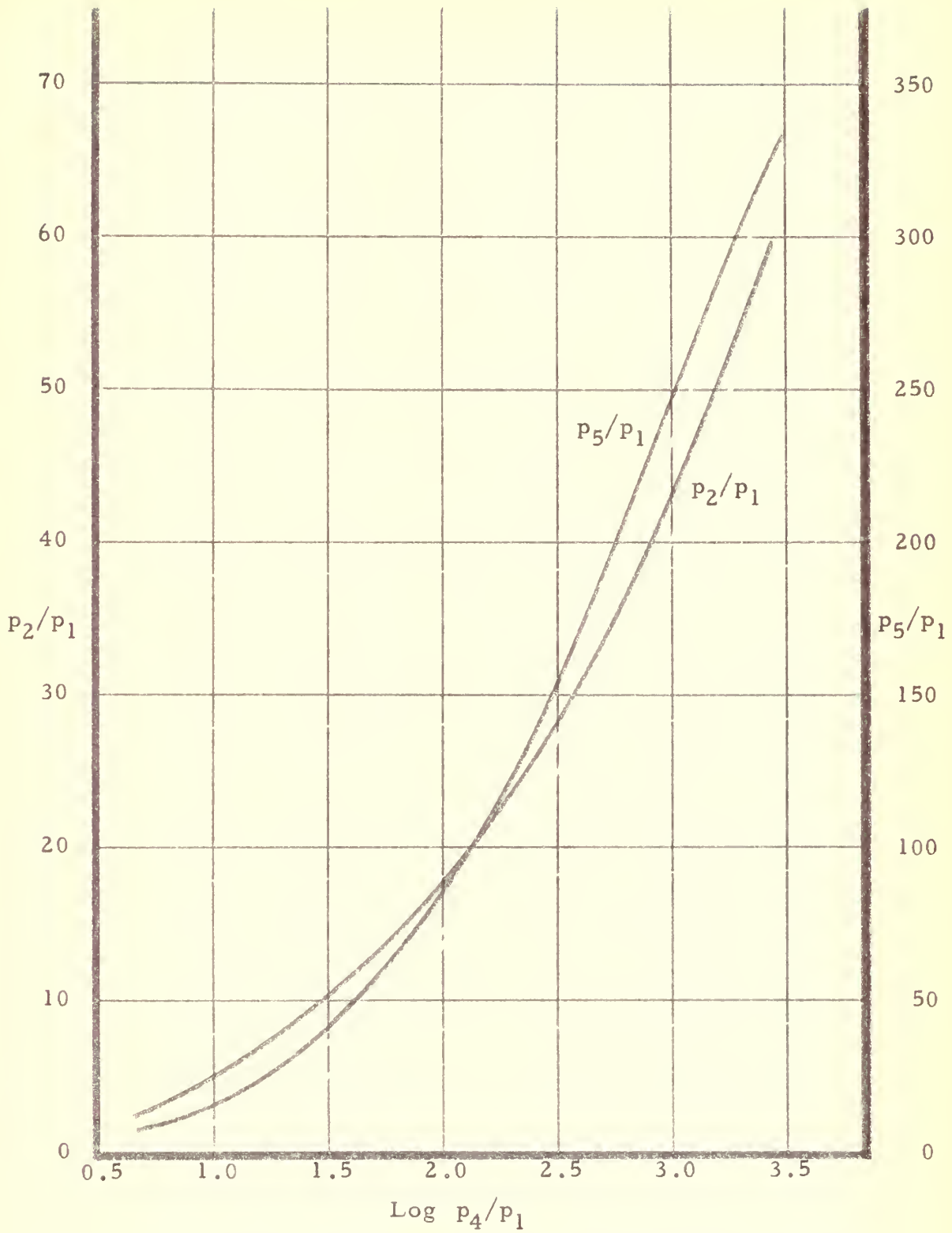


Fig. 20. Pressure ratios, $p_2/p_1$ and $p_5/p_1$ vs. log $p_4/p_1$ for a mixture of 95 °/o argon and 5 °/o acetylene; $\gamma = 5/3$.

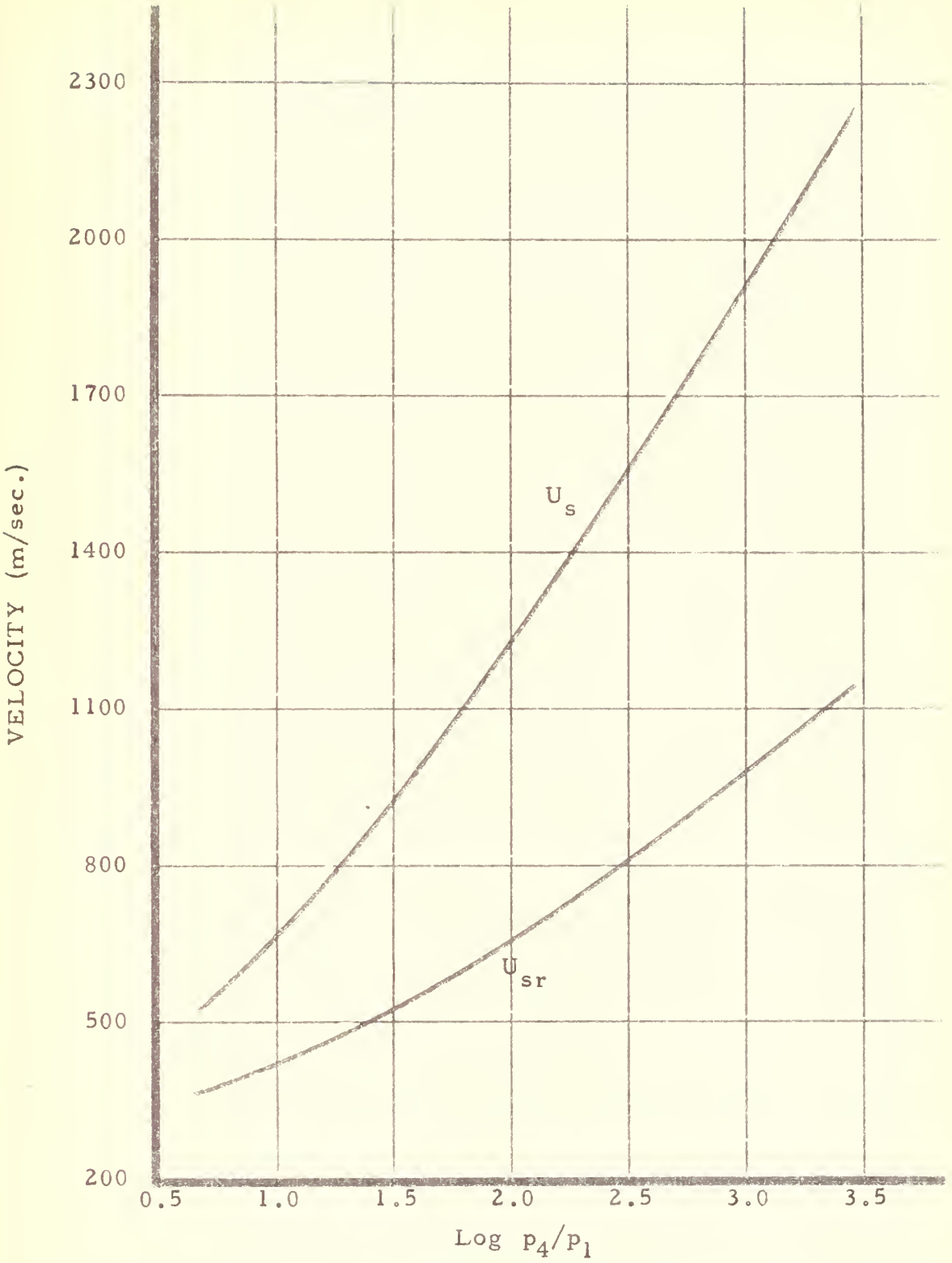


Fig. 21. Incident and reflected shock velocities vs. log $p_4/p_1$ for a mixture of 95 °/o argon and 5 °/o acetylene; $\gamma = 5/3$.

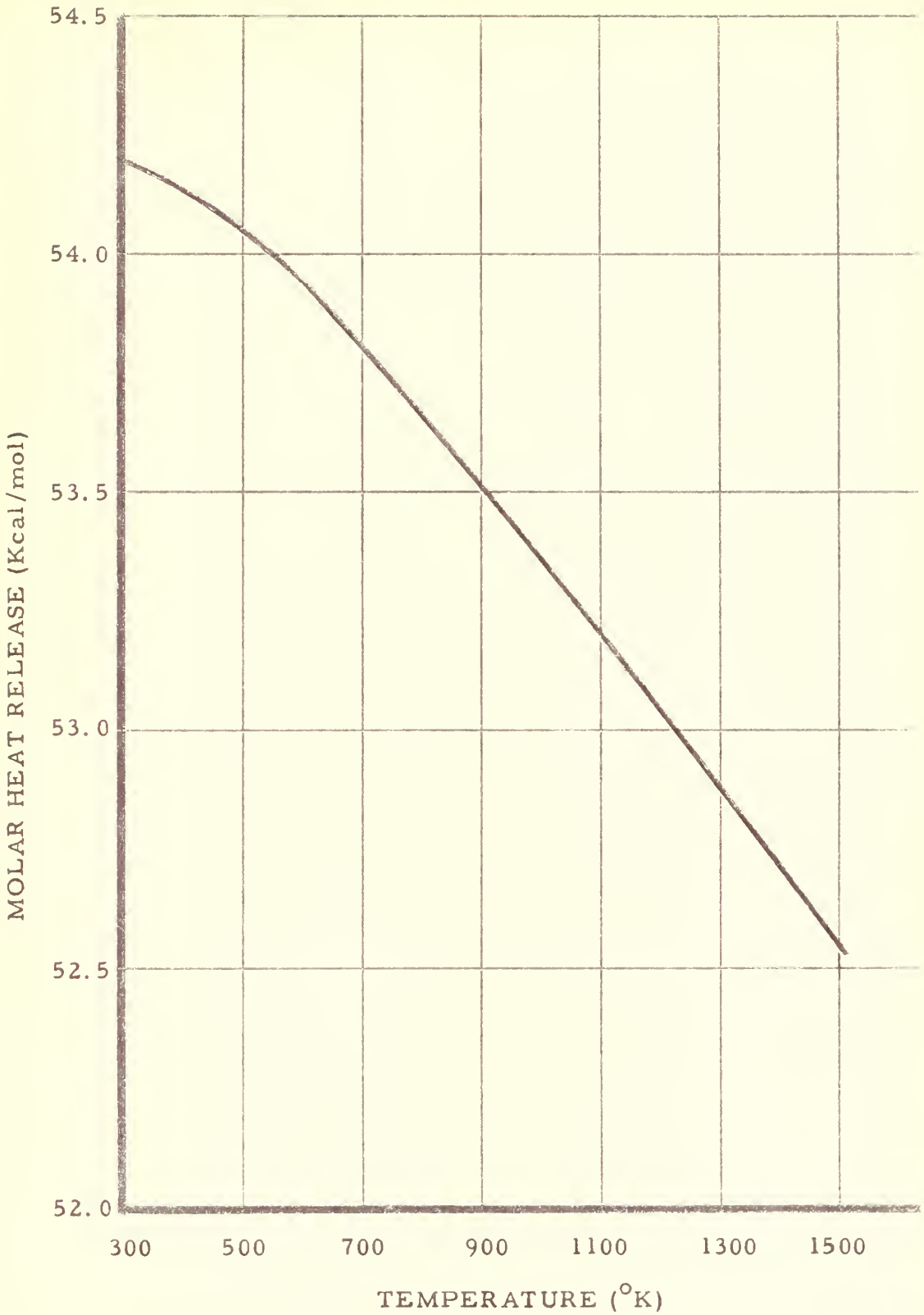


Fig. 22. Molar heat release (Q) vs. temperature for the decomposition of acetylene to solid carbon and hydrogen; $\gamma$ = equilibrium value.

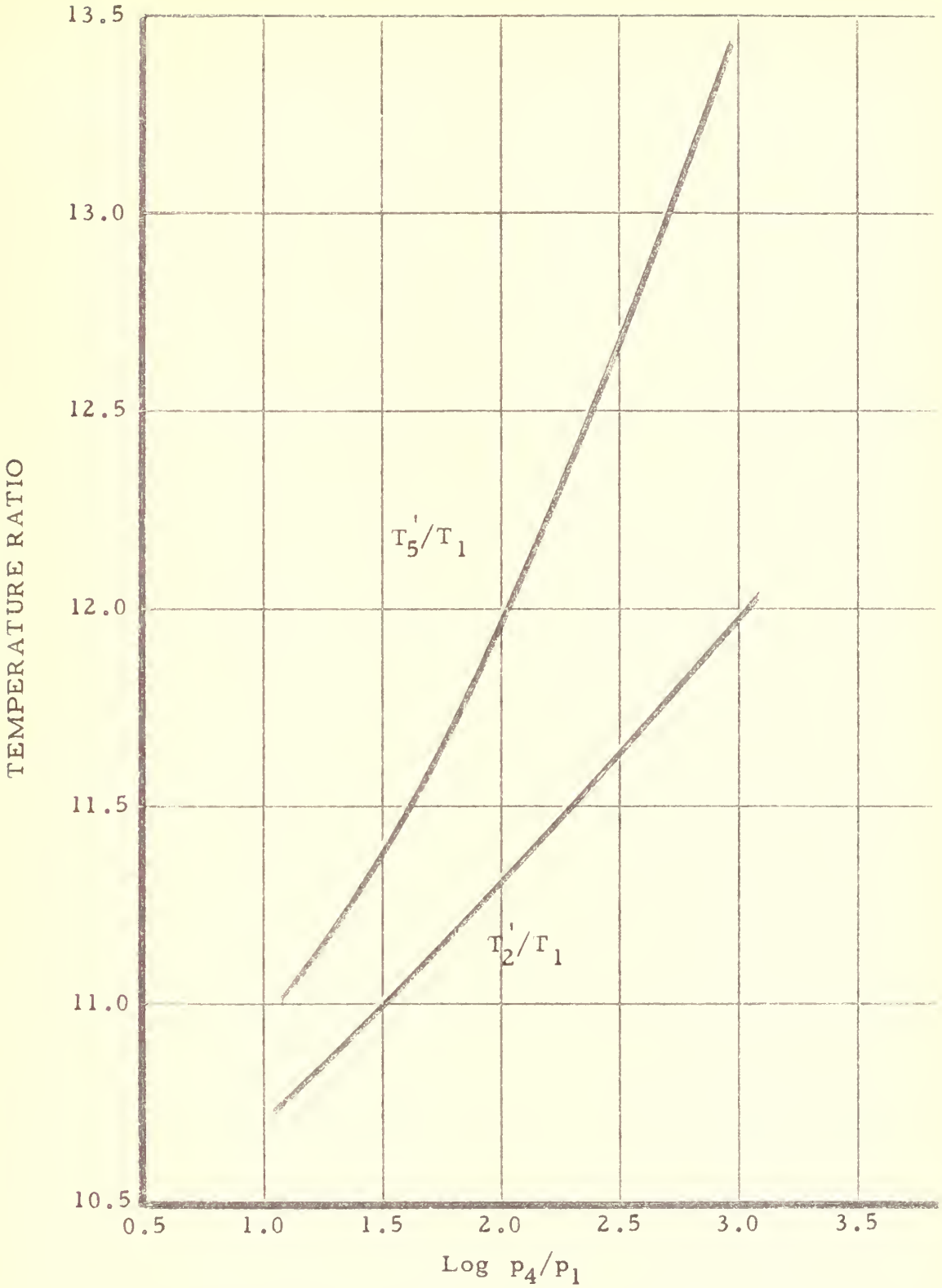


Fig. 23. Temperature ratios, $T_2'/T_1$ and $T_5'/T_1$ vs. log $p_4/p_1$ for acetylene; constant-pressure reaction; $\gamma$ = equilibrium value.

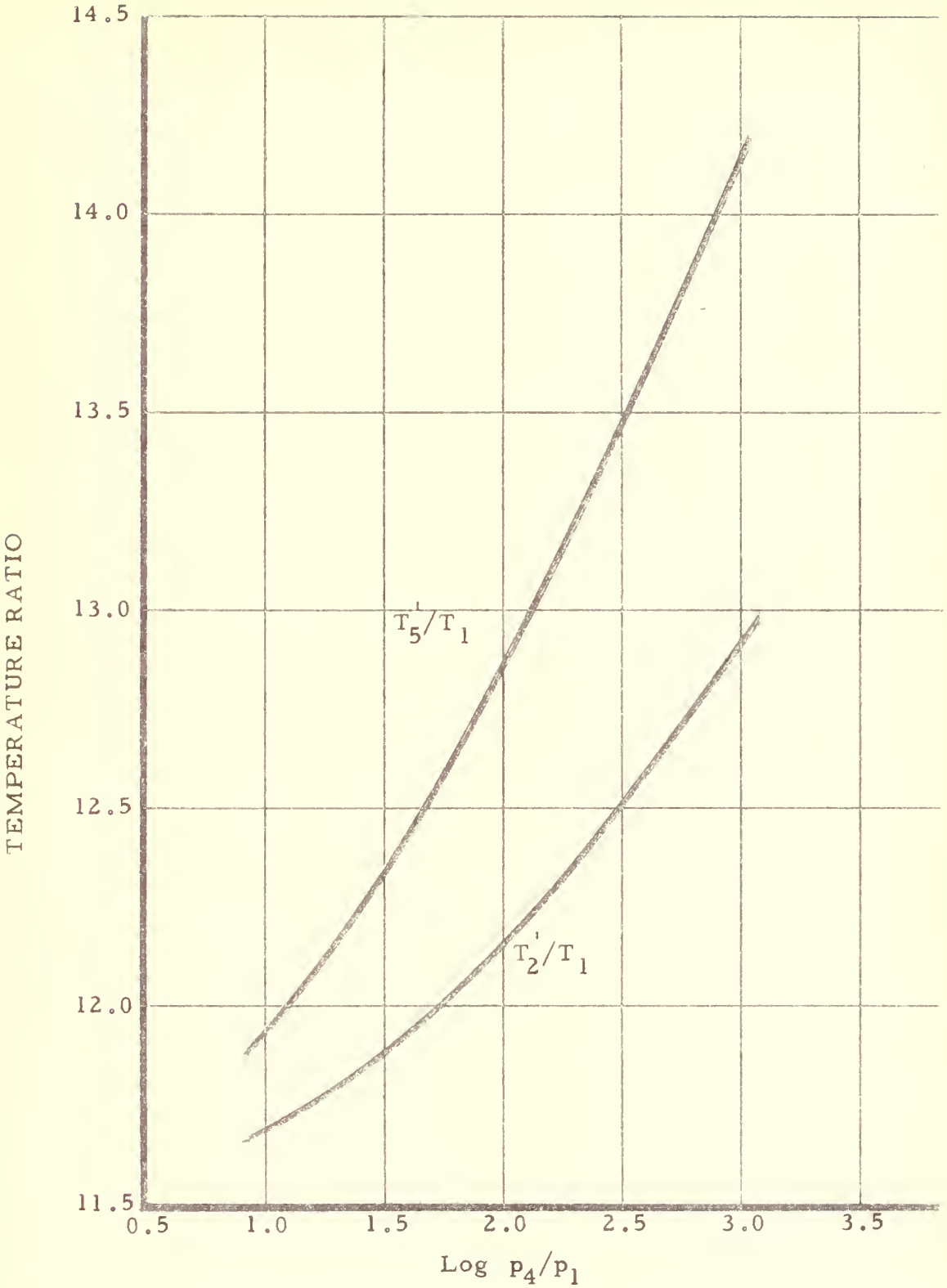


Fig. 24. Temperature ratios $T_2'/T_1$ and $T_5'/T_1$ vs. log $p_4/p_1$ for acetylene; constant-volume reaction; $\gamma$ = equilibrium value.

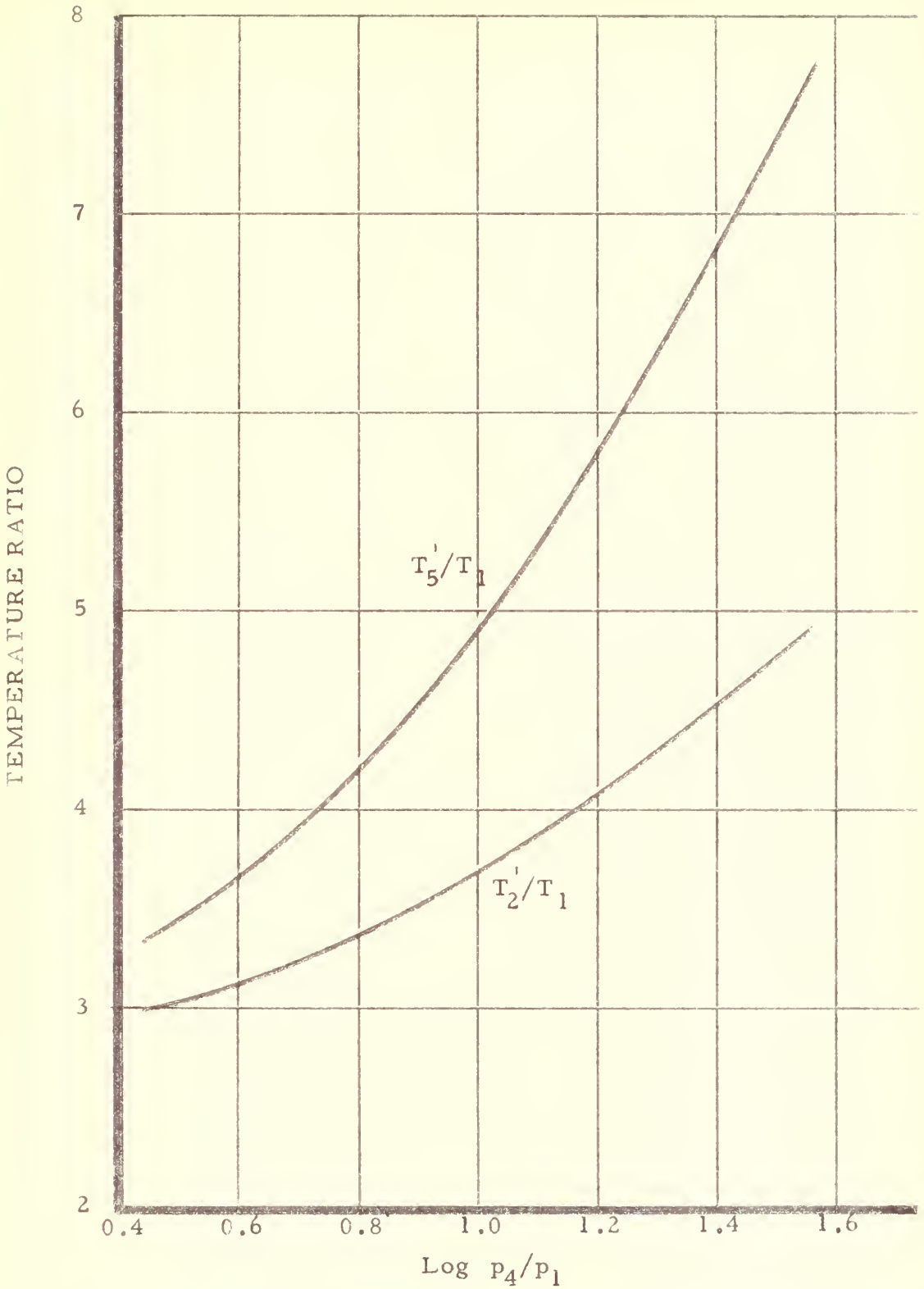


Fig. 25. Temperature ratios $T_2'/T_1$ and $T_5'/T_1$ vs. log $p_4/p_1$ for a mixture of 95 °/o argon and 5 °/o acetylene; constant-pressure reaction; $\gamma$ = equilibrium value.

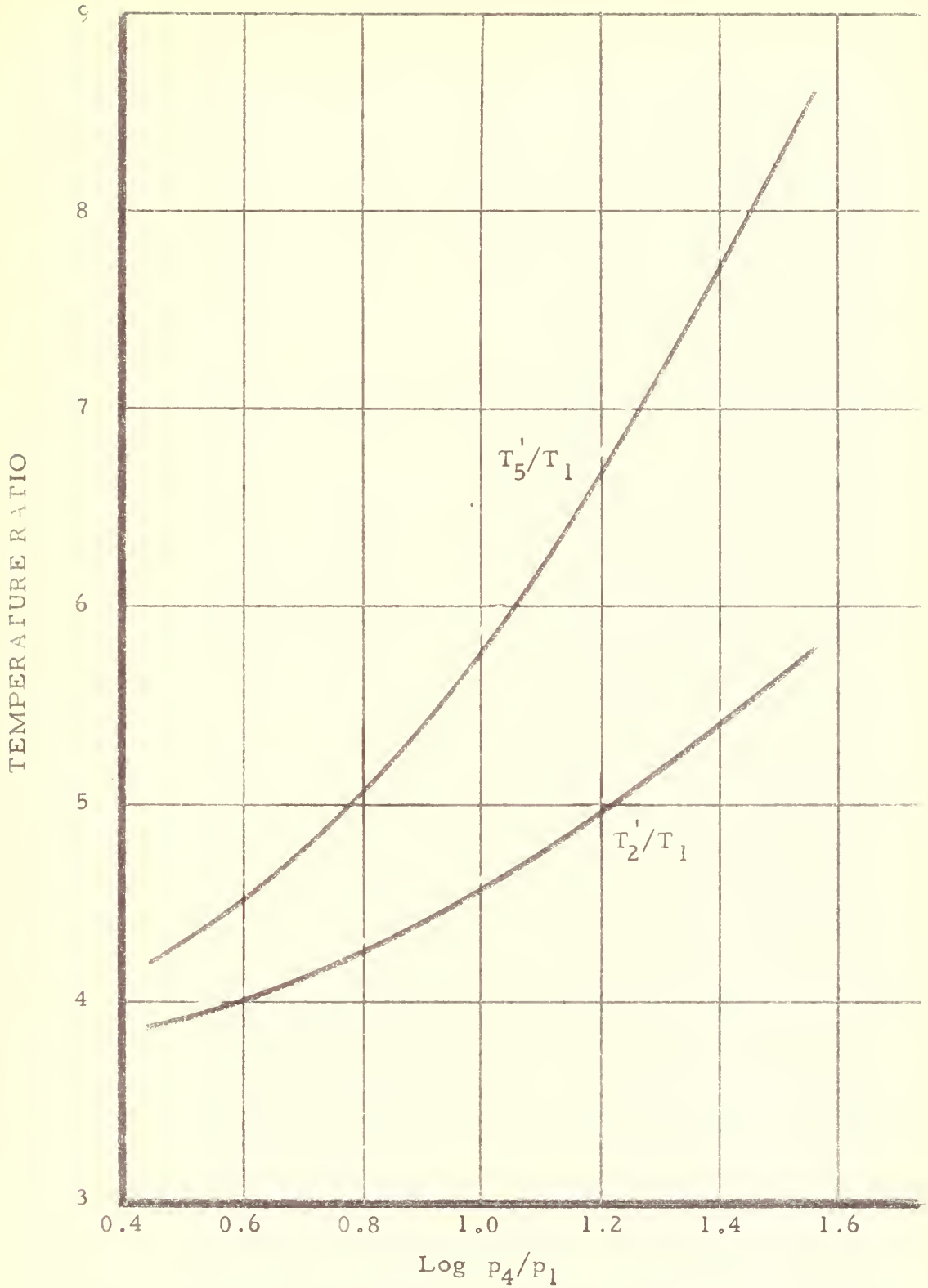


Fig. 26. Temperature ratios, $T_2'/T_1$ and $T_5'/T_1$ vs. log $p_4/p_1$ for a mixture of 95 °/o argon and 5 °/o acetylene; constant-volume reaction; $\gamma$ = equilibrium value.

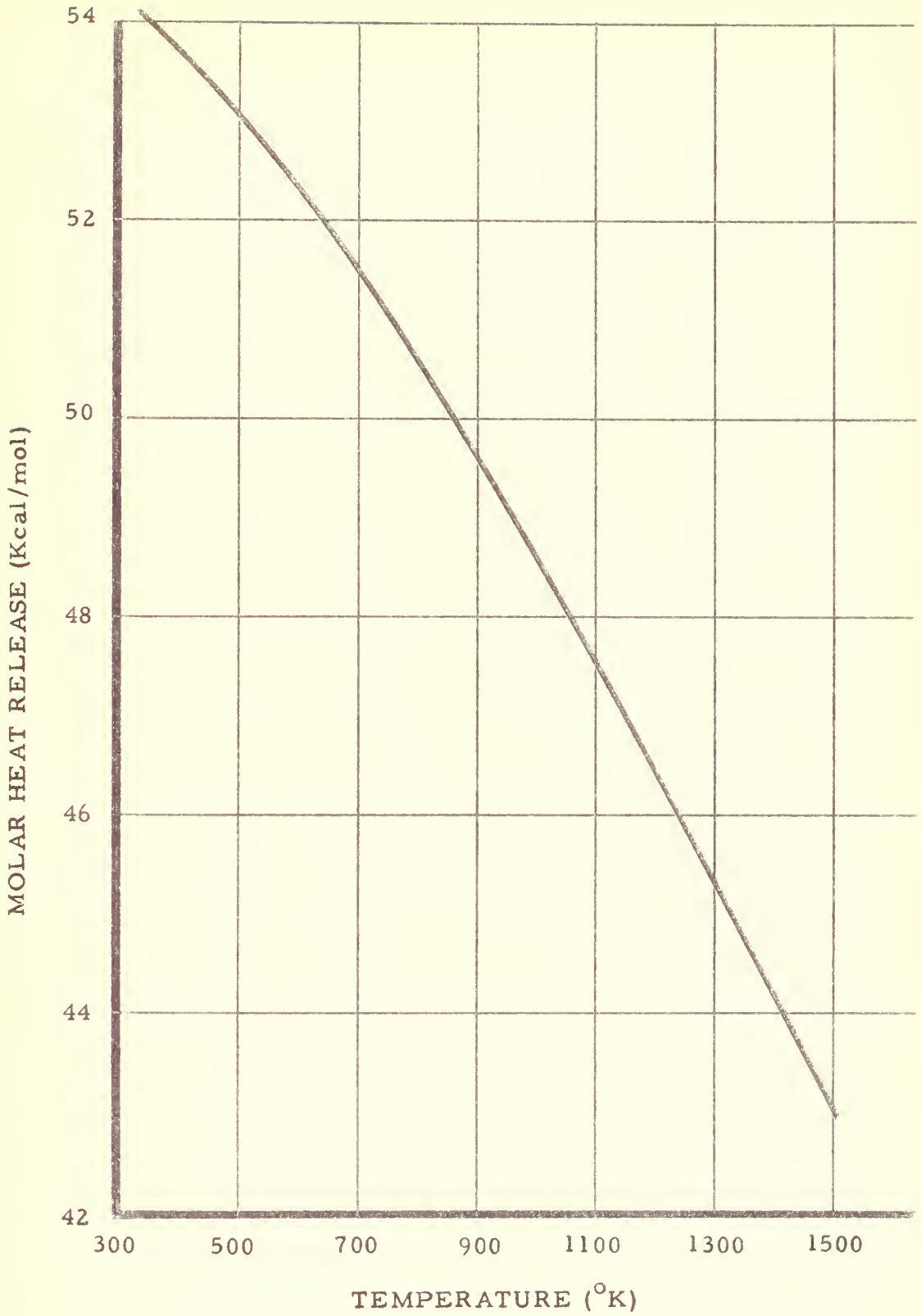


Fig. 27. Molar heat release (Q) vs. temperature for the decomposition of acetylene to solid carbon and hydrogen; $\gamma$ = 7/5 or 5/3 for $C_2H_2$ and $H_2$ .

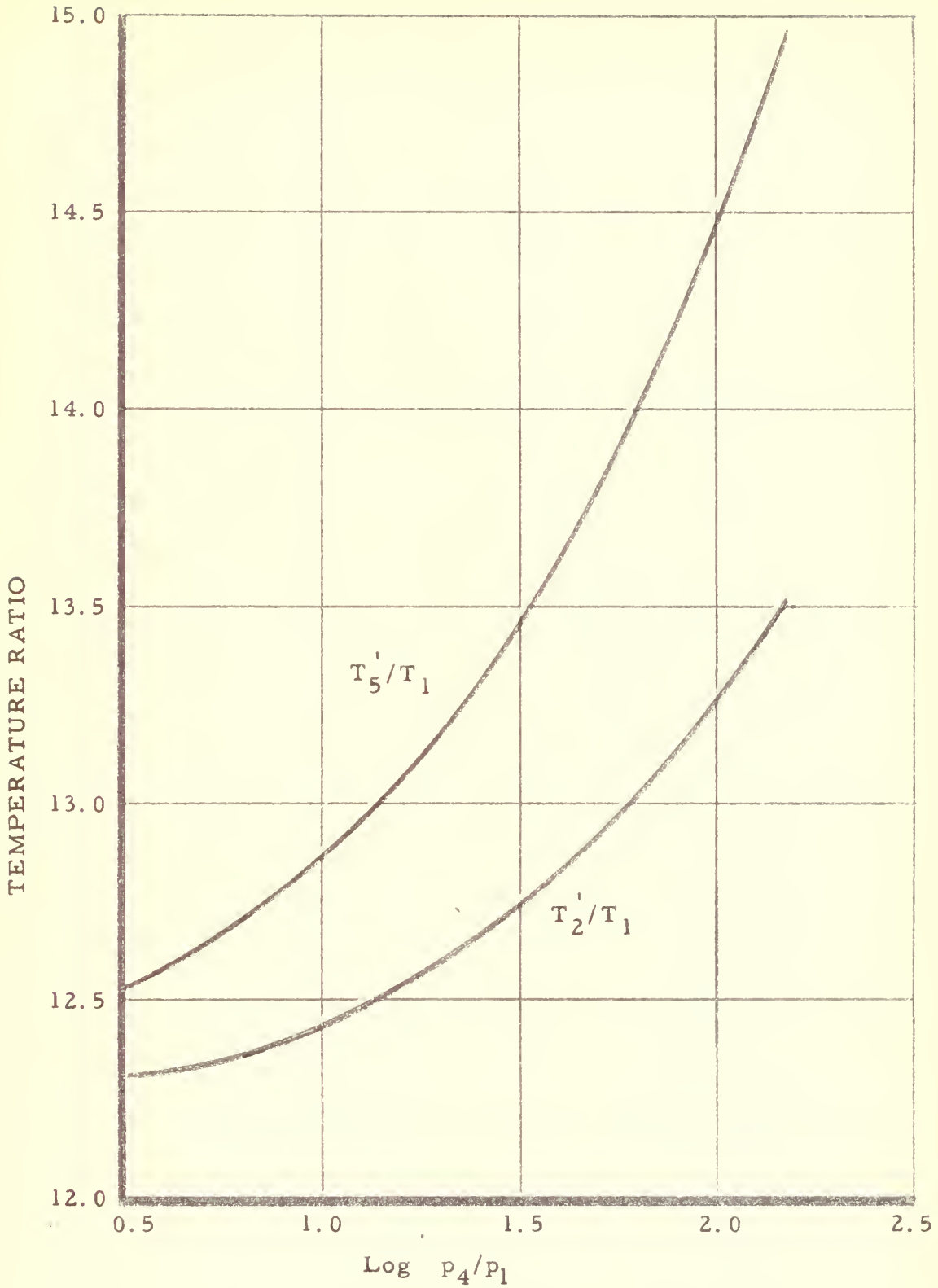


Fig. 28. Temperature ratios $T_2'/T_1$ and $T_5'/T_1$ vs. log $p_4/p_1$ for acetylene; constant-pressure reaction; $\gamma = 5/3$.

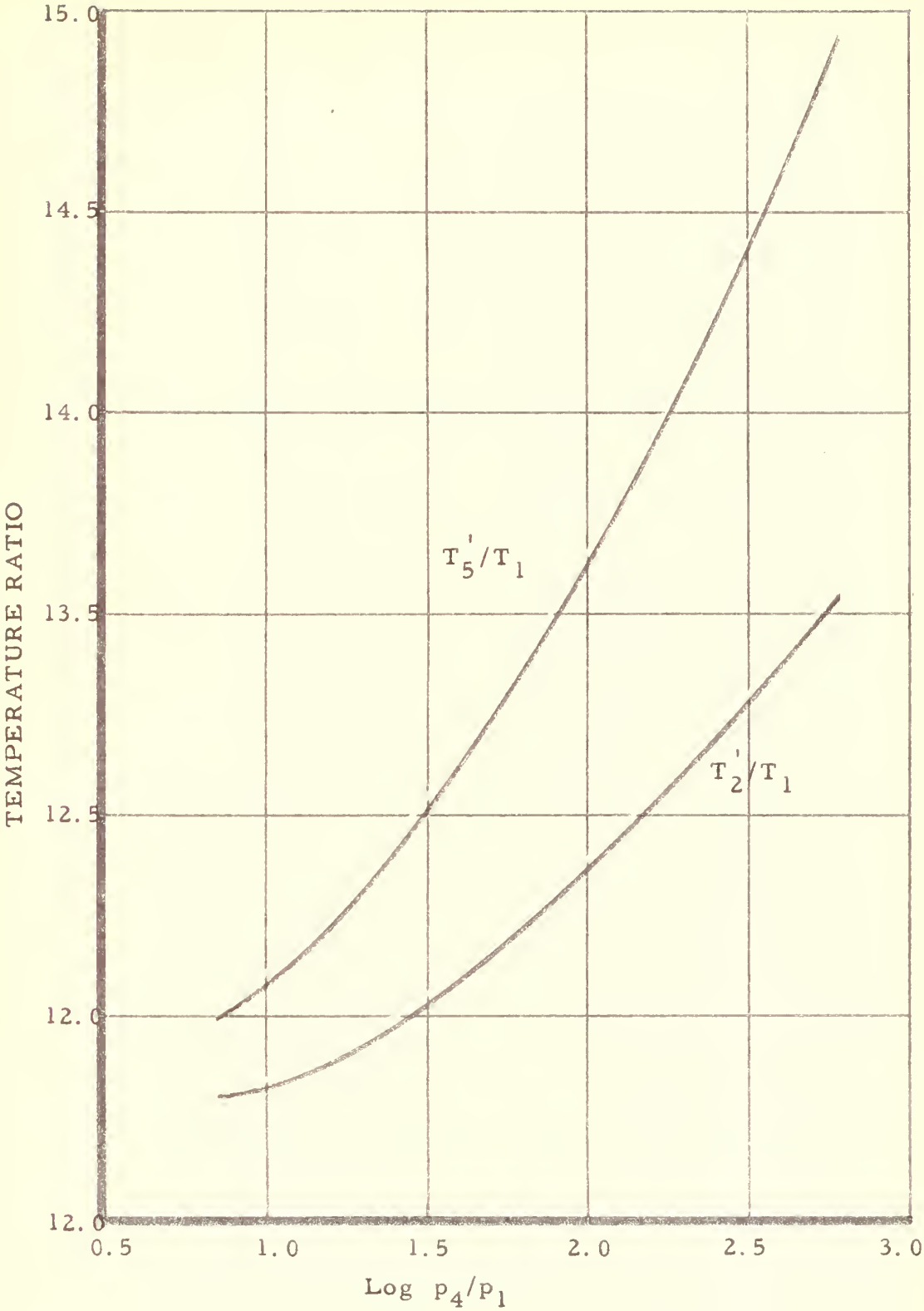


Fig. 28a. Temperature ratios $T_2'/T_1$ and $T_5'/T_1$ vs. log $p_4/p_1$ for acetylene; constant-volume reaction; $\gamma = 7/5$.

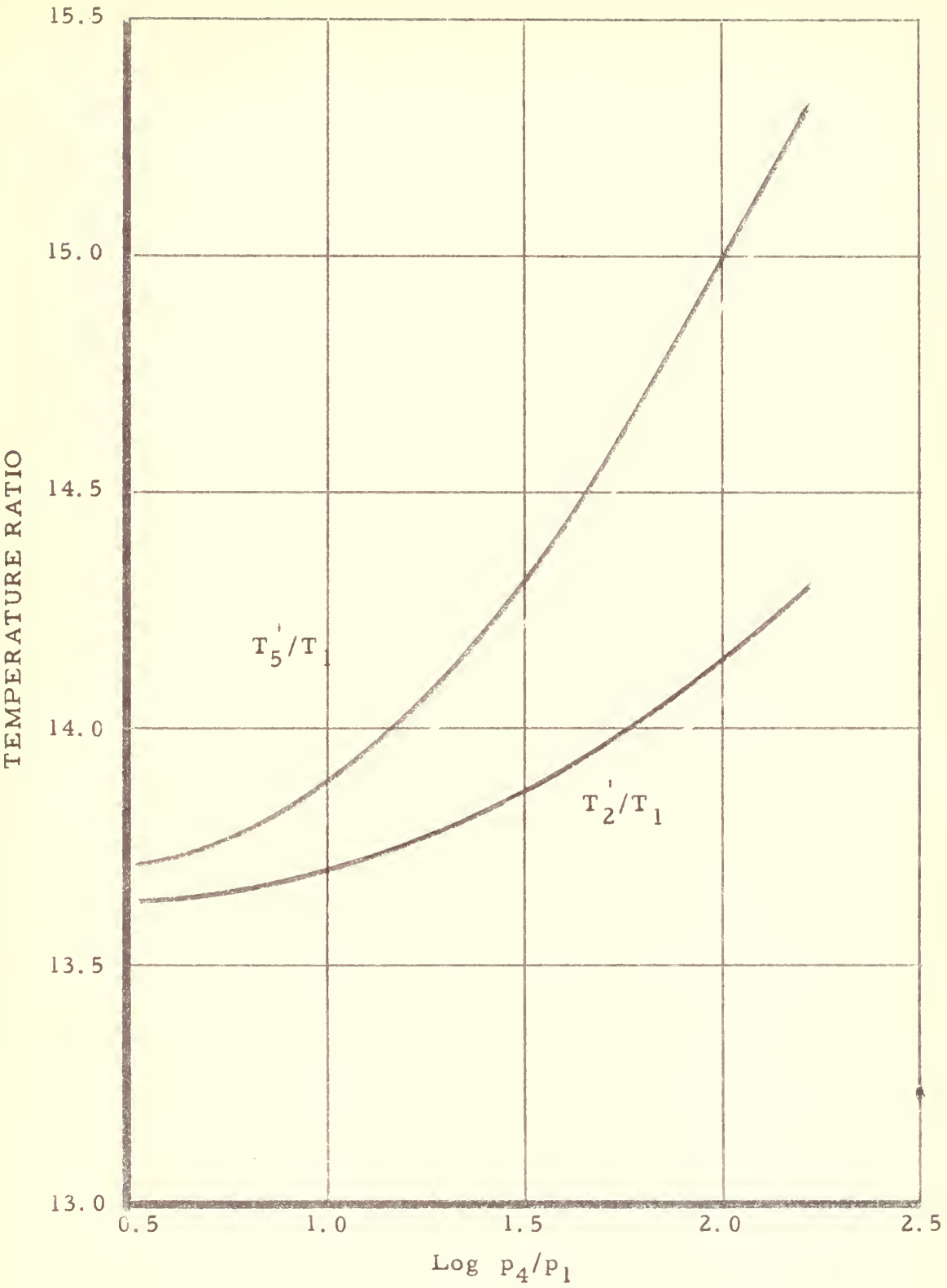


Fig. 29. Temperature ratios $T_2'/T_1$ and $T_5'/T_1$ vs. log $p_4/p_1$ for acetylene; constant-volume reaction; $\gamma = 5/3$.

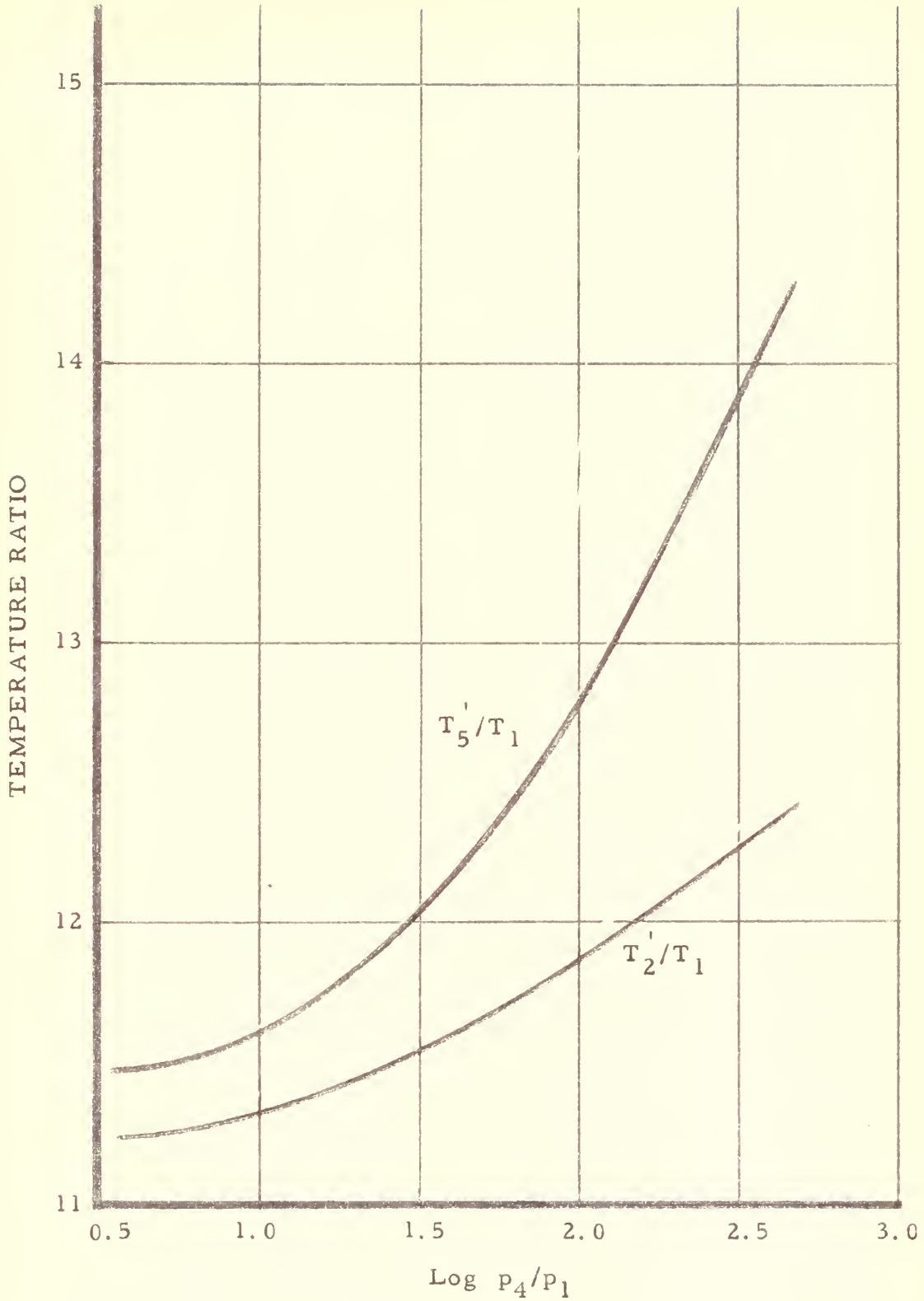


Fig. 30. Temperature ratios $T_2'/T_1$ and $T_5'/T_1$ vs. log $p_4/p_1$ for acetylene; constant-pressure reaction; $\gamma = 7/5$.

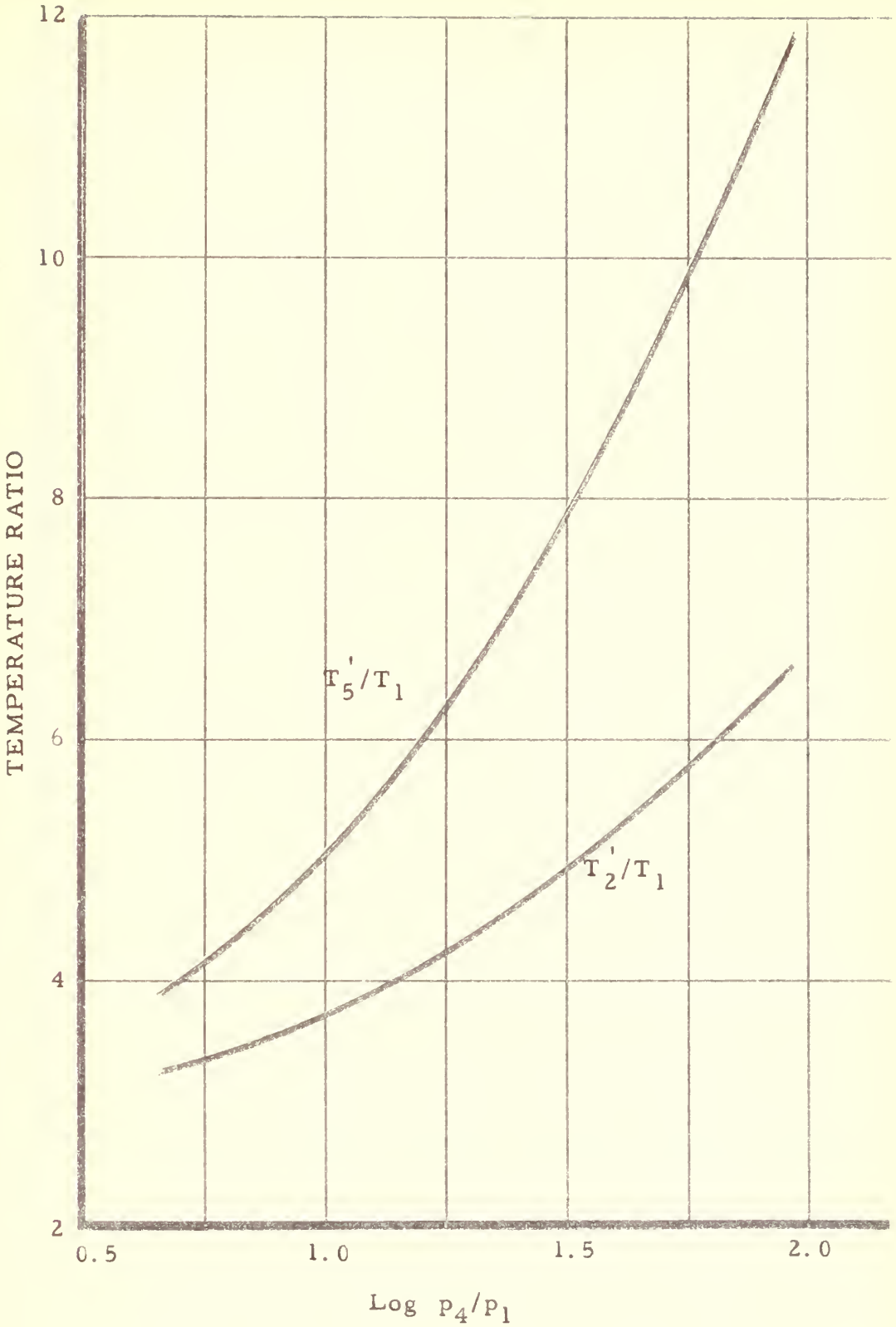


Fig. 31. Temperature ratios $T_2'/T_1$ and $T_5'/T_1$ vs. log $p_4/p_1$ for a mixture of 95 °/o argon and 5 °/o acetylene; constant-pressure reaction; $\gamma = 5/3$.

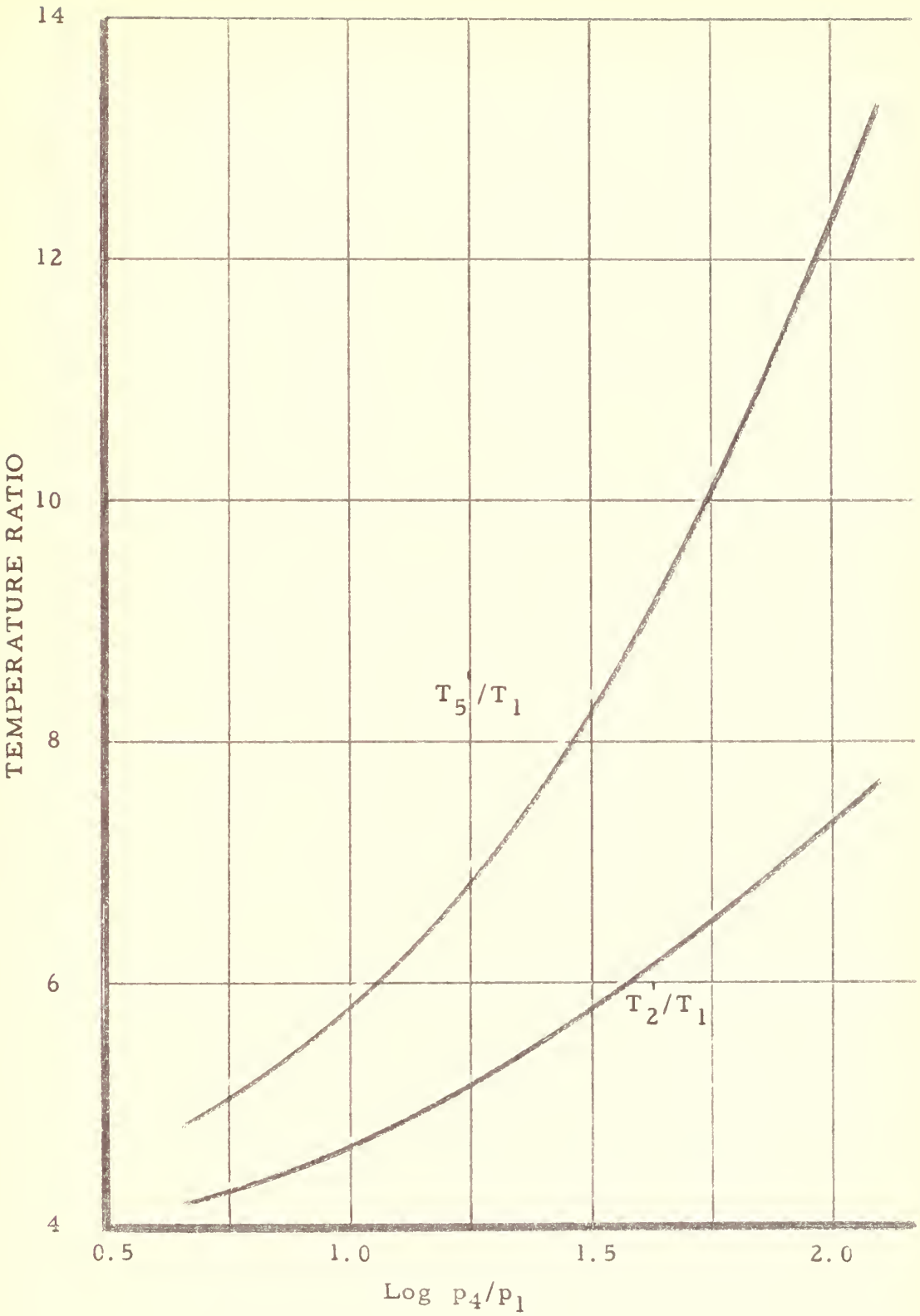


Fig. 32. Temperature ratios $T_2'/T_1$ and $T_5'/T_1$ vs. log $p_4/p_1$ for a mixture of 95 °/o argon and 5 °/o acetylene; constant-volume reaction; $\gamma = 5/3$.

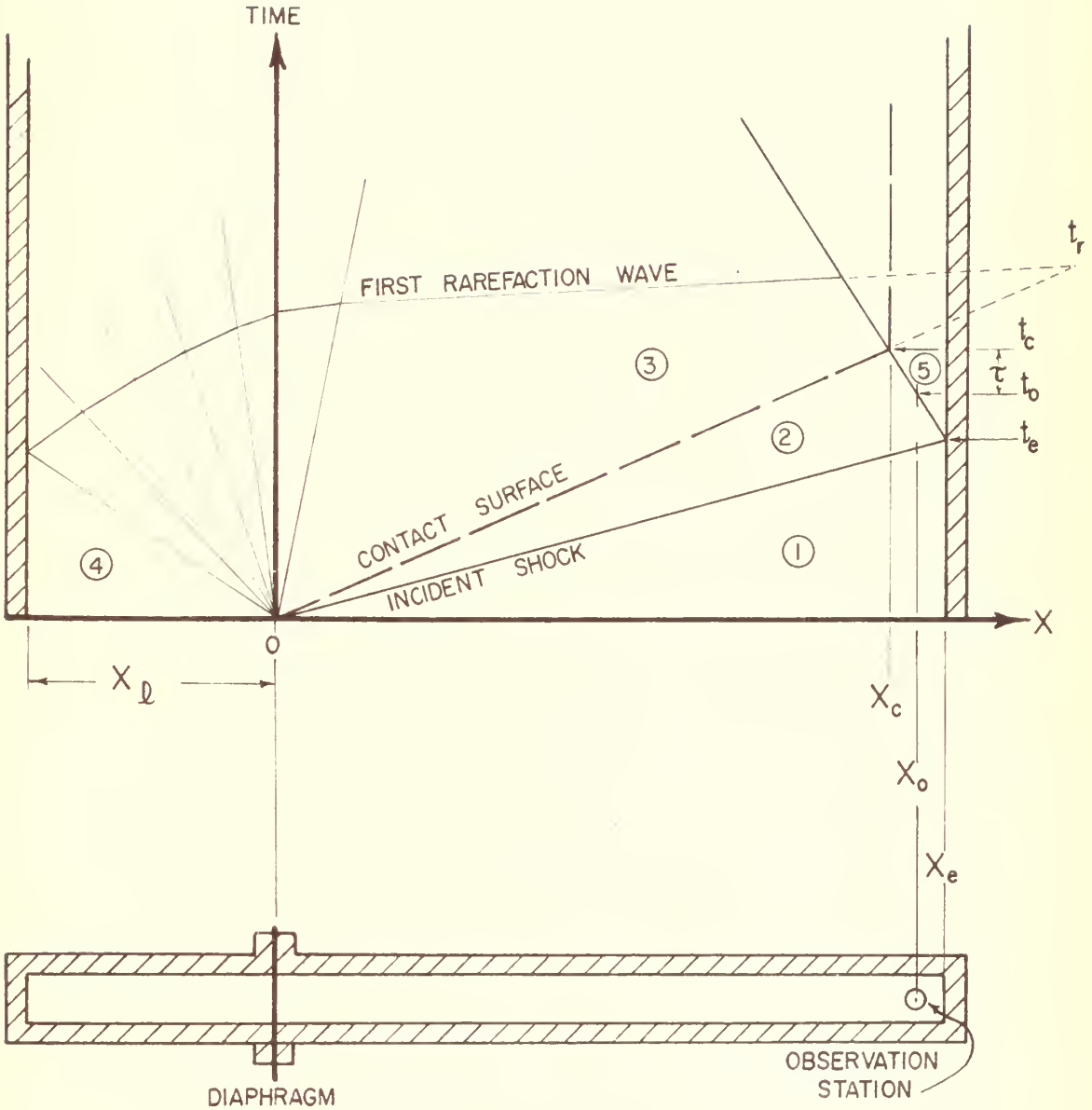


Fig. 33. The x-t diagram, showing coordinates defined in Section IV.

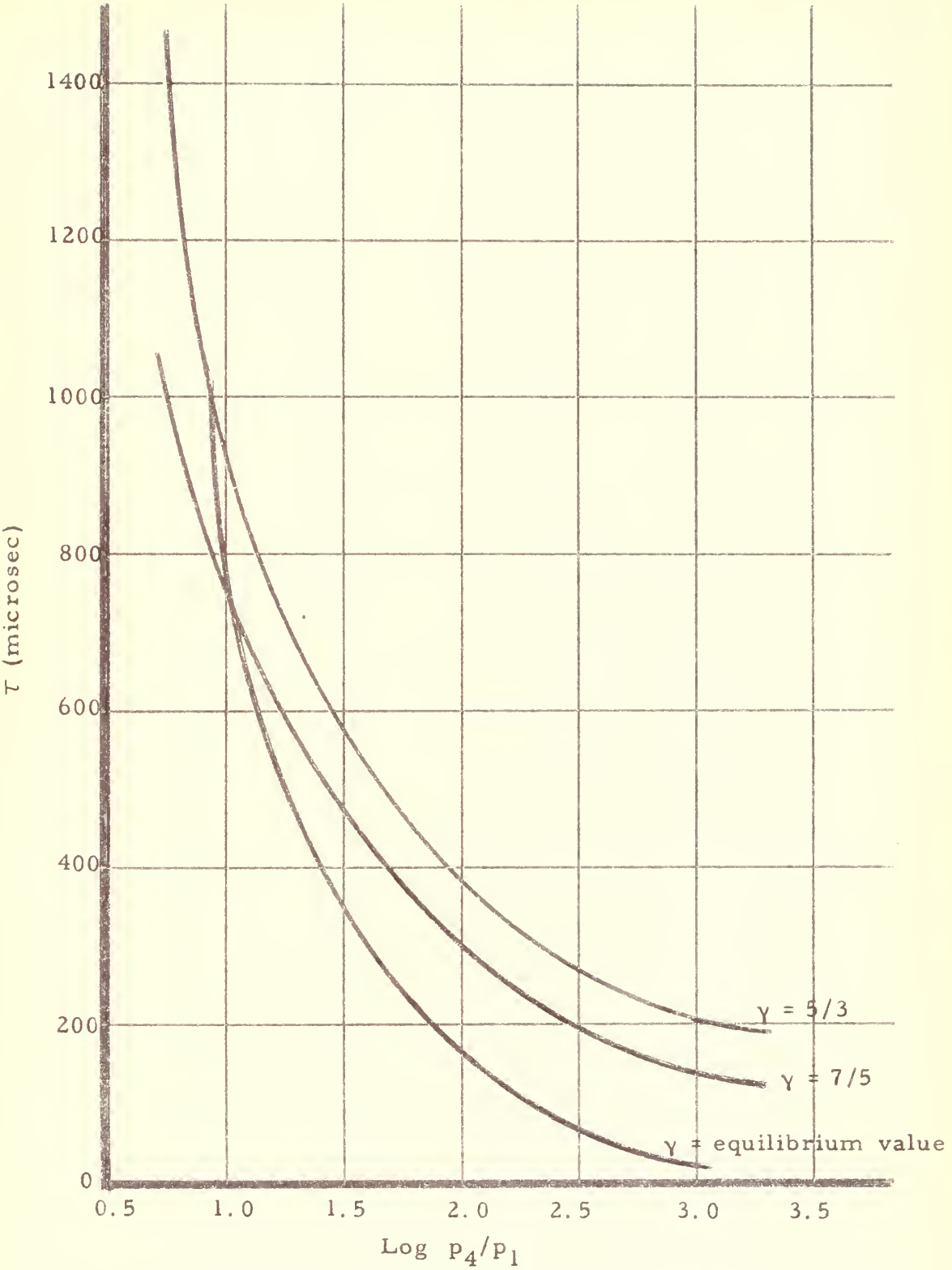


Fig. 34. Minimum time ($\tau$) at $T_5$ vs. log $p_4/p_1$ for acetylene.

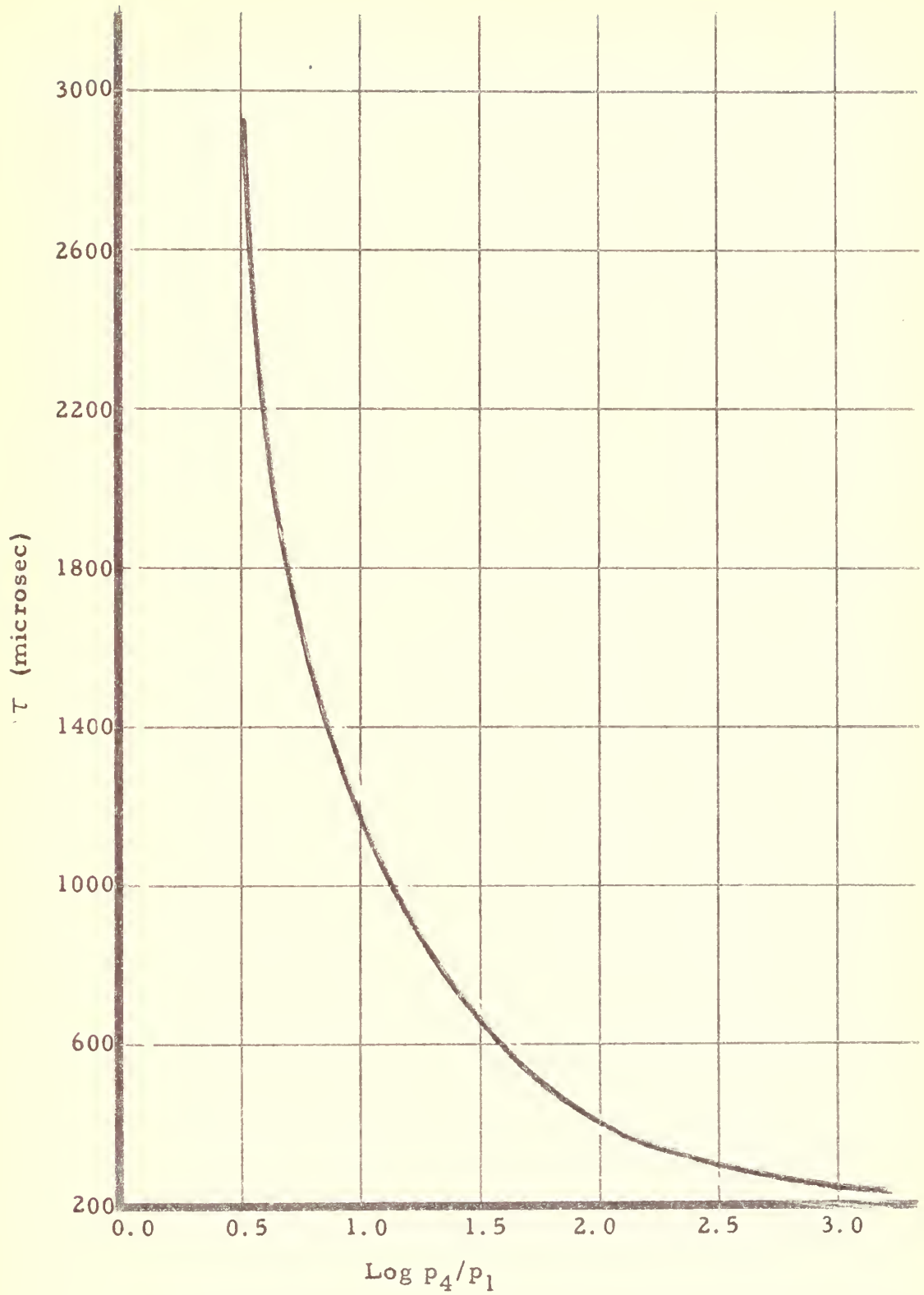


Fig. 35. Mininium time ($\tau$) at $T_5$ vs. log $p_4/p_1$ for a mixture of 95 °/o argon and 5 °/o acetylene.

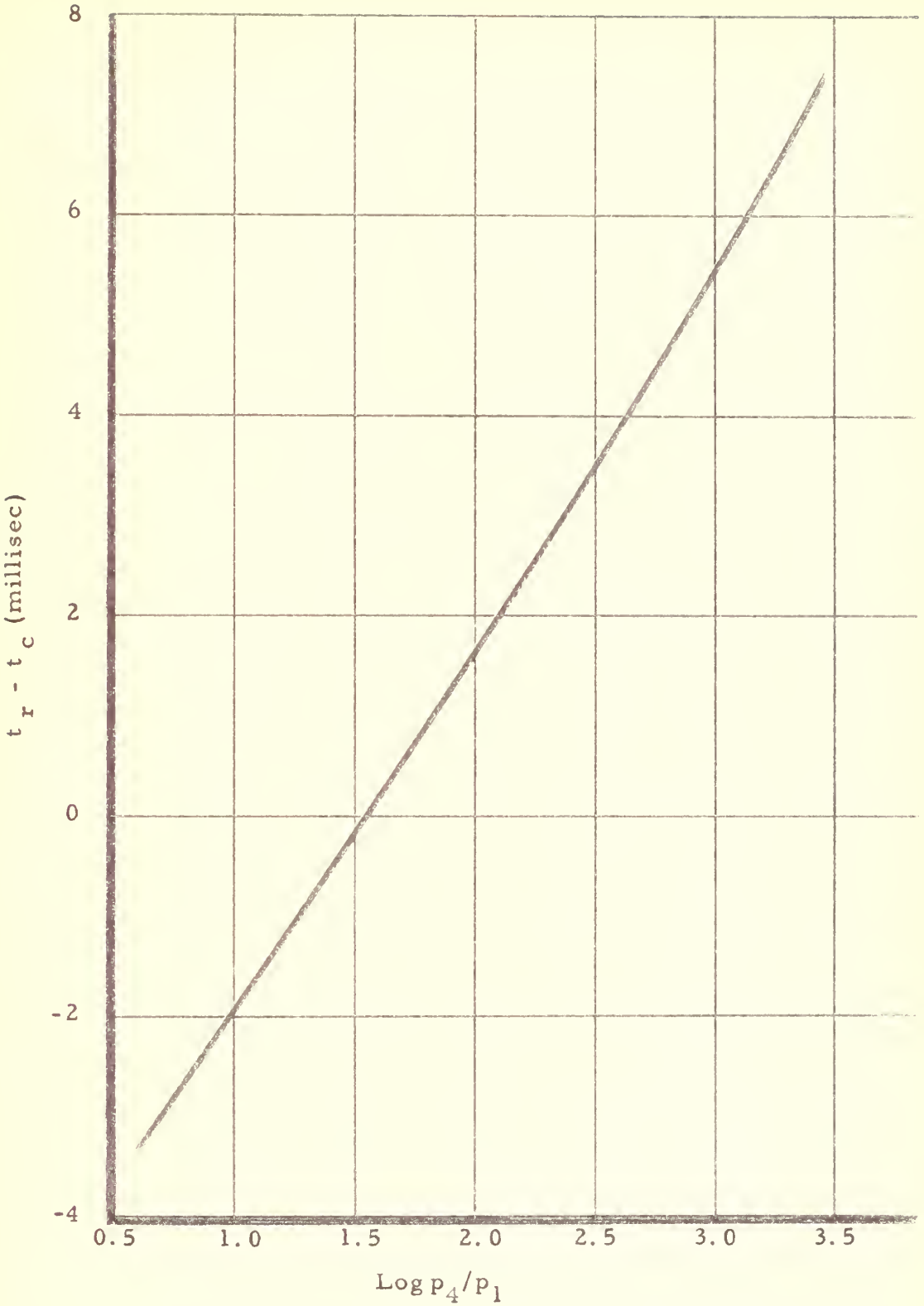


Fig. 36. The time $(t_r - t_c)$ vs. log $p_4/p_1$ for acetylene.

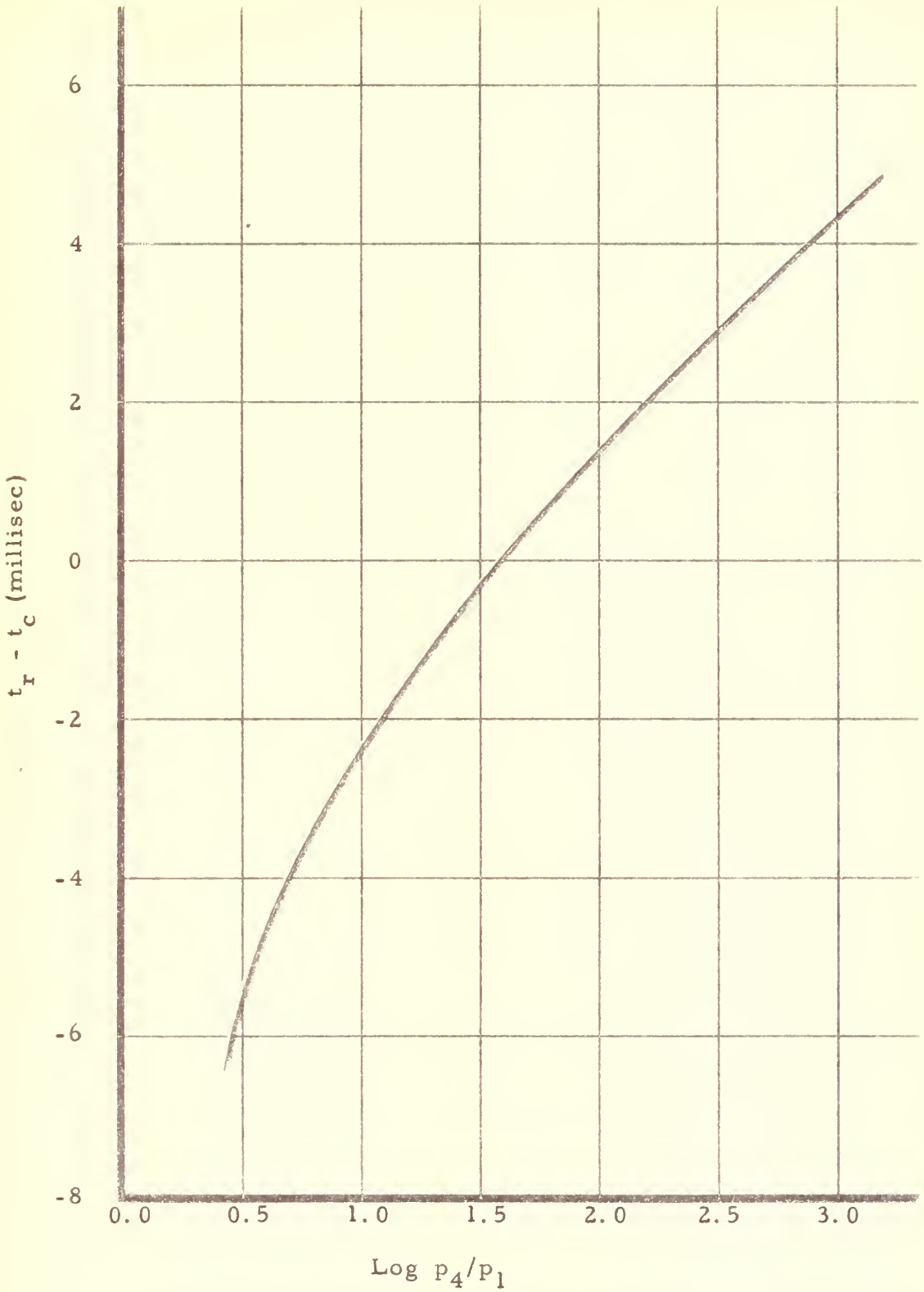


Fig. 37. The time $(t_r - t_c)$ vs. log $p_4/p_1$ for a mixture of 95 °/o argon and 5 °/o acetylene.

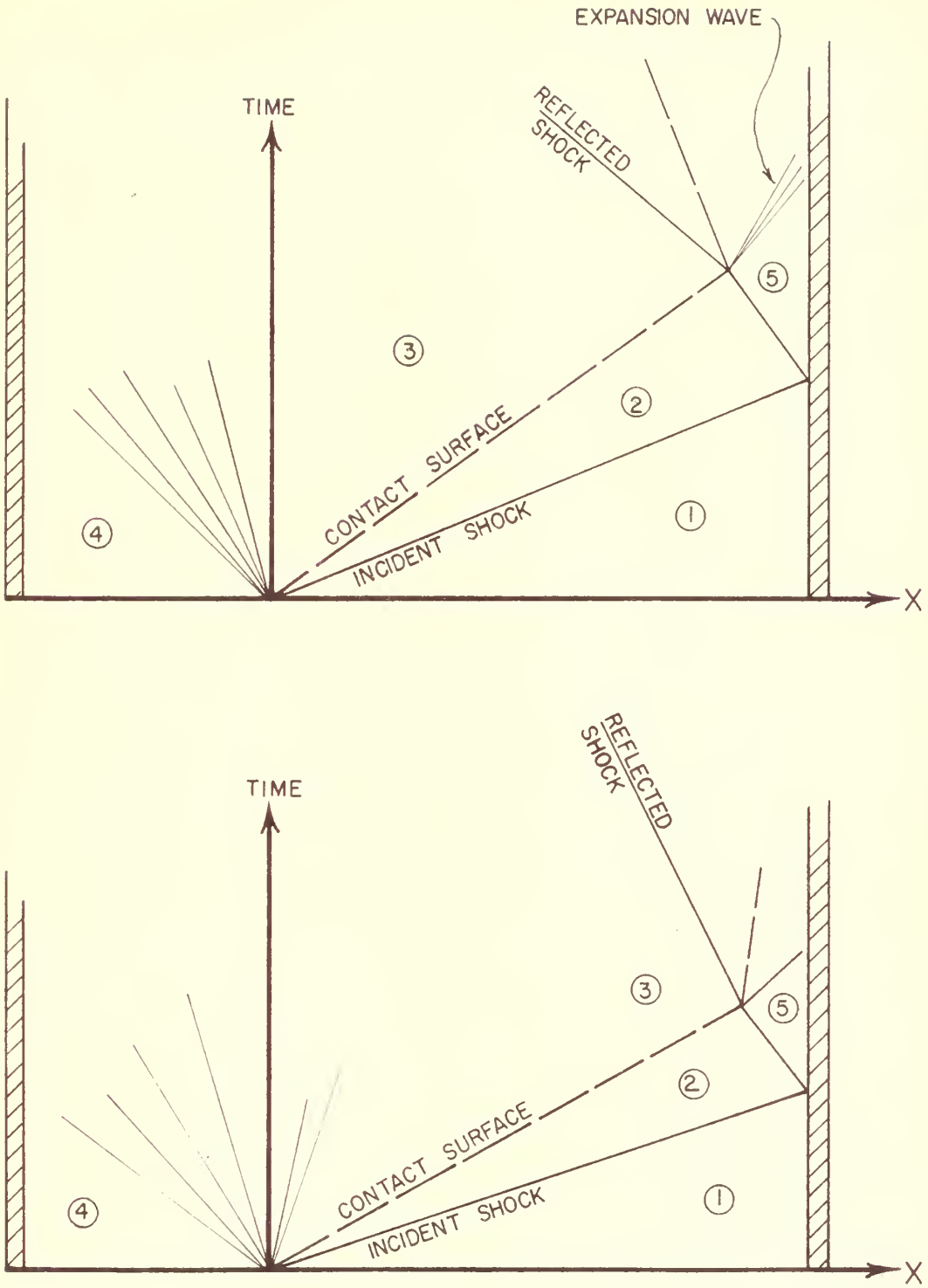


Fig. 38. Two x-t diagrams, showing wave reflection resulting from the interaction between the reflected shock and the contact surface.

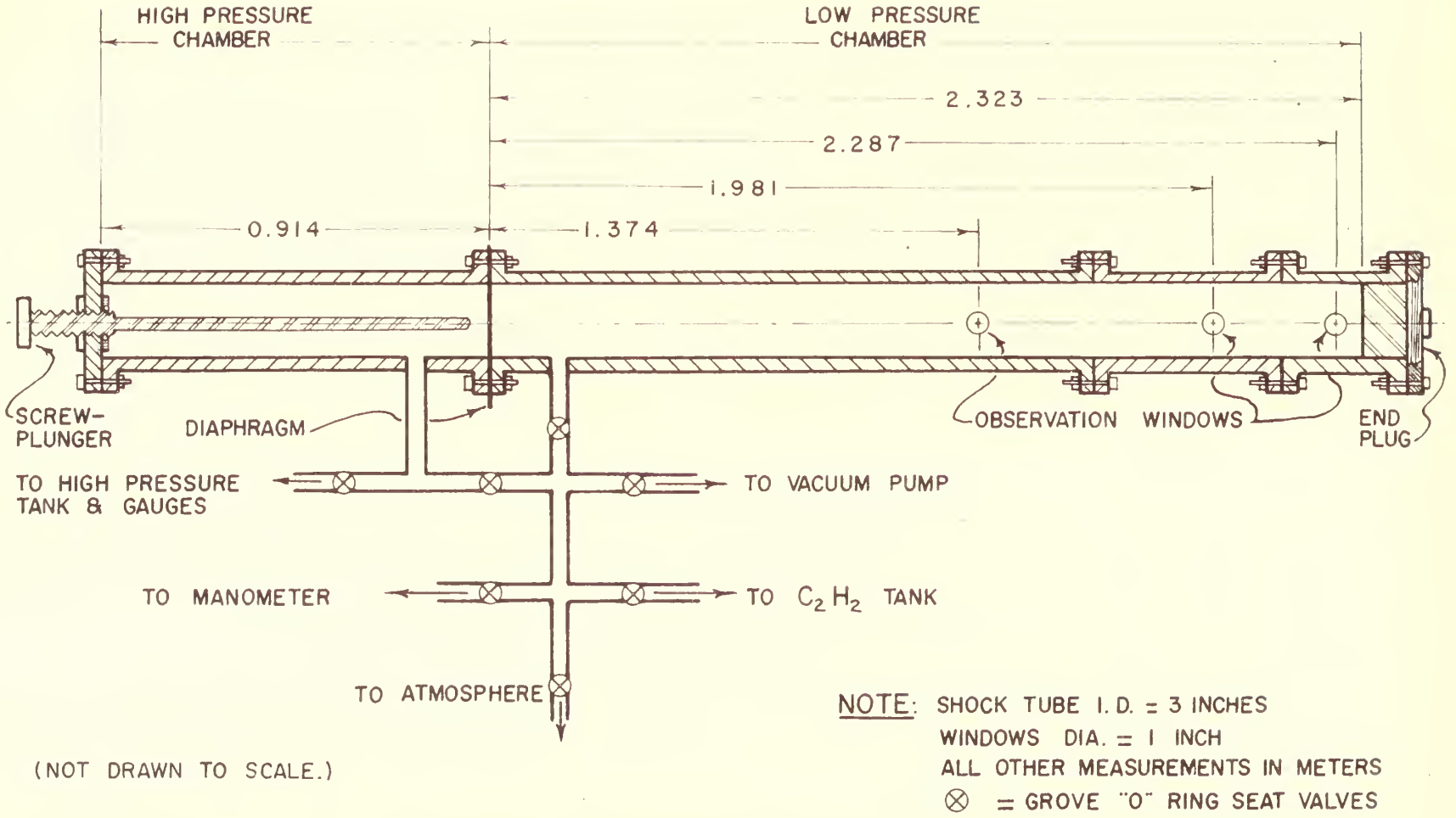


Fig. 39. Schematic diagram of the shocktube and gas supply manifold.

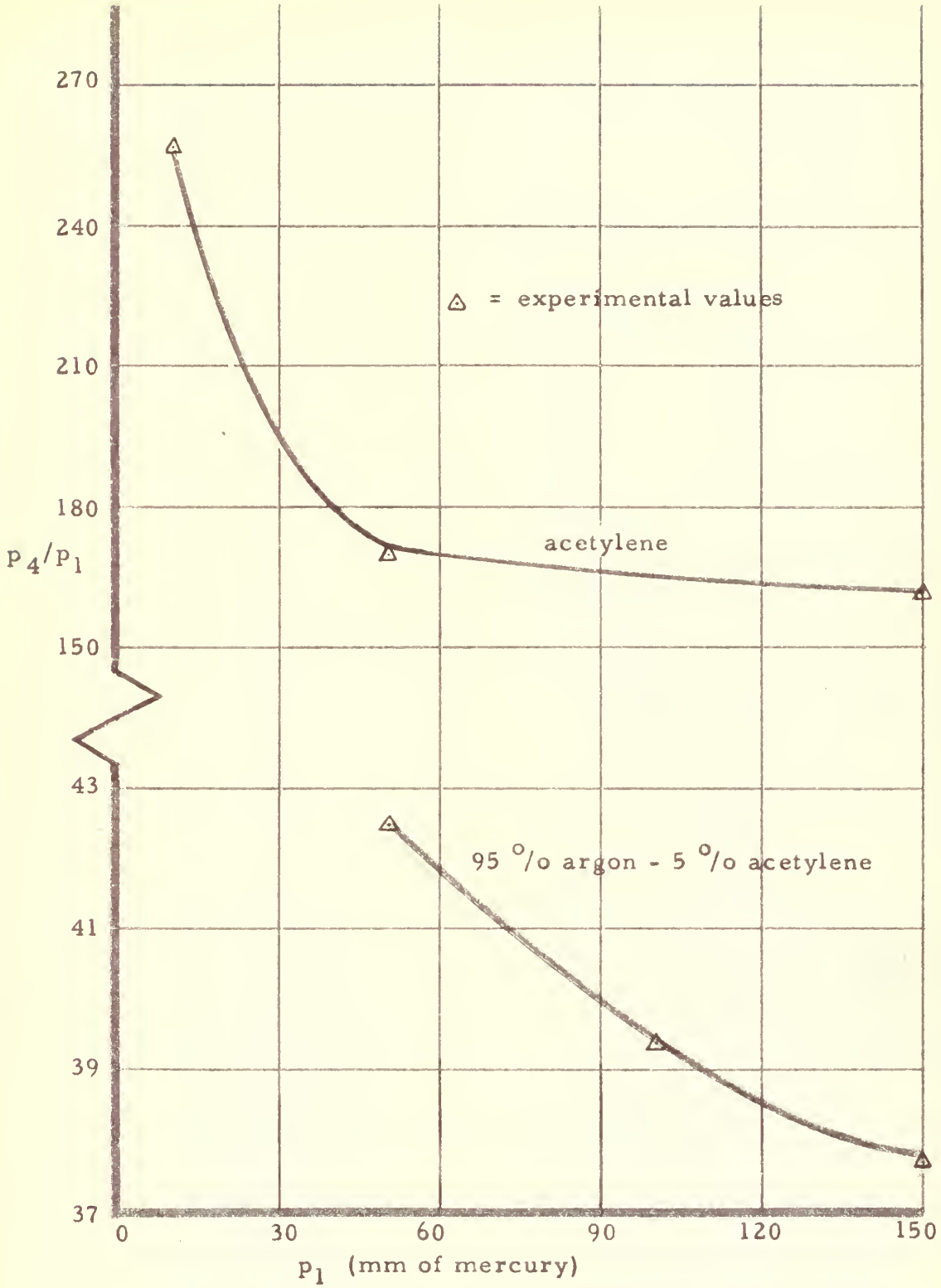


Fig. 40. Minimum pressure ratio ($p_4/p_1$) vs. initial pressure ($p_1$) required for carbon formation.

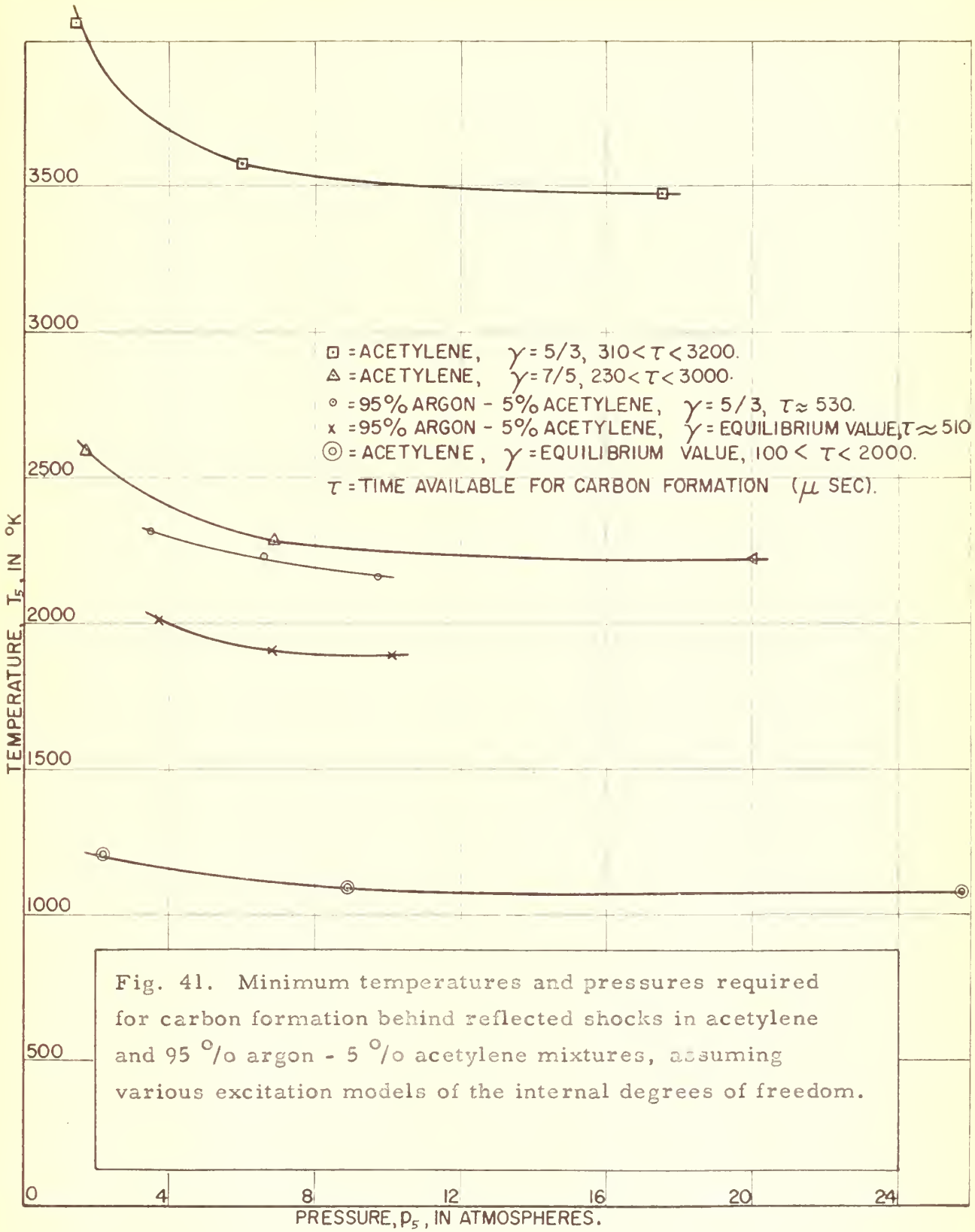
3500
3000
2500
2000
1500
1000
500
0
4
8
12
16
20
24
TEMPERATURE, $T_5$, IN °K
PRESSURE, $p_5$, IN ATMOSPHERES.
⊡ = ACETYLENE, $\gamma = 5/3$, $310 < \tau < 3200$.
△ = ACETYLENE, $\gamma = 7/5$, $230 < \tau < 3000$.
◦ = 95% ARGON - 5% ACETYLENE, $\gamma = 5/3$, $\tau \approx 530$.
x = 95% ARGON - 5% ACETYLENE, $\gamma$ = EQUILIBRIUM VALUE, $\tau \approx 510$
◎ = ACETYLENE, $\gamma$ = EQUILIBRIUM VALUE, $100 < \tau < 2000$.
$\tau$ = TIME AVAILABLE FOR CARBON FORMATION ($\mu$ SEC).

Fig. 41. Minimum temperatures and pressures required for carbon formation behind reflected shocks in acetylene and 95 °/o argon - 5 °/o acetylene mixtures, assuming various excitation models of the internal degrees of freedom.

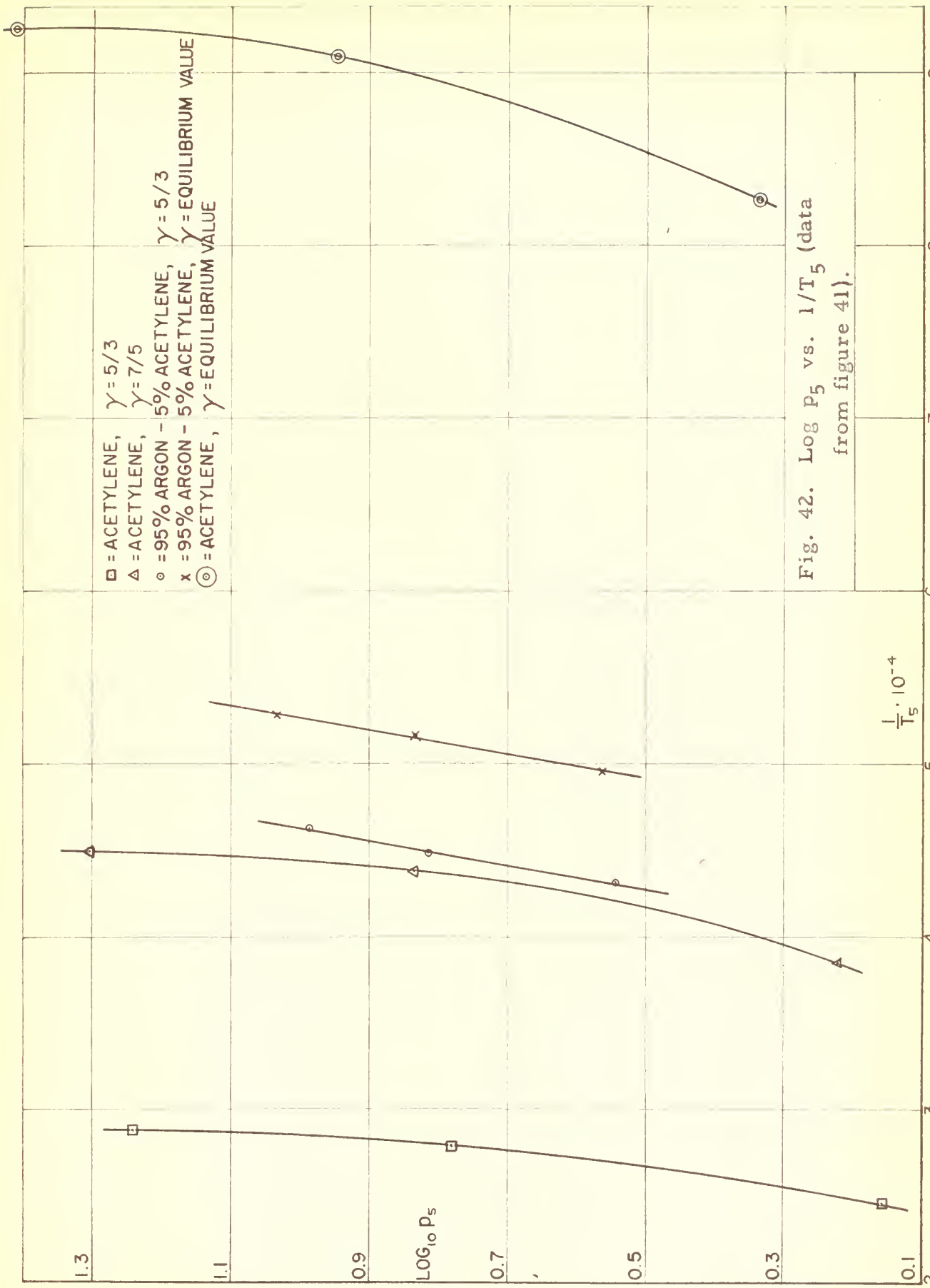


Fig. 42. Log $p_5$ vs. $1/T_5$ (data from figure 41).

Fig. 43. Emitted spectral intensity distribution measured behind carbon-forming shocks in acetylene.

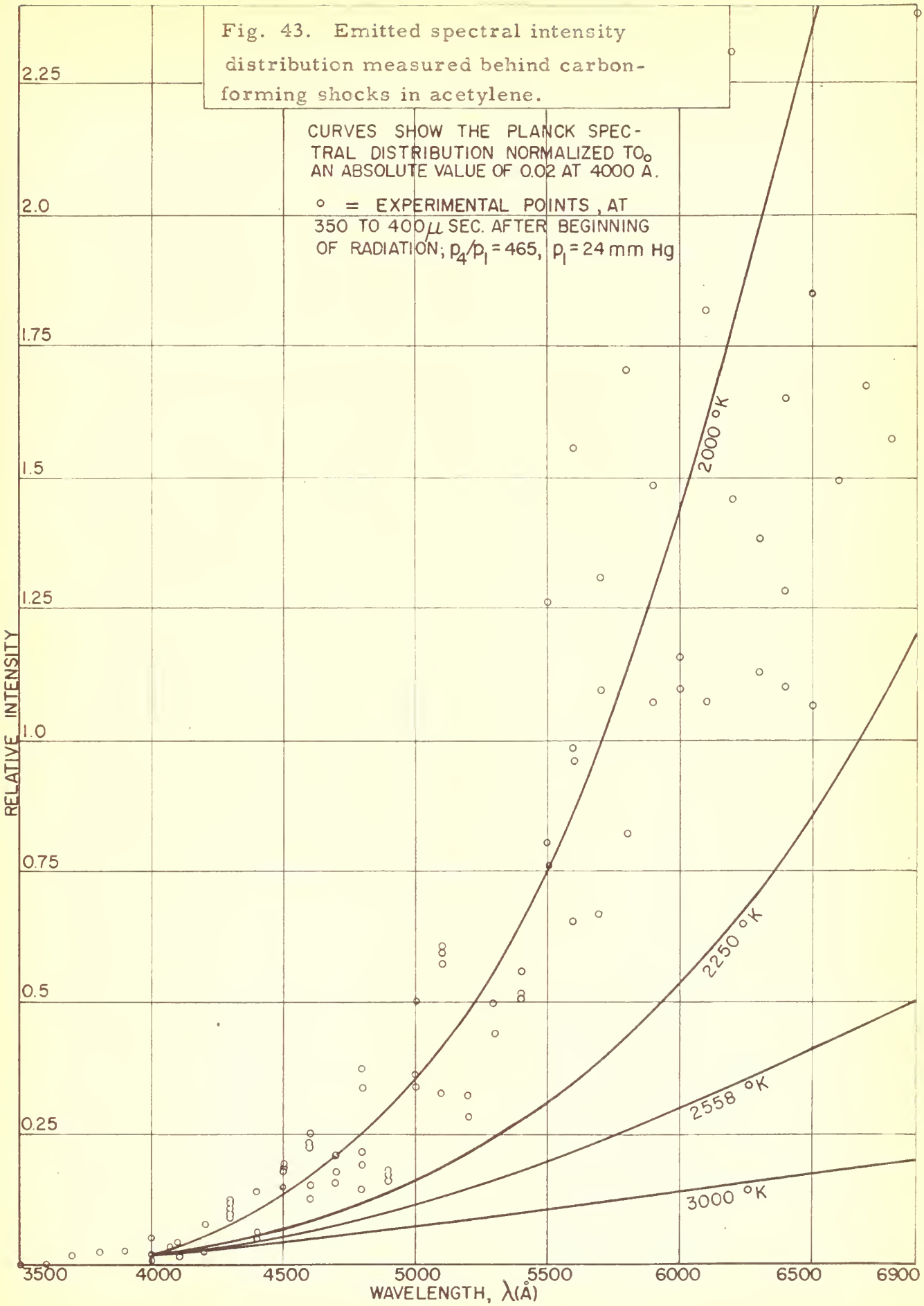

5479

JA1160

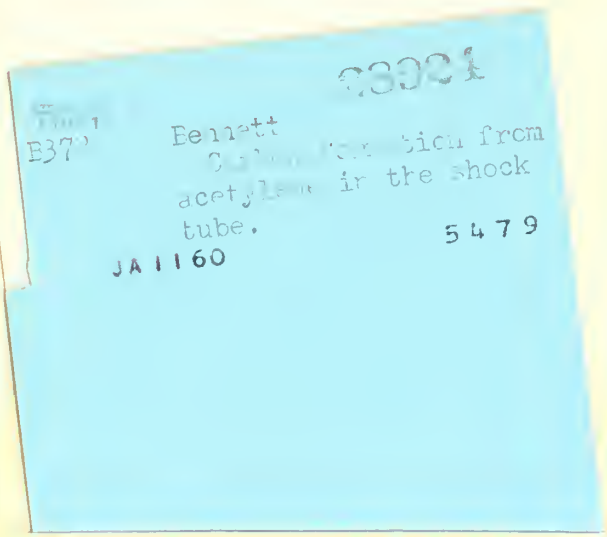

thesB372
Carbon formation from acetylene in the s
3 2768 002 13705 1
DUDLEY KNOX LIBRARY